1985

Nuclear magnetic resonance studies of amorphous silicon hydrides: proton spin dynamics

Charles Gordon Fry
Iowa State University

INFORMATION TO USERS

This reproduction was made from a copy of a document sent to us for microfilming. While the most advanced technology has been used to photograph and reproduce this document, the quality of the reproduction is heavily dependent upon the quality of the material submitted.

The following explanation of techniques is provided to help clarify markings or notations which may appear on this reproduction.

1. The sign or "target" for pages apparently lacking from the document photographed is "Missing Page(s)". If it was possible to obtain the missing page(s) or section, they are spliced into the film along with adjacent pages. This may have necessitated cutting through an image and duplicating adjacent pages to assure complete continuity.

2. When an image on the film is obliterated with a round black mark, it is an indication of either blurred copy because of movement during exposure, duplicate copy, or copyrighted materials that should not have been filmed. For blurred pages, a good image of the page can be found in the adjacent frame. If copyrighted materials were deleted, a target note will appear listing the pages in the adjacent frame.

3. When a map, drawing or chart, etc., is part of the material being photographed, a definite method of "sectioning" the material has been followed. It is customary to begin filming at the upper left hand corner of a large sheet and to continue from left to right in equal sections with small overlaps. If necessary, sectioning is continued again—beginning below the first row and continuing on until complete.

4. For illustrations that cannot be satisfactorily reproduced by xerographic means, photographic prints can be purchased at additional cost and inserted into your xerographic copy. These prints are available upon request from the Dissertations Customer Services Department.

5. Some pages in any document may have indistinct print. In all cases the best available copy has been filmed.

University Microfilms International
300 N. Zeeb Road
Ann Arbor, MI 48106

Fry, Charles Gordon

NUCLEAR MAGNETIC RESONANCE STUDIES OF AMORPHOUS SILICON-HYDRIDES: PROTON SPIN DYNAMICS

Iowa State University PH.D. 1985

PLEASE NOTE:

In all cases this material has been filmed in the best possible way from the available copy. Problems encountered with this document have been identified here with a check mark ✓.

1. Glossy photographs or pages _____
2. Colored illustrations, paper or print _____
3. Photographs with dark background ✓
4. Illustrations are poor copy _____
5. Pages with black marks, not original copy _____
6. Print shows through as there is text on both sides of page _____
7. Indistinct, broken or small print on several pages _____
8. Print exceeds margin requirements _____
9. Tightly bound copy with print lost in spine _____
10. Computer printout pages with indistinct print _____
11. Page(s) _____ lacking when material received, and not available from school or author.
12. Page(s) _____ seem to be missing in numbering only as text follows.
13. Two pages numbered _____. Text follows.
14. Curling and wrinkled pages _____
15. Dissertation contains pages with print at a slant, filmed as received _____
16. Other _____

_____

_____

University
Microfilms
International

Nuclear magnetic resonance studies of amorphous silicon hydrides: Proton spin dynamics

by

Charles Gordon Fry

A Dissertation Submitted to the Graduate Faculty in Partial Fulfillment of the Requirements for the Degree of DOCTOR OF PHILOSOPHY

Department: Chemistry
Major: Physical Chemistry

Approved:

Signature was redacted for privacy.

In Charge of Major Work

Signature was redacted for privacy.

For the Major Department

Signature was redacted for privacy.

For the Graduate College

Iowa State University
Ames, Iowa

1985

TABLE OF CONTENTS

LIST OF FIGURES

LIST OF TABLES

I. INTRODUCTION

Amorphous is, in itself, an interesting word, meaning "without form or shape." Throughout its long history, it has somehow managed to conjure up concrete images out of the abstract thought. In modern science, however, we find it important to make precise our usage of amorphous. And, in fact, a huge effort is currently being put forth to such a cause. The reasons for this effort are not hard to understand: such diverse physical phenomena as the tensile strength of polymers and the electronic mobility in semiconductors are greatly dependent on what exactly the amorphous structure of a material happens to be. In the most basic terms, the physics of amorphous materials is one of the least developed areas of all theoretical physics. It is with these thoughts in mind that this thesis is written.

A. Spin Diffusion in Amorphous Systems

As B. Mandelbrot[1] has taught us with the use of fractals, one must define the scale with which one is interested in to clarify an observation. Amorphous materials are a case in point: macroscopically, >1 μm, systems truly appear amorphous, lacking in the long-range order expected of crystalline solids. Conversely, observing atomic dimensions, <5A, the system will appear structurally ordered, an example

of which is the observation in amorphous materials of a well-defined nearest-neighbor peak in the radial distribution function. This seeming dichotomy is an essential property of all amorphous solids.[2]

The statements of loss of long-range order with conservation of short-range order make clear the necessity of defining the intermediate region in between, from 10-1000A. Great strides have been made using both macroscopic and microscopic techniques for structural characterization of amorphous materials. From the macroscopic side, diffraction techniques can now routinely observe resolutions of 100A, and some recent experiments show resolution down to 10A. Unfortunately, X-ray techniques suffer from their inherent insensitivity to hydrogen and other light nuclei, whereas neutron scattering suffers from self-scattering problems and requires enormous amounts of sample (as does NMR, in the minds of thin film scientists!). Even so, these techniques have provided a wealth of information about a-Si:H.

From the atomic dimensions, there has recently been a surge of interest in expanding the spatial information available from nuclear magnetic resonance (NMR) into the dimensions appropriate for characterizing the term "amorphous". These experiments require no new technical innovations, and lack only in a complete understanding of the basic physics involved. In order to study dimensions >5A,

NMR spectroscopists use the phenomenon of spin diffusion.[3-5] Spin diffusion entails the process wherein magnetic dipole transitions cause magnetization to "walk" thru a region. Using an experiment first devised by Goldman and Shen,[6] and recently extended by Cheung and Gerstein,[7] one can determine domain sizes and shapes by experimentally starting the walk at a predetermined point, and measuring the time needed to remagnetize a domain. Multiple quantum experiments have shown promise for measuring small domains (containing perhaps up to 100 protons) in certain systems.[8-11] In these experiments, the communication of spins by spin diffusion can be measured as the total number of mixed states obtained after a period of time. The number of such mixed states, measured by observing the highest order multiple quantum transition possible, defines the domain size. Lastly, two-dimensional NMR experiments are now using spin-diffusion of not only protons, but also of rare nuclei to extend the available information. Spin diffusion between quadrupolar nuclei has been investigated as a function of spinning speed,[12-14] whereas in other cases spin diffusion is used to determine whether a spectral line is homogeneously or inhomogeneously broadened.[15] In addition, spin diffusion between ^{13}C nuclei has been used to define whether a sample is only macroscopically heterogeneous or microscopically heterogenous.[16]

This very current interest in using spin diffusion has firm foundations, and a promising future. Interest in the basic dynamics of spin diffusion is justified. Application of the phenomenon to new systems would appear to be a worthy task.

B. Amorphous Silicon Hydride

Perhaps it is advisable to briefly distinguish points of practical importance about amorphous silicon hydride (a-Si:H) films before becoming too involved in what essentially must be an extended discussion about technical aspects of the material. First, I emphasize the optimism presently abundant about the use of a-Si:H in devices. The USDOE's goal of photovoltaics generating 1% of the US's energy needs by the year 2000 has an estimated dollar value of $36 billion per year.[17] A-Si:H becomes a factor in this industry because:[17-22] i) it has a relatively high absorption coefficient (~20 times better that c-Si), thus greatly reducing the gross material needs, ii) it can be easily deposited over large areas, iii) it may be easily doped to control the bandgap, and iv) the deposition process is relatively cheap. Moreover, the overriding concern about the use of a-Si:H as a component in photoconversion devices has been its achievable conversion efficiency. Efficiencies of 10-12% have been

stated as being necessary before the material would be considered truly competitive with existing technologies.[17-22] Over a year ago the barrier of 12% was broken,[23] about which Bolton stipulated,[17] "... a-Si cells will be a very strong contender for the next generation of commercial solar cells."

Our main concerns are the problems remaining. In broad terms, these problems are:[17-22] i) the thermal stability of the films over long periods of time, ii) the effects of long term irradiation, and iii) causes for the short carrier lifetimes where recombination is a major loss mechanism. Johnston states[19] that a-Si:H is exceptional in that much basic research is still needed to improve deposition processes and conversion efficiencies. I have approached solving these problems in the production of a-Si:H by studying the annealing behavior of the films, and by attempting to characterize the defect structures responsible for light-induced effects and recombination in these materials.

Amorphous silicon hydride films are an important example of a material in which deviations away from the idealized amorphous solid, the model which I shall use being the continuous random network[24,25] (CRN), are essential to the film's properties. It is becoming accepted that many of the early problems in studying a-Si:H came from an incomplete understanding of the importance of these deviations or

defects, and for a certain period of time from a lack of knowledge that these defects in good films even existed. It appears that many diverse, often seemingly contradictory, results obtained on nominally similar films came from a-Si:H's strong dependence on these deviations from the CRN, deviations which are strongly dependent on preparative conditions. For example, studies on amorphous silicon (a-Si) and germanium (a-Ge) provided evidence that certain defects, called dangling bonds, give deep states in the semiconductor gap, whereas other defects coming from reconstruction of void surfaces give shallow or weak states in the gap. The combined density of these defect states is always so high in a-Si that the mobility gap is filled, allowing transport to occur only by hopping which gives poor electronic properties. While hydrogen (H) decreases, or passivates, most of these defect states in a-Si:H, H can create other kinds of structural defects from the CRN. Obviously, the characterization of these structural defects is important to an understanding of the electronic properties of this material, and necessary for production of controlled device grade materials.

In the characterization of structural defects of a-Si:H, NMR has proven to be uniquely powerful.[26] As mentioned, for a period of time results were published which were interpreted to mean that "good" glow-discharge films were

structurally homogeneous (see section II.A.3). The first use of NMR by Reimer et al.[27] still provides the strongest evidence that all a-Si:H films are heterogeneous in the hydrogen environments. Evidence since then has led to the conclusion that a-Si:H is such a complex system structurally that Bustarret et al.[28] describes "... a-Si:H as a whole class of materials in itself." NMR has continued to be of such essential importance in the study of a-Si:H that three reviews pertaining to NMR have appeared in the literature.[27,29,30]

Still, many important questions remain about the structure of a-Si:H, and its effect on electronic properties. One specific question concerns the size and spatial distribution of the proton domains observed by proton NMR. A clear choice for studying such features is the Goldman-Shen experiment,[6] utilizing spin diffusion to obtain domain sizes and shapes, and perhaps also information about the separation between the domains.[7] This was the project which initiated the present study.

During the study of spin diffusion using the Goldman-Shen sequence, anomalous results were obtained. Apart from simple curiosity, an extended study of these anomalous features was deemed important for a number of reasons. First, it was established that the anomalous results originated from only a small portion of the total proton concentration. A chance to

obtain more detailed information about the proton structure appeared probable. It has been conjectured that for some electronic properties in a-Si:H only a small portion of the total number of protons is involved.[31] One example of this is the predicted occurrence of molecular hydrogen (m-H_2) in a-Si:H.[32] M-H_2 may be important not only for the interpretation of certain features of the NMR spectra of these materials, but also for understanding the process of annealing (related to the deposition substrate temperature) and the so-called Staebler-Wronski effect.[31] Since m-H_2 must be confined by void structures, the void characteristics might be obtained from information obtained about the m-H_2.

Second, most of the NMR experiments previously done have been basic ground work experiments - the behavior of T_2 and T_1; see section II.C - and many have not had unambiguous results. An example of this fact is the differences observed in both proton[33,34] and silicon-29[35,36] NMR of samples prepared by glow-discharge as compared to samples prepared by sputtering. Thus, more work is needed to clarify the results already obtained from NMR (see the discussion in section II.C).

Lastly, a point in favor of continued studies using NMR on a-Si:H is related to a widely known source of puzzlement about a-Si:H. This factor is the known disparity between the amount of hydrogen uptake necessary to make a good

semiconductor, compared to the number of dangling bonds[37,38] - unpaired electrons situated on silicons - known to be the main source of photovoltaic degradation in a-Si:H. Hydrogen is present in the best materials in amounts at least 100 times higher than necessary in order to passivate all the dangling bonds. One important example where a small number of hydrogen could be involved in determining electronic behavior, already alluded to, is the so-called Staebler-Wronski or light-induced effect.[31] It is observed that irradiation of some a-Si:H films causes huge (up to five orders of magnitude), reversible (annealing at 150^{o}C reverses the process) changes in the film's photoconductivity, luminescence and defect densities.[31,37] So far, this effect has resisted an accepted explanation. In addition, it seems reasonable to assume that if electronic defects could be minimized, while also minimizing the amount of hydrogen - which must create structural defects, if only compositionally - a better photovoltaic material would be obtained. Thus, any investigation of unusual behavior of hydrogen, especially of hydrogen in small concentrations may have important implications for the material in general.

C. Statement of the Problem

The present research on a-Si:H using NMR involves three main questions. First, with the use of the Goldman-Shen[6] spin diffusion experiment, can domain sizes and shapes be determined[7] in a-Si:H? Specifically, can a measure of the clustered proton domain (see section II.C) be obtained, along with a dimension for the domain separation? Second, noting the simplicity of the a-Si:H system in terms of a lack of proton motions, can spin diffusion itself be more fully understood, especially in terms of the Goldman-Shen experiment? Once these parameters are determined, can a more suitable understanding of the proton spin-lattice relaxation be realized? And last, can any detailed features of the proton spin dynamics be isolated and understood using any and all the techniques available to state-of-the-art NMR spectroscopist? Of specific interest would be the ability to observe and isolate features arising from a small fraction of the main proton content.

II. BACKGROUND AND LITERATURE SURVEY

A. Structural and Chemical Characterization of a-Si:H

In 1975, Spear and LeComber wrote their landmark paper[39] illustrating that amorphous silicon hydride (a-Si:H) films could be doped, allowing a control of the film's electrical conductivity over seven orders of magnitude. This immensely important practical aspect of a-Si:H films has led to a still increasing explosion of publications concerning these materials. The fact that interest is still increasing is not hard to understand upon remembering the statements made in the introduction. As with any new field undergoing such an expansion in literature, a summary of the reviews, compilations and conference proceedings discussing a-Si:H should be useful in leading prospective workers to specific literature of interest.

Recently, two books[40,41] and a four part series[42] have been published which deal exclusively with a-Si:H. Both of these sets contain excellent up-to-date reviews covering almost all current research on a-Si:H. In addition to the above, an older volume edited by Brodsky[43] is very useful, containing reviews of most aspects of amorphous semiconductors (a-sc), including a-Si:H. Written in a more introductory style is the proceedings of the Kyoto 1980 Summer Institute, which also reviews a-sc with many

discussions specifically concerning a-Si:H.[44] A number of other reviews have been published dealing with a-Si:H. Fritzsche,[37,45,46] Knights and Lucovsky,[47] and Paul and Anderson[48] give in-depth reviews of experimental results and interpretations on a-Si:H. Theoretical reviews discussing electronic properties,[49-51] defects[52-54] and topology[55-58] of a-Si:H and a-sc in general have appeared, as well as reviews covering luminescence,[59] vibrational spectra,[60] and nuclear[26,29,30] and optically detected[61] magnetic resonance studies on a-Si:H. Also deserving mention are three reviews discussing a-Si:H solar cells.[18,62,63] A number of conference proceedings contain technical papers concerning a-Si:H.[64-72] I reiterate that the two sets of texts[40-42] mentioned at the beginning of this discussion contain the most up-to-date reviews, written by many authors, covering all aspects of research on a-Si:H, and these treatises should probably be consulted before searching the earlier reviews or conference proceedings.

Briefly, I shall discuss some of the literature discussing a-sc which may be of interest. Mott and Davis[73] and Ziman[74] serve as excellent texts reviewing and discussing the theoretical physics of non-crystalline systems. The application of a-sc, and a-Si:H as one specific system of a-sc, in solar cells[17-20,22,40-44,75-77] and thin film devices[21,78,79] has been treated in many places, of which

only a few are listed here. The experimental determination of structure in non-crystalline materials has been discussed at length,[80-85] as well as the use of light scattering in solids.[86] Three recent reviews, not yet mentioned, covering aspects of a-sc, of which a-Si:H is treated as one subsystem, are important for broader interpretations and implications to the physics of a-sc.[87-89] Some older conference proceedings covering a-sc are important especially for early theoretical and experimental work on a-Si and a-Ge.[90-98] Papers about a-sc written for general audiences may be of interest.[99-103] The classic papers of Anderson,[104] who evolved the basic background for mobility, and Mott,[105] who introduced the basic band theory of non-crystalline materials deserve mention here.

In the following sections, a review of the large amount of information available about a-Si:H will not be attempted; more than adequate reviews have been introduced above. Instead, the generally accepted notions about a-Si:H will be presented, with pertinent supporting references. And important questions or problems still unresolved which are important for the work presented here will be emphasized.

1. Amorphous nature

An obvious, but perhaps not readily apparent how important, aspect of characterizing a-Si:H is determining

whether the material is in actuality amorphous - having a complete lack of long range order - or instead possesses microcrystalline features. In general, the previous quote of Bustarret et al. rings true.[28] Raman spectroscopy has clearly shown that amorphous-, polycrystalline-, and microcrystalline-Si:H films all exist under certain conditions,[106] but for most a-Si:H studied, including the films studied here, the common assertion is that these films are truly amorphous.[106] Still, it is important to give precision to the use of the term "amorphous".

An understanding of the amorphous nature of a-Si:H requires an understanding of the earlier work done on a-Si, both because the latter system provides the basic groundwork for a-Si:H, and because many basic properties of the two systems are similar. Much early work on a-Si involved finding a model system which would correctly predict the radial distribution function (rdf) obtained from x-ray diffraction. Historically, amorphous tetrahedrally bonded solids provided a difficult system to describe for many years. Moss and Graczyk,[107] when presenting their experimental rdfs of a-Si, pictured the theoretical state of affairs as: "... it is unfortunately true with amorphous solids that, far from having a surfeit of good fits to models, one usually cannot find any model which gives a passable fit."[107] Moreover, it appears that frustration

became so abundant that rdfs were believed by many workers in the area as being fairly useless.[58] A breakthrough appeared in 1971, wherein Polk[24] applied ideas dating back to Zachariasen[25] for the construction of his continuous random network (CRN) model for a-Si and a-Ge.

The CRN contains important ideas for all amorphous tetrahedrally bonded systems. These include:

i) completely saturated covalent bonds (i.e., the coordination number is four) to prevent defect sites,

ii) minimal changes in bond lengths and small but important changes in bond angles, and

iii) loss of long-range order through variation in dihedral angles.

Polk[24] showed that this model adequately described the rdf of Moss and Graczyk.[107] The CRN model has been extended many times,[108-112] including a-Si:H for which Weaire et al.[113] built the first model using the CRN concept. In any case, the essential points as stated above remain the same. After considerable study using a variety of techniques including theoretical modeling, x-ray, electron, and neutron diffraction, extended x-ray absorption fine structure (EXAFS), Raman scattering, and even ^{29}Si NMR, the CRN model is accepted as the basic starting point for modeling results of structural studies of a-Si:H.[106] From the width of the first peak in the rdf the first-neighbor separations are

found to be nearly constant (to perhaps ±0.02A), whereas the bond angles vary ~±5%.[106] The obvious, essential information left to be characterized is to what extent, and how, the actual structure deviates from the classical CRN model.

2. Characterization of a-Si

To start, we must understand how a-Si (or a-Ge) deviates from the pure CRN. A-Si has poor photovoltaic properties irrespective of preparation or annealing. The cause is the large density of defect states in the gap. Electron spin resonance (ESR) provides the most direct measure of these states, by measuring directly the dangling bond density. This inference may be misleading, however, since a variety of techniques[114,115] has shown that the total number of dangling bonds is many times smaller than the estimated number of unsaturated silicons residing on the surfaces of voids. This fact has prompted the assertion that most of the unsaturated silicon reconstructs,[116] similar to the well-known reconstruction of clean Si surfaces.[117] The current belief is that dangling bonds provide "deep" states or levels in the gap, whereas the reconstructed, or weak, Si-Si bonds also contribute to the gap state density.[53,100,116]

To give an explicit example, Phillips[116] conjectured that flat surfaces in voids of a-Si appear as Si(111) surfaces, and labeled these sites as T_3^0. The edges of the voids

where the Si(111) surfaces meet are described as appearing as a line of Si(100) sites, labeled T_2^0. The reconstruction then is conjectured to occur for both surfaces. The (111) surface reconstructs through a (2x1) reconstruction, giving:

$$2\ T_3^0 \rightarrow T_3^+ + T_3^-$$

having no sites observable by ESR. The (100) edge dimerizes giving one lone electron per the orginal T_2^0 site. I note here an interesting observation from this work. Phillips points out that ~3 at% of hydrogen would be necessary to passivate all defect sites in a-Si (i.e., all T_3 and T_2 sites).[116] This value stands out because results of NMR studies indicate that an ~3 at% hydrogen concentration is associated with a particular H environment in all a-Si:H's.[26] The reason for this particular H concentration in a-Si:H is not understood. A reasonable question is whether the 3 at% inferred from NMR is related to the intrinsic number of defects originally in a-Si, whereas other features of the NMR studies would pertain to H-created defects? This point will be discussed in more detail in Section II.C.1.

An important role of hydrogen in producing a good photovoltaic material is then seen to consist of more than just passivating dangling bonds, but also of passivating the weak reconstructed bonds in the original a-Si network. This result resolves some of the uncertainty of why so much more

hydrogen is necessary to produce a good a-Si:H film than would appear to be needed just from the a-Si dangling bond densities. It also introduces the important question of how much reconstruction, believed to exist at some concentration,[54] is left in a hydrogenated film. Optically induced ESR studies provide evidence that in good a-Si:H films having $\sim 10^{15}$ dangling bonds, there also exists $\sim 10^{17}$ weak bonds.[47]

3. Characterization of a-Si:H

Phillips has explained why a-Si materials have never achieved good photovoltaic properties.[56] The foundation of his arguments resides in the postulate that any amorphous material with an average coordination number, N_c, greater than $6^{1/2}$ (derived from the number of degrees of freedom available to the material) cannot be constructed strain-free. Moreover, this postulate takes into account the realities of thin film growth, and specifically a-Si:H growth,[57] whereas computer[108-110] and stick-and-ball[24,113] models do not. It is well known that thin film growth starts from nucleation centers, from which further growth creates "islands."[118] The essential factor, then, in producing a void-free thin film material depends on whether or not the islands can coalesce.[48,57] When $N_c > 6^{1/2}$, Phillips argues that the strain energy is too high for islands to coalescence void-

free.[56,57] Hydrogen, in this respect, plays the important role of lowering the coordination number of a-Si:H to a region in which relatively strain-free lattices can be constructed.

In this context, it appeared possible that given the correct H concentration and deposition conditions, a strain-free, void-free film could be produced. Early work did in fact appear stating that films displayed no heterogeneity under transmission electron microscopy (TEM).[119] Since then, a number of studies have shown that at least some films have void and grain structure. Electron microscopy work[120,121] gives perhaps the clearest indication of inhomogeneities. Poor quality (high dangling bond density) films showed columnar structure having diameters of ~100A with clear interstitial, or tissue, regions.

Even so, it was believed that good films still possessed no heterogeneity. The electron micrographs showed no features indicating heterogeneity for the good films.[120,121] Studies utilizing IR[122-124] and hydrogen evolution[125-128] appeared to suggest, when combined with the electron microscopy studies, that the good films were compositionally homogeneous in hydrogen. In the IR studies, this inference resulted from the observation that good films have only absorption from ≡SiH bonding, whereas poor films display $=SiH_2$, $-SiH_3$, and the polymeric $(SiH_2)_n$ structures.[122-124]

In the hydrogen evolution studies, poor materials showed a low temperature evolution peak at ~350^{o}C in addition to the evolution at higher temperatures seen in good materials.[125-128] In addition, neutron scattering[129,130] correlated fairly well with the electron microscopy, showing strong anisotropic scattering, indicating rod-like structures ~60A in diameter, in the materials where the electron microscopy showed clear microstructure.[120,121] These studies showed no evidence of structural inhomogeneities in good (low dangling bond density) materials. Barna et al.[119] and Graczyk,[131] using electron diffraction, also concluded that good materials showed no obvious deviations from the CRN model. Graczyk suggested that the poor materials might have two phase compositional inhomogenities.[131] Small angle x-ray scattering (SAXS) studies[129,132] led to similar conclusions. Here, poor materials showed indications of voids, which D'Antonio and Konnert[132] suggested were predominantly <10A in diameter, whereas the good films showed almost no scattering intensity.

It might seem, then, that good a-Si:H films have no structural or chemical heterogeneity. More recent studies, however, have supplied strong evidence that good films are not homogeneous. Some sputtered films Postol et al.[130] studied using neutron diffraction were nominally good films, and intense scattering at small angles was observed. More

recently, Bellissent et al.,[133,134] also studying sputtered films using small angle neutron scattering (SANS), have confirmed Postol et al.'s observations, and suggested a correlation distance of ~30A and radius of gyration of 125A. This result implies that voids are far from spherical in shape. Complimentary results were found by Bouldin et al.[135] using extended x-ray absorption fine structure (EXAFS) to study a-Ge:H films. They also concluded that voids exist which have one dimension ~30A and another >100A. But with respect to the compositional structure of hydrogen, NMR has had the greatest impact. Since the first study of Reimer et al.,[27] proton NMR has clearly shown compositional heterogeneity in the proton distributions in all a-Si:H films.[26] NMR studies will be reviewed in section II.C, but this initial work[27] concurred with, and gave impetus to a picture of a-Si:H films in which heterogeneity plays a most important role in determining the properties of films of device grade quality.[47,48,106]

A leading picture, already alluded to, used to describe this heterogeneous structure of a-Si:H is the island-tissue model.[47,48,54,57] Here the film is pictured as growing from each nucleation center, and forming columns, or islands, of relatively defect-free a-Si:H. The islands are connected by the tissue region, a region of much lower density having a high concentration of defects. This model of the film has

been used to explain anomalies in conductivity and thermopower versus temperature measurements.[48] It also seems in reasonable agreement with the known dependence of film quality on deposition parameters. A few of these parameters can, in a simplified manner, be described as follows:

i) slow deposition rates produce better films,

ii) substrate temperatures ranging from T_s = ~200-400^{0}C make better films, relative to T_s at other temperatures, and

iii) high silane concentrations make better films.

This island-tissue model can be used to describe many experimental results.[48] An example is the two peaks observed in annealing studies, which appear to be correlated with hydrogen evolving at lower temperatures from the tissue regions, and from the islands at the higher temperature evolution peak. But caution must adhered to when applying this model. For example, IR studies show that there is no direct correlation of the annealing peaks to mono- or dihydride silicon.[136,137]

In conclusion, the importance of structural defects to the electronic properties of a-Si:H has been emphasized in this brief review. Atomic scale defects occur not only from dangling bond sites in the amorphous matrix, but also from Si-Si reconstruction of surfaces within the bulk material. Larger scale defects definitely occur in poor materials as

voids and grains, islands and tissue. An important goal of this work is to better define and characterize these defects and heterogeneities in both poor and good quality films.

B. Nuclear Magnetic Resonance; Theory

The technique of nuclear magnetic resonance (NMR) entails studying the resonant interaction of radiation with a nucleus' (in this work, a proton's) magnetic moment, $\vec{\mu}$, described by

$$\vec{\mu} = \gamma \hbar \vec{I} \tag{1}$$

where $\hbar\vec{I}$ is the nuclear spin angular momentum, and γ is the magnetogyric ratio. The study of NMR dates back to the classic work of Purcell, Torrey, and Pound at Harvard,[138] and independently to Bloch, Hansen and Packard at Stanford[139,140] in the mid-1940s. Since then, NMR has enjoyed enormous utility, especially for the structural elucidation of organic compounds. The technique has also had considerable success in the study of solids, with recent interest promoted by the combined use of Fourier Transform (FT) techniques with dedicated laboratory computers.

Excellent texts therefore exist detailing the theory and techniques of NMR. Abragam's classic text[4] still sets the standard for the theory of relaxation and line shapes.

Several texts also provide excellent introductions to NMR and its application to solids.[141-144] The monographs of Haeberlen[145] and Mehring[146] provide reviews and details of modern NMR techniques applied to solids. Gerstein and Dybowski[147] furnish a more introductory level, and more readable, discussion of multiple-pulse techniques than given in Haeberlen or Mehring. Bax[148] details the use of two-dimensional techniques applied to liquids and solids. Many other excellent texts exist discussing NMR, but those mentioned above provided the basis for the brief review given here.

Nuclear interactions in light, non-quadrupolar nuclei are in general very weak, having energies of < 1K, and detection of these interactions by direct resonance methods becomes possible only when the nuclei are bathed in a strong static magnetic field. The interaction of the nuclear magnetic moment with the static field, $\vec{B}_0$, is represented by the Zeeman Hamiltonian:

$$H_z = -\vec{\mu}.\vec{B}_0 \equiv -\gamma\hbar B_0 I_z \qquad (2)$$

when the z axis is defined parallel to the static field direction. Resonance then occurs for the allowed single quantum transitions of $\Delta I_z = \pm 1$ when an electromagnetic field perpendicular to the z-axis is applied to the spin system with an energy

$$\Delta E = \hbar\omega_o = \gamma\hbar B_o \tag{3}$$

The description of a system of N spins-1/2 at equilibrium in a static field $\vec{B}_o$ is given by classical statistics

$$\frac{N_\alpha}{N_\beta} = e^{\gamma\hbar B_o/kT} \sim 1 + \frac{\gamma\hbar B_o}{kT} \tag{4}$$

α denoting I_z=1/2, β I_z=-1/2. Equation (4) leads directly to Curie's law for the macroscopic magnetization

$$\vec{M} = N\vec{B}_o \frac{\gamma^2\hbar^2 I(I+1)}{3kT} \tag{5}$$

Bloch et al. first demonstrated that in many cases simple first-order kinetics could be used to describe the time dependence of $\vec{M}$ interacting with a magnetic field, $\vec{B}$:[139,140]

$$\frac{d\vec{M}}{dt} = \gamma\vec{M} \times \vec{B} - \frac{M_x\vec{i} + M_y\vec{j}}{T_2} - \frac{M_z - M_o}{T_1}\vec{z} \tag{6}$$

This equation phenomenologically describes the relaxation of the macroscopic magnetization described by equation (5) back to equilibrium after a disturbance. In general, relaxation of $\vec{M}$ perpendicular to the magnetic field, called the transverse or spin-spin relaxation rate, T_2^{-1}, depends on any interaction with other magnetic fields. The relaxation

of $\vec{M}$ parallel to $\vec{B}$, called the longitudinal or spin-lattice relaxation rate, T_1^{-1}, can occur only from interactions with magnetic fields perpendicular to $\vec{B}$. Moreover, T_1 processes require an energy transfer between the spin system and the lattice. This process requires a resonant transition of $\Delta I_z = \pm 1, \pm 2, \ldots$. T_1 therefore depends intimately on motions having frequency components at $\omega = \gamma B$. T_2, on the other hand, can have significant contributions from variations in local fields in the z direction, as well as from resonant transitions.

In general, the evolution of the spin system can be described in the following way. The time-dependent wavefunction of the system, $\psi(t)$, can be formed from a linear combination of basis states which form a complete set:

$$\psi(t) = \sum_i c_i(t)\, \phi_i \tag{7}$$

The density matrix is defined as

$$\rho_{ij}(t) = \overline{c_i(t)\, c_j^*(t)} \tag{8}$$

where the bar implies an ensemble average. The value of any observable A is then

$$\langle A \rangle = \mathrm{tr}\, \{\rho A\} \tag{9}$$

In equation (8), it is important to note that the diagonal density matrix elements, ρ_{ii}, equal the probability of finding the system in the i^{th} basis state. The diagonal elements then provide the relative populations of the basis states. Off-diagonal elements describe the "coherence" of the |i-j| quantum order.

From the Liouville-von Neumann equation, the time dependence of the density operator follows

$$i\hbar \frac{d\rho}{dt} = [H,\rho] \tag{10}$$

where H is the total Hamiltonian of the system. A solution of equation (10) is found to be[147]

$$\rho(t) = U(t)\ \rho(0)\ U^{-1}(t) \tag{11}$$

where U(t) is a unitary operator. The evaluation of equation (11) then describes the system at any time, and equation (9) can be used to calculate an observable. Obviously, if the Hamiltonian, H, is time-independent

$$U(t) = \exp(-iHt/\hbar) \tag{12}$$

For a system starting at equilibrium, the density operator for all temperatures above ~2K can be evaluated using using the expansion ($\omega_0=\gamma B_0$)

$$\rho(0) = \frac{\exp[-(\gamma\hbar B_0 I_z)/kT]}{Z} \propto 1 - \hbar\omega_0 I_z/kT \tag{13}$$

Thus, in many cases, $\rho(0) \propto I_z$ will be a sufficient starting point for calculating observables in equations (9) and (11).

The useful information obtained from NMR comes from the perturbations on the Zeeman interaction. These perturbations are the chemical shift, H_{cs}, scalar coupling, H_J, spin-rotation, H_{sr}, homonuclear, H_D^{II}, and heteronuclear dipole-dipole, H_D^{IS}, and quadrupole, H_Q, interactions. The total Hamiltonian is

$$H = H_{ext} + H_{int} \tag{14}$$

where

$$H_{ext} = H_{rf} + H_z \tag{15}$$

and

$$H_{int} = H_{cs} + H_J + H_{sr} + H_D^{II} + H_D^{IS} + H_Q + H_L \tag{16}$$

H_{rf} represents the interaction of the rf pulses, and H_L the Hamiltonian containing the other degrees of freedom in the system, jointly called the "lattice". The internal Hamiltonians are

$$H_{cs} = \gamma \vec{I} . \overleftrightarrow{\sigma} . \vec{B}_o \tag{17}$$

$$H_J = \sum_{i \neq j} \vec{I}_i . \overleftrightarrow{J} . \vec{I}_j \tag{18}$$

$$H_{sr} = \Sigma \vec{I}_i . \overleftrightarrow{C} . \vec{J} \qquad (19)$$

$$H_D^{II} = \sum_{i<j} \frac{\hbar \gamma_i \gamma_j}{r_{ij}^3} \left[\vec{I}_i . \vec{I}_j - \frac{3(\vec{I}_i . \vec{r}_{ij})(\vec{I}_j . \vec{r}_{ij})}{r_{ij}^2} \right] \qquad (20)$$

$$H_Q = \frac{eQ}{2I(2I-1)\hbar} \vec{I} . \overleftrightarrow{V} . \vec{I} \qquad (21)$$

In equation (19), $\vec{J}$ is the molecular rotational angular momentum. $\vec{r}_{ij}$ is the vector connecting spin i to spin j, and eQ is the electric quadrupole moment. H_D^{IS} is identical to H_D^{II} except for replacing $\vec{I}_j$ with $\vec{S}_j$ in equation (19). The symbols $\overleftrightarrow{A}$ in equations (16), (17), (18), and (20) represent second rank tensors. Rapid isotropic tumbling at a rate much faster than an interaction strength will average the second rank interaction into its isotropic value: $A = tr\{A_{\alpha\beta}\}/3$. This is in general the case for all interactions in a liquid or gas, and leads to the more familiar chemical shift Hamiltonian

$$H_{cs} = \gamma \hbar \sigma \vec{I} . \vec{B} \qquad (22)$$

where σ is the isotropic chemical shift observed in liquid-state NMR. If motions are not rapid enough to fully average the tensor interactions, then in general five quantities must be known in order to completely determine a symmetric tensor.

The dipole-dipole interaction is of special interest to this work. The dipolar Hamiltonian, equation (20), can reexpressed as[149]

$$H_D = \hbar\gamma^2 \Sigma(A + B + C + D + E + F)/r^3 \quad (23)$$

where $$A = I_z I'_z (1-3\cos^2\Theta) \quad (24)$$

$$B = -1/4 (1-3\cos^2\Theta) (I_+ I'_- + I_- I'_+) \quad (25)$$

$$C = -3/2 \sin\Theta\cos\Theta e^{-i\phi} (I_z I'_+ + I_+ I'_z) \quad (26)$$

$$D = -3/2 \sin\Theta\cos\Theta e^{i\phi} (I_z I'_- + I_- I'_z) \quad (27)$$

$$E = -3/4 \sin^2\Theta e^{-i2\phi} I_+ I'_+ \quad (28)$$

$$F = -3/4 \sin^2\Theta e^{i2\phi} I_- I'_- \quad (29)$$

Of special interest in the dipolar Hamiltonian is the B term, equation (25). This term expresses the mutual interaction of two nucleus' transverse component of spin, and allows for an exchange of magnetization with no net change in energy of the spin system. The B term represents processes of mutual spin "flip-flops" which gives rise to the phenomenon of spin diffusion.

It will always be true for this work that the Zeeman interaction >> other interactions. It is then convenient to transform into the interaction frame of the Zeeman Hamiltonian, called the "rotating frame". To first order in

perturbation theory, only interactions commuting with H_z, called the "secular" terms, will be significant in equation (9), and therefore

$$\tilde{\rho}(t) = e^{-iH_z t} \rho(t) e^{iH_z t} \tag{30}$$

Inserting equation (30) into (9) gives

$$i\hbar \frac{d\tilde{\rho}(t)}{dt} = [\tilde{H}, \tilde{\rho}(t)] \tag{31}$$

where

$$\tilde{H} = e^{iH_z t} H e^{-iH_z t} \tag{32}$$

An rf-pulse $H_{rf} = -2\hbar\omega_1 I_y \cos\omega_0 t$ where $\omega_1 = \gamma B_1$ has a secular term of just $H_1 = -\hbar\omega_1 I_y$. A resonant rf pulse phased along the y-axis in the rotating frame then changes $\rho(0) \propto I_z$ into

$$\rho(t) = e^{-i\hbar\omega_1 I_y t} I_z e^{i\hbar\omega_1 I_y t} = I_z \cos\omega_1 t - I_x \sin\omega_1 t \tag{33}$$

A 90_y pulse then is defined for $\omega_1 t = \pi/2$, and $\tilde{\rho}(t)$ immediately after the pulse will be $\tilde{\rho}(0)_+ \propto -I_x$. Most calculations and descriptions will be made with reference to the rotating frame (as opposed to the lab frame). The $\tilde{}$ will therefore be omitted where a discussion in the rotating frame is obvious.

1. Line shapes

Although the formalism expressed above in equations (9) and (11) is useful for many calculations, certain advantages exist in using the method of moments.[4,150] The main advantages of the moments method is that the calculations start from first principles, and exact solutions in many cases can be derived without a knowledge of the eigenfunctions of the system. Abragam details the moments method in Chap. IV of his monograph,[4] and only a brief outline based on his discussion will be presented here.

The n^{th} moment of a resonance curve is defined as

$$M_n = \int_{-\infty}^{\infty} (\omega - \omega_0)^n f(\omega)\, d\omega \qquad (34)$$

where $f(\omega)$ is the line shape function of the resonance curve. Since the Fourier transform of the time evolution of the magnetization gives $f(\omega)$, it is apparent that the moments are even terms in the expansion of the system's time evolution ($g(t) = \int e^{i\omega t} f(\omega) d\omega$).

Two basic line shape functions will be used here. The first is the Gaussian distribution

$$g(\omega) = \frac{1}{\Delta \sqrt{2\pi}} \exp\left[\frac{-(\omega-\omega_0)^2}{2\Delta^2}\right] \qquad (35)$$

For this shape function, $M_2^g = \Delta^2$, $M_4^g = 3\Delta^4$ so that $M_4^g/(M_2^g)^2 = 3$. The full-width at half-maximum (FWHM $\equiv 2\delta$) is easily found to be $2\delta = \Delta \sqrt{(8 \ln 2)}$.

The second line shape function is the Lorentzian function

$$L(\omega) = \frac{\delta}{\pi} \frac{1}{\delta^2 + (\omega - \omega_o)^2} \qquad (36)$$

This function leads to an infinite second moment; it must be cut off in the wings for the integrals in equation (34) to converge. In general the calculated $M_4^L/(M_2^L)^2$ for a Lorentzian line is much larger than three, whereas a Gaussian line will have $M_4^g/(M_2^g)^2 \sim 3$.

The method of moments takes into account the fact that the spin system may be strongly coupled through the dipolar Hamiltonian. Van Vleck calculated moments[150] for a spin system experiencing a static dipolar interaction. The calculation proceeds from equation (11). In the rotating frame, the signal observed is proportional to $\langle I_x \rangle$, and $\rho(0)_+$ following a $90^o{}_y$ pulse will be proportional to I_x. Therefore

$$M_x = \langle I_x(t) \rangle = tr\{ e^{iH_1 t} I_x e^{-iH_1 t} I_x \} \qquad (37)$$

where H_1 is the perturbation Hamiltonian. Expanding the exponentials in equation (37) leads to

$$\frac{d^n \langle I_x(t) \rangle}{d^n t} = (i)^n tr\{[H_1,[H_1,[\ldots[H_1,I_x]\ldots]]_n I_x\} \qquad (38)$$

From the expansion of the time evolution's Fourier transform, it is apparent that

$$M_{2n} = (-1)^n \left. \frac{d^{2n}\langle I_x(t)\rangle}{dt^{2n}} \right|_{t=0} \div \langle I_x(0)\rangle \qquad (39)$$

Now it can be seen from equations (38) and (39) that[4]

$$M_2 = - \frac{tr\{[H_1, I_x]^2\}}{tr\{I_x^2\}} \qquad (40)$$

$$M_4 = - \frac{tr\{[H_1, [H_1, I_x]]^2\}}{tr\{I_x^2\}} \qquad (41)$$

For a static homonuclear dipole-dipole interaction, $H_1 = H_D^{II} = \hbar\gamma^2\Sigma(A+B)/r^3$, equation (40) gives the Van Vleck formula[150]

$$M_2 = \frac{3}{4}\gamma^4\hbar^2 I(I+1) \sum_j \frac{(1-\cos^2\Theta_{ij})^2}{r_{ij}^6} \qquad (42)$$

where $\vec{r}_{ij}$ is the vector from spin i to spin j, and Θ_{ij} is the angle between $\vec{r}_{ij}$ and $\vec{B}_0$. In general, line shapes dominated by static H_D^{II} interactions are close to Gaussian. In powders, the angle Θ_{ij} is averaged, and since

$$\Sigma \rightarrow \frac{I}{2\pi} \int_0^I$$

$$\sum_j (1-\cos^2\Theta_{ij})^2 = \frac{\pi}{2\pi} \int_0^\pi (1-\cos^2\Theta_{ij})^2 \sin\Theta d\Theta = \frac{4}{5} \qquad (43)$$

For a cubic lattice of lattice spacing d, $\sum_j r_{ij}^{-6} = 8.5d^{-6}$. The Van Vleck formula (42) then becomes

$$M_2 = 5.1\gamma^4\hbar^2 I(I+1)d^{-6} \tag{44}$$

There are two cases wherein H_D^{II} can give a line shape more approximately Lorentzian than Gaussian.[4] The first of these is the dilute spin case. Here, a regular lattice is randomly filled with protons, but only for less than one percent of the total number of sites. A Lorentzian line shape results primarily from intensity in the wings coming from the small number of protons which are in adjacent lattice sites. A Lorentzian line shape can be derived more generally, but only with an important assumption. If the B term of H_D^{II}, equation (25), becomes nonsecular, a Lorentzian line shape will be obtained.[4] The B term becomes nonsecular when one spin has a large frequency shift from its nearest neighbor, i.e., the interaction effectively becomes heteronuclear. When this happens, mutual spin flips require an energy transfer from the lattice, and B no longer commutes with H_z. For this case, Abragam finds[4]

$$\delta \sim 3.8\gamma^2\hbar\eta \tag{45}$$

where η is the density of protons, and δ is defined in equation (36). In terms of T_2, equation (45) is found to be

$$T_2 = 2.65\times10^{17}/\eta \qquad (\eta \text{ in } cm^{-3},\ T_2 \text{ in sec})$$

or

$$FWHM = \eta/8.3\times10^{17} \qquad (\eta \text{ in } cm^{-3},\ FWHM \text{ in Hz}) \tag{46}$$

2. The Carr-Purcell-Meiboom-Gill sequence

A sequence of great importantance in this thesis is the Carr-Purcell-Meiboom-Gill (CPMG) sequence.[151] A schematic representation of the sequence is shown in Figure 1a. This sequence is useful because it refocuses interactions linear in I_z, and can therefore give information about the scalar coupling and/or homonuclear dipole-dipole interactions (both bilinear in $\vec{I}$) which might otherwise be obscured.

The first two pulses in the CPMG sequence can be dated back to Hahn,[152] and will be called here the Hahn echo sequence, 90_x-τ-180_y-τ-echo. The echoing of interactions linear in I_z can be understood vectorally, as shown in Figure 1b. Two spin isochromats having different shifts (chemical shift, field inhomogeneity, Knight shift, or in the case of two isolated spins, heteronuclear dipolar) are shown in the rotating frame. After the time τ, the isochromats have rotated by $\Theta_i = \Delta\omega_i\tau$ away from the y-axis in the x-y plane. The 180_y pulse inverts Θ_i, but not the direction of the offset $\Delta\omega_i$. After another interval τ, the isochomat returns to the y-axis with $\Theta_i = 0$, giving an echo in the time decay. The next 180_y pulse simply repeats the process.

Figure 1. The Hahn echo

a) Schematic of the CPMG sequence. 2τ equals the cycle time, t_c, the dotted line depicts the magnetization echo.

b) Vector diagram of the Hahn echo. The long, darkened arrow implies one isochromat of an inhomogeneously broadened magnetization vector.

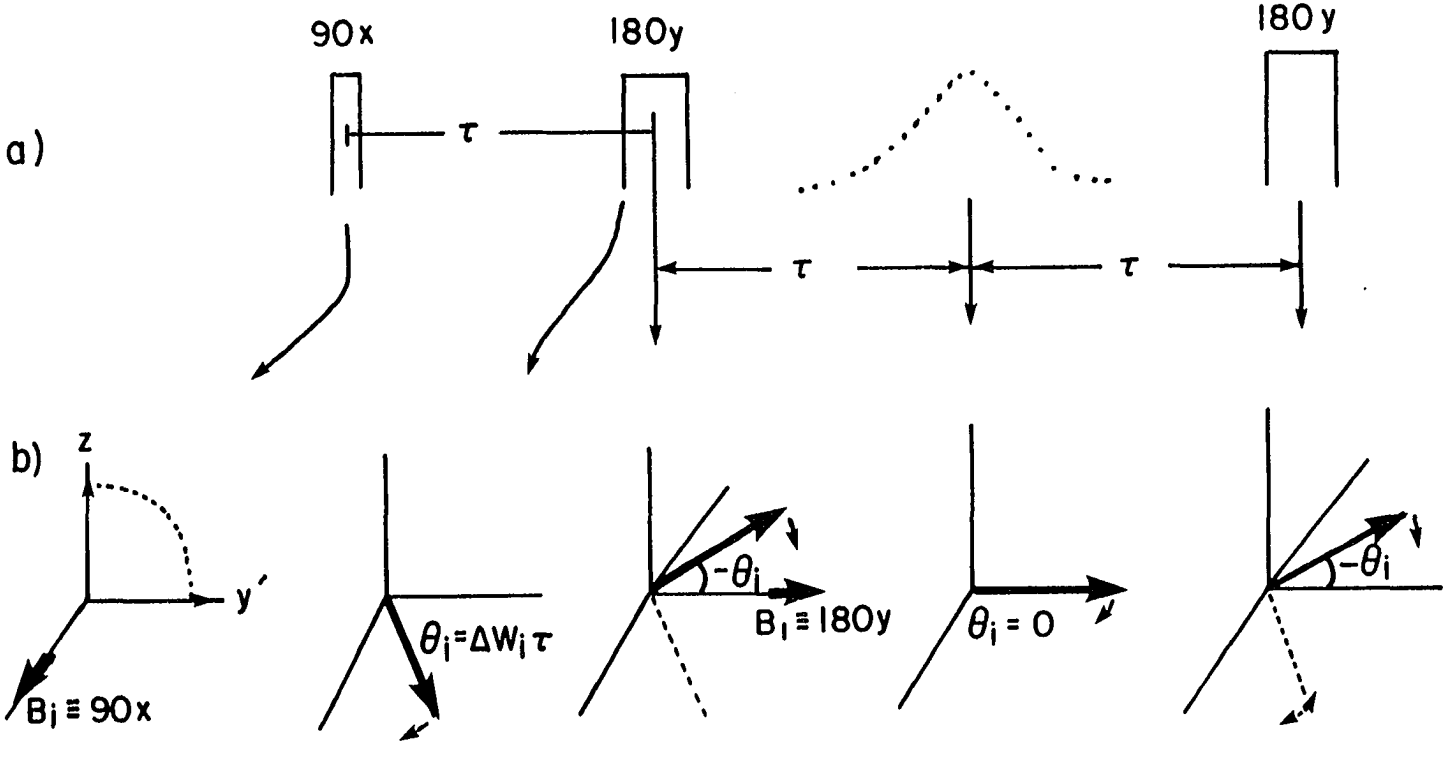
a)
90x
180y
180 y
τ
τ
τ
b)
z
y'
$B_i \equiv 90x$
$\theta_i = \Delta W_i \tau$
$-\theta_i$
$B_i \equiv 180y$
$\theta_i = 0$
$-\theta_i$

Carr and Purcell extended Hahn's original two pulse sequence to 90_x-τ-$(180_x$-2τ-$)_n$.[153] The problem with the Carr-Purcell sequence is that any small error in the 180_x pulse width will add up for each additional pulse. Meiboom and Gill[151] realized that a sequence with 180_y pulses instead of the 180_x pulses would cancel pulse width errors in the 180^0 pulse width setting. Again, this can easily be visualized using a vector picture. Suppose the 180_y pulse is actually set to 179^0. The first 179_y pulse will rotate an isochromat at Θ_i to $-\Theta_i$, but the isochromat will also end up 1^0 above the x-y plane. After 2τ, the isochromat returns to $+\Theta_i$, but is still 1^0 above the x-y plane. The next 179_y pulse then rotates the isochromat back into the x-y plane. (Farrar and Becker[142] have excellent illustrations of this effect.) Thus, under a CPMG experiment, only the even echoes will be used.

Later on, I will use the CPMG experiment to obtain an upper limit on the strength of "echoing" protons' homonuclear dipolar interaction. It is important therefore to determine how well the CPMG sequence cancels different pulse errors, and what the effect of these errors is on the dipolar Hamiltonian.

Since the sequence 90_x-τ-180_y-2τ-180_y-τ is periodic and cyclic (defined below), average Hamiltonian theory[145-147] can be used to express the time development of the echo peaks, at

integer multiples of 4τ. Average Hamiltonian theory is based on the pulse sequence being cyclic

$$U_{rf} = T \exp[-i\int_0^{t_c} H_{rf}(t)dt] = 1 \qquad (47)$$

where T is the Dyson time-ordering operator, and on the sequence being periodic

$$H_{rf}(t+t_c) = H_{rf}(t) \qquad (48)$$

where t_c is the cycle time, which for the CPMG sequence is 4τ. For the CPMG sequence, the first order term is

$$\int_0^{t_c} H_{rf}(t)dt = \pi(I_y+I_y)$$

and all higher order terms vanish, since they all involve commutators of I_y with itself. Thus, the sequence is cyclic, $U_{rf}(t_c)=1$, and it is obviously periodic. The calculation of the time development is then performed by transforming to the interaction frame of the Hamiltonian of interest;

$$\rho(t) = U_{rf}\tilde{\rho}U_{rf}^{+} = U_{rf}U_{int}\tilde{\tilde{\rho}}U_{int}^{+}U_{rf}^{+} \qquad (49)$$

If only times $t=nt_c$ are used, where n=integer, then $U_{rf}=1$. For these times,

$$U_{int}(t_c,0) = \exp\{-it_c[\bar{H}_{int}^{(0)} + \bar{H}_{int}^{(1)} + \ldots]\} \qquad (50)$$

where the Magnus expansion[147] was used as the solution to the Liouville equation for U_{int};

$$i \frac{dU_{int}}{dt} = \tilde{H}_{int} U_{int} \tag{51}$$

and

$$\tilde{H}_{int}(t) = U_{rf}^{+} H_{int} U_{rf} \tag{52}$$

Convergence of the Magnus expansion requires $t_c |H_{int}^{hom}| \ll 1$, where H_{int}^{hom} denotes all homogeneous, plus lifetime, interactions. This criterion is obvious in the CPMG sequence, since if the cycle time is not much smaller than the T_2 of the dipolar interaction, no coherence will be left after a few cycles.

The zeroth and first order terms in the Magnus expansion are calculated as[145-147,154]

$$\bar{H}_{int}^{(0)} = -\frac{1}{t_c} \int_0^{t_c} \tilde{H}_{int}(t) dt \tag{53}$$

$$\bar{H}_{int}^{(1)} = -\frac{i}{2t_c} \int_0^{t_c} dt' \left[\tilde{H}_{int}(t'), \int_0^{t'} dt'' \tilde{H}_{int}(t'')\right] \tag{54}$$

From equation (50), the effective Hamiltonian at the cycle times nt_c is

$$\bar{H}_{int} = \bar{H}_{int}^{(0)} + \bar{H}_{int}^{(1)} + \ldots \tag{55}$$

Following the techniques clearly discussed in Gerstein and Dybowski,[147] the terms of the internal average Hamiltonian in equation (55) can be derived. For an internal Hamiltonian

$$H_{int} = H_o + H_D^{II} \tag{56}$$

where H_o is the sum of all interactions linear in I_z, the following average Hamiltonians are found:

$$\bar{H}_o^{(i)} = 0 \qquad \text{for all } i \tag{57}$$

$$\bar{H}_{ok}^{(1)} = 0 \qquad k = \delta,\varepsilon,P,T \tag{58}$$

$\bar{H}_{ok}^{(1)}$ represents the first-order cross terms between the offset Hamiltonian and the error Hamiltonians for pulse width error, $k=\delta$, B_1 inhomogeneity, $k=\varepsilon$, phase misadjustment, $k=P$, and phase transients, $k=T$.[154] The results in (57) and (58) demonstrate that the CPMG sequence does a very effective job of echoing, or averaging to zero, offset Hamiltonians, and also canceling experimental errors which might affect this averaging.

There are, however, some undesirable sources of error displayed even in zero-order. Taking proper account of finite pulse widths,[147] t_w (=2-3μs for a typical experiment), the following terms can be derived:

$$\bar{H}_\delta^{(0)} = -2\,\frac{\delta_y}{t_c}\,I_y \tag{59}$$

$$\bar{H}_\varepsilon^{(0)} = \frac{2}{t_c}\sum_i \varepsilon_i I_{yi} \tag{60}$$

$$\bar{H}_P^{(0)} = 0 \tag{61}$$

$$\bar{H}_D^{(0)} = H_D^{II} + \frac{3t_w}{t_c}(I_{zi}I_{zj} - I_{xi}I_{xj}) \tag{62}$$

where the Hamiltonians show only spin terms (spatial terms remain unaffected). Equation (62) shows that dipolar information may be affected by finite pulse widths ($3t_w/t_c \sim$ .04-.01 is typical in this work). These errors, however, will appear to make the CPMG decay faster than if H_D^{II} was the only interaction term in equation (62). Experimentally, the error terms can be investigated by using model compounds, and studies of this kind are under way in our group. (Experimental details of the CPMG sequence are discussed in the next section.) But, in general, error contributions will make the dipolar interaction appear to be stronger than it truly is. I will, therefore, use the CPMG sequence to obtain only an upper limit on the strength of H_D^{II}, which then gives a lower limit on distances obtained from H_D^{II}. Useful information pertaining to void sizes in the a-Si:H will be obtained in this manner, as discussed later in this work.

C. NMR Studies of a-Si:H

Since Reimer et al. first published proton NMR results[27] on a-Si:H, NMR has provided useful, and sometimes

controversial interpretations about the material (see Refs. 26, 29 and 106). The bulk of the proton NMR work has been done at Caltech by Reimer, Vaughan, and Knights,[27,35,155-160] at the Naval Research Labs by Carlos and Taylor,[33,161-164] at the Ames Laboratory by Lowry, Jeffrey, Barnes and co-workers,[34,36,165-167] and at Washington University by Norberg, Fedders and coworkers.[32,168-171] The NMR results have followed two basic directions. The first area has involved the study of the proton line shape, obtained through the Fourier transform of the proton free-induction decay (FID), and the interpretation of this line shape to proton morphology and film quality. The second direction of NMR work has been the study of the proton spin-lattice relaxation, T_1^{-1}, and the investigation of the origins of its behavior.

1. Line shape analysis

Perhaps the most intriguing results obtained from the proton NMR of a-Si:H come from the similarities of the proton line shape seen regardless of sample preparation, including samples prepared by glow-discharge or by rf-sputtering.[26,106]

A typical line shape, measured during the course of this work on VAN150 at 220MHz, is shown in Figure 2. This figure includes the usual fit (using PEAK15, see section III.C) comprised of a superposition of a broad Gaussian line on a

Figure 2. Fourier transform of a FID of VAN150 at 220MHz. The crosses are the raw data, the broad Gaussian peak has FWHM = 34 kHz and the narrower Lorenztian has FWHM = 5.0 kHz; the relative intensities are 51% for the Gaussian, 49% for the Lorenztian (corrected gives 44 and 56%, respectively).

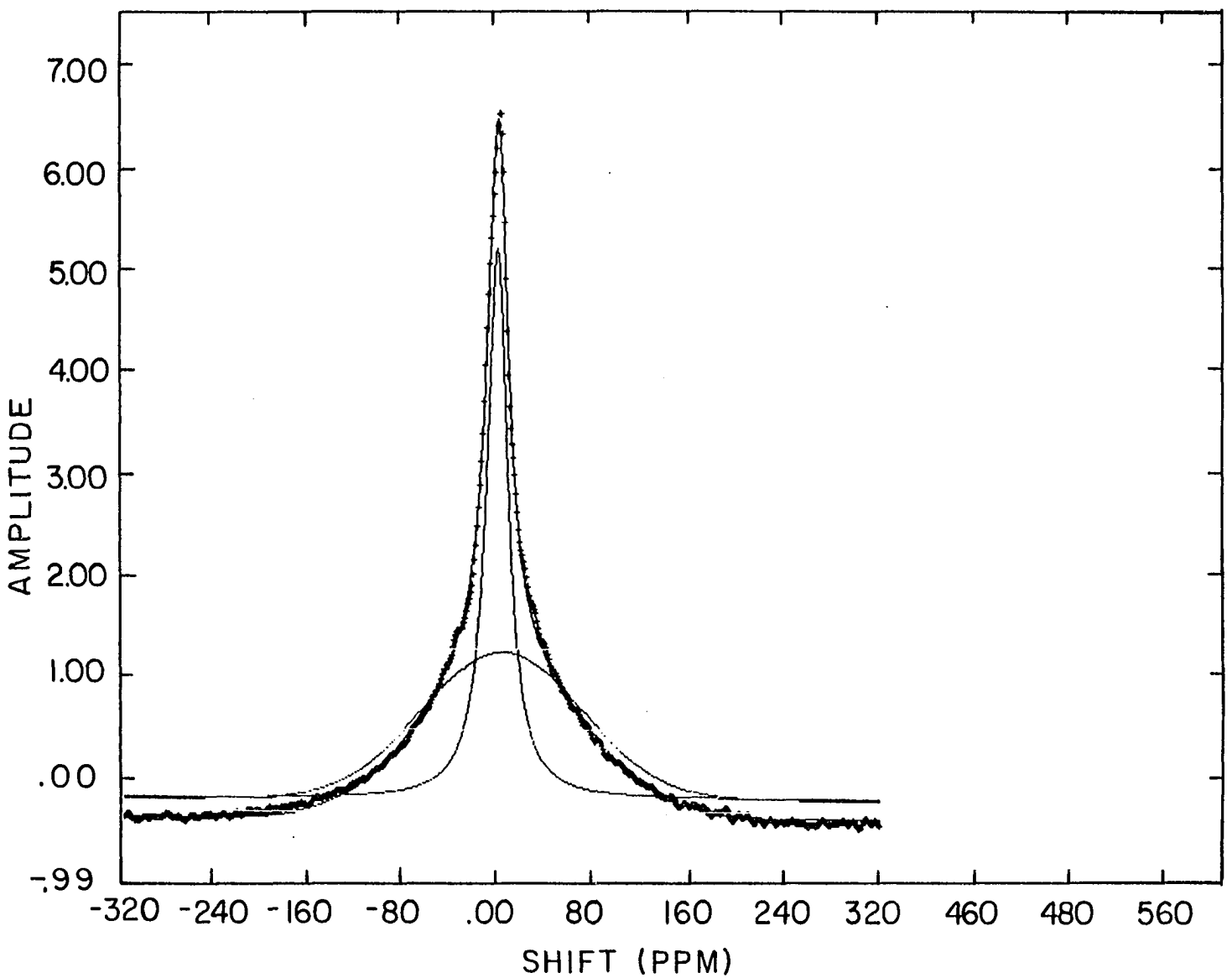
7.00
6.00
5.00
4.00
3.00
2.00
1.00
.00
-.99
AMPLITUDE
-320 -240 -160 -80 .00 80 160 240 320 460 480 560
SHIFT (PPM)

narrower Lorentzian line. These two line shapes are reported in the literature,[27,33,155,157,165,166] with the full-width-at-half-maximum (FWHM) in all samples equaling 25±4 kHz for the broad Gaussian line, and 3.5±0.5 kHz for the narrower Lorentzian line. Moreover, in all unannealed samples having proton concentrations >5 at%, the Lorentzian line represents ~3-4 at% H.

Still more features of the line shape common to all samples have been reported. The line shapes were reported to be independent of temperature to liquid-He temperatures[27,165] (but see the discussion below about molecular hydrogen), and the linewidths were shown to be dominated by homonuclear dipole-dipole interactions.[27] Hole-burning[155] and spin echo[33] measurements conclusively proved that the two lines come from protons in spatially distinct regions. Again, these features are present regardless of sample quality. The NMR results therefore show the important fact of distinct proton heterogeneity in all samples, a feature not observed in SEM/TEM or IR studies on good samples.[106]

It is important to note that the observation of two distinct line shapes in the proton spectra provides evidence that at least two distinct proton regions exist in the sample. Carlos and Taylor noted this fact,[33,161] and carefully analyzed a FID in an attempt to observe any third proton species. They could only identify two distinct decay

rates, but as Carlos and Taylor pointed out,[33] this still does not rule out the possibility that more than two proton morphologies exist in a-Si:H, only that a) if a third (or more) species exists having a significantly different FWHM from ~25 kHz or ~4 kHz, then this species must be present in the material only in small concentrations (<5% of the total H content), and/or b) other morphologies may exist, but must give a FWHM close to 25 or 4 kHz.

a. Moments analysis and the Gaussian line shape In an attempt to define, or at least restrict, the possible bonding configurations of hydrogen in the a-Si:H films, moments analyses have been carried out.[33,155,165,166] The first three groups mentioned above used equation (42) with the powder averaging of Θ_{ij} to estimate linewidths due to specific proton bonding configurations. The use of equation (42) is facilitated by defining a parameter, $\xi \equiv$ the effective number of nearest neighbors, which is reminiscent of the Madelung constant[172]

$$\sum_i \frac{1}{r_{ij}^6} = \frac{\xi}{r_{nn}^6} \qquad (63)$$

where r_{nn} is the distance from the nearest neighbor to the j^{th} spin. Equation (42) then becomes

$$FWHM(Hz) = 1.90\times10^{5}\left[\frac{\xi}{r_{nn}(A)^{6}}\right]^{1/2} \quad (64)$$

The use of equation (64) for differing proton bonding configurations is presented in Table 1; a number of the entries are not reported in the literature.

All the bonding configurations in Table 1 would give rise to a Gaussian line shape (SiH_2 or SiH_3 would need variations in bond lengths, or strong next-nearest neighbor interactions

Table 1. Moments analysis for proton linewidths due to specific proton bonding configurations

Bonding configuration	Nearest neighbor bond length, d(A)	Number of nearest neighbors, ξ	FWHM (kHz)
SiH_2	2.37	1	14.3
SiH_3	2.37	2	20.2
$(SiH_2)_n$	2.37	1.3	16.3
Si(111):H	3.83	6.32	8.5
Si(100):H_2	1.51	1.05	56.5
monovacancy	1.47	3	104.
divacancy	1.47	2.005	85.
trivacancy	1.47	2.005	85.
two parallel	2.57 (b=0)[a]	3.6	21.2
Si(111):H	2.0 (b=0)	1.3	27.1
surfaces	3.83 (b=1)	7.3	9.1

[a] b equals the smallest proton-proton distances perpendicular to the surfaces (see Figure 3).

to broaden the expected line shape,[4] a Pake doublet for SiH_2,[173] into a Gaussian line shape). The generally accepted interpretation is that the broad Gaussian line (~25 kHz) is mainly due to hydrogenated surfaces in the a-Si:H, plus SiH_2, SiH_3 and/or $(SiH_2)_n$ bonding in the poorer materials.[26,33,155,165] The identification of the origin of the line 8.5 kHz in width for the hydrogenated Si(111):H surface has caused some contention in the literature.[33] This ambiguity can be resolved if a modification is made in the interpretation.

A possible bonding configuration that could give rise to the broad Gaussian line not discussed in the literature is a close approach of two hydrogenated surfaces, as depicted in Figure 3. As seen from Table 1, if the surfaces come sufficiently close, the FWHM for the Si(111) surface can become very close to the observed width. One example might be the surfaces of two islands in the region of contact. As discussed in Section II.A.3, the two surfaces do not have enough degrees of freedom to coalesce[56,57] - i.e., the lattices do not have enough mobility to match the necessary bond angles or bond lengths for Si-Si bonds to form surface to surface. But if the growth rate is slow enough, the surfaces can continue to grow until they become very close to each other. Other possibilities for the configurations leading to the broad Gaussian line will be discussed later.

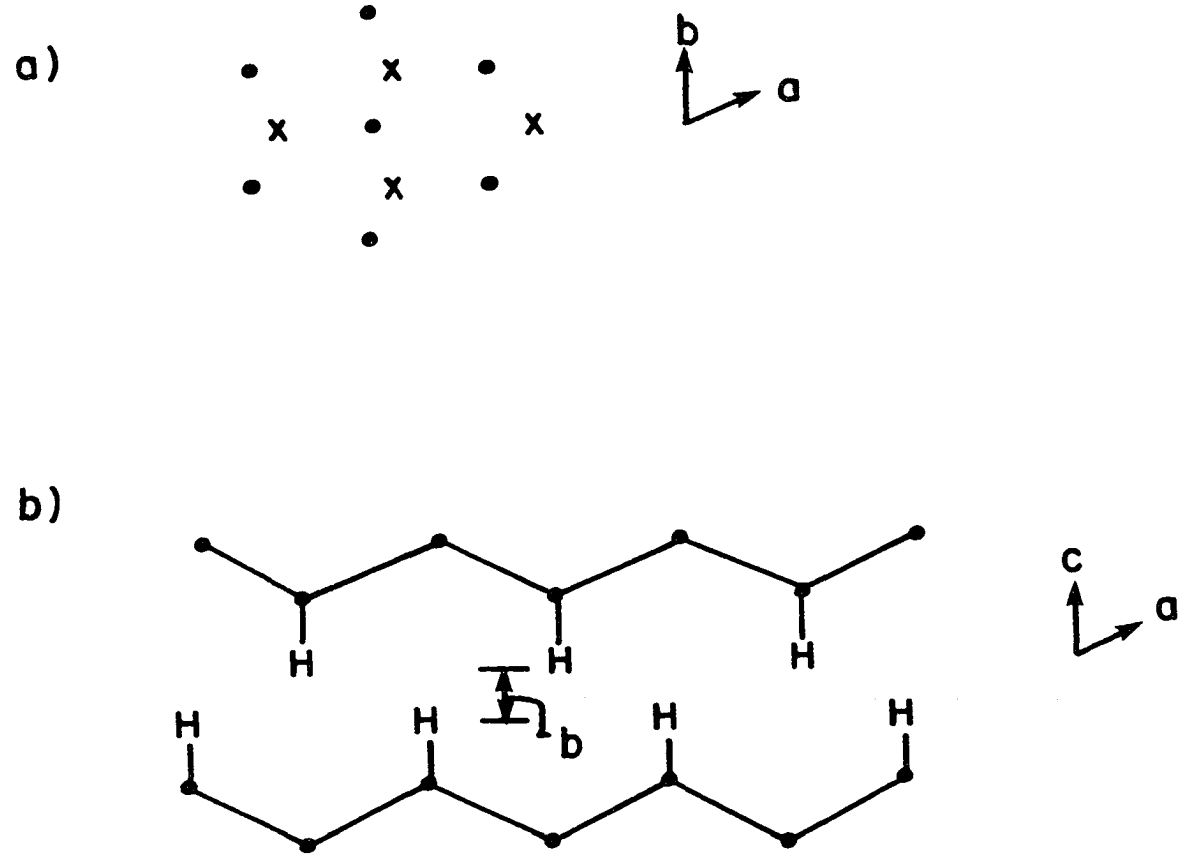

Figure 3. Parallel Si(111) surfaces illustrating a possible proton environment leading to the broad NMR line.
a) Looking down perpendicular to the surface planes, the x's represent hydrogen bonded to one surface, the dots to the hydrogen bonded to the other surface.
b) Looking at a cross-section of the surface, where b is the separation of the protons perpendicular to the surfaces.

Another important point, not stated in the literature, is the following. It is quite easy to see, if one experiments with a stick-and-ball model, that any small rigid void of <10 Si vacancies which is considered fully hydrogenated would give a line shape much broader than 25 kHz. For such small voids, relaxation of the lattice to give Si(111) type surfaces is impossible. Thus, NMR results clearly show that small, fully hydrogenated rigid voids do not exist in appreciable amounts (having >5% of the total H content) in a-Si:H films.

b. The Lorentzian line shape The origin of the narrower, Lorentzian line has in general caused less speculation, at least within the NMR community, but has generated some debate about why it is Lorentzian instead of Gaussian.[33,155,165,166] Later in this section, I will pose some questions about the standard interpretation.

As discussed previously, a Lorentzian line shape can be associated with a system of protons experiencing predominantly homonuclear dipolar interactions. This result obtains if the proton system is very dilute, or if the B term in H_D^{II} for some reason becomes nonsecular.[4] In a later section, evidence will be given that the B term is not nonsecular for most of the protons associated with the

Lorentzian line (indeed, relaxation studies take this point for granted; see Section II.C.2). Moreover, the concentration is too high to make an argument for the dilute case,[4,155] unless one accepts the interpretation of Lowry et al. that in an amorphous solid, the lattice spacing of a unit cell becomes relatively small, thus decreasing the conditions for dilution.[165,166] This approach appears to have some justification. Myles et al. have shown theoretically from first principles that a random array of atoms shows Lorentzian character at higher concentrations than in the derivation for a perfect lattice.[174]

Reimer et al.[155] and Lowry et al.[165,166] used both spin counting and average densities obtained from moments analyses to calculate the amount of space-filling of the protons. Both groups agreed on the interpretation that the Lorentzian line comes from a random distribution of monohydride groups in the islands, or bulk regions of the film. (From here on, I will use monohydride meaning the protons giving rise to the Lorentzian line shape.) Reimer et al. calculated the average spacing, r_0 = 7.7Å, and the standard deviation, σ = 1.7Å, of the random (Gaussian) distribution of monohydride spacings equaling 1.7Å.[155] It was also concluded that in films with lower H content, the monohydrides leading to the Lorentzian line could not fill the lattice (excluding the portion containing the broad Gaussian protons). A "buffer zone"[155]

or "nonhydrogenated Si network"[165,166] region was therefore necessarily present as a third phase in a-Si:H films.

The necessity of having nonhydrogenated areas in a-Si:H is perhaps most easily seen using the argument presented by Carlos and Taylor.[33] Using the relation of Myles et al.,[174] which states that the linewidth varies directly with the concentration of spins at low concentrations, $c < 0.1$, Carlos and Taylor[33] proceeded with equation (45). Assuming the monohydrides space themselves at the crystalline Si density such that $\eta = 4.94 \times 10^{22}/cm^3$, then

$$FWHM(Hz) = 3.8\gamma^2\hbar\eta = 4.51 \times 10^4$$

Since FWHM $\propto$ c, each at% of monohydride will give ~450 Hz linewidth. The observed linewidth is ~4 kHz, whereas the concentration is ~3.5 at%. The monohydride species must therefore cluster in some way to decrease their average separation.[33]

While the interpretation of monohydride clustering is reasonable, the assignment of monohydrides as random bonding arrangements within the bulk of high density silicon[155,165,166] is contentious. Weaire et al.[113] found while building a CRN (continuous random model; see section II.A.1) of a-Si:H that it is extremely unlikely that a lone hydrogen atom could be bonded within the Si matrix without causing nearby defects. Weaire, in fact, directly addresses

the problem of the interpretation made from the NMR results.[175] It is the opinion of the present author that Weaire's objections are valid. There does not seem to be any substantial evidence (although see Ref. 129; it seems this work may be the origin of this argument) that the Lorentzian monohydrides must be associated with the bulk of the material. As Weaire points out, this bonding model does not conform with normal CRN models. While annealing studies have suggested that the monohydrides associated with the Lorentzian line anneal out of the material at higher temperatures than some protons giving rise to the broad line,[33,155,158,162] this interpretation could reasonably be explained by having both proton distributions occurring on Si surfaces.

Consider the possibility of the monohydrides occurring on a Si surface. In order to give the narrow linewidth of 4 kHz, the surface could be only partially hydrogenated. The dangling bonds left over would reconstruct to give no (or very low) ESR observable dangling bond density. As discussed previously, such reconstruction of Si surfaces is well known.[117] The monohydrides would anneal at higher temperatures than surface di- or trihydrides, consistant with annealing studies on clean Si surfaces.[176] I will return to this premise later in this work, after the experimental results have been presented.

2. Relaxation studies

Proton spin-lattice relaxation, T_1^{-1}, in a-Si:H created considerable interest because of the unusual temperature dependence of T_1.[26,106] Most a-Si:H films display a deep minimum in T_1 at ~30K.[26,161] Initially, Carlos and Taylor proposed that disorder-modes caused the behavior of the relaxation,[161] but it was shown that the number of such modes necessary to give the observed behavior of T_1 would be so high as to be directly observable.[177,178] No such evidence exists. Conradi and Norberg, following work on entrapped molecular hydrogen (m-H_2) in solid noble gas matrices[179,180] surmised that the relaxation could be explained as being due to a small number of entrapped m-H_2 in the a-Si:H lattice having a very fast T_1 which then relax the rest of the protons by spin diffusion to the m-H_2.[32] Carlos and Taylor[164] soon provided convincing evidence that m-H_2 are indeed the relaxation sink giving rise to the observed temperature dependence of T_1. In those studies, samples were cooled to liquid-helium temperatures for periods of months, and a large increase in T_1 at the minimum was observed. This effect was interpreted as a conversion of spin-1 ortho-H_2 to spin-0 para-H_2. A number of workers have indirectly determined m-H_2[33,164,168,169,181,182] and m-D_2[168,169] from the nuclear spin-lattice relaxation data fitted to the theory of Conradi and Norberg.[32]

Recently, two groups using low temperature calorimetry measured the heat of the ortho- to para-H_2 conversion,[183,184] allowing quantitative determination of the m-H_2 in annealed samples. Then observation of m-H_2 was made using IR absorption.[185,186] The IR results suggest the m-H_2 is at high densities, ~800 amagats, and resides in small voids containing <100 H_2 molecules.[186]

Very recently, Boyce and Stutzmann have reported the direct observation of m-H_2 in a-Si:H[187] from the m-H_2 Pake doublet formation[188] observed by proton NMR at low (<30K) temperatures. This study confirmed the IR result which indicated that the m-H_2 was at high densities in the sample. Fedders et al.[189] have shown that only m-H_2 residing on the surfaces of the voids can contribute according to the theory of Conradi and Norberg.[32,179,180,190] This result follows from the needed decrease in the EQQ (electric quadrupole-quadrupole interaction) in bulk m-H_2 to give the observed phonon-dominated T_1 behavior. From this result, Boyce and Stutzmann determined the void sizes to be ~20A in diameter.[187]

Some a-Si:H samples do not have spin-lattice relaxation characteristics as described by Conradi and Norberg. Lowry et al. observed nonexponential T_1's in their sputtered samples,[34,167] and proposed a three-bond disorder mode to explain their results.[191] Some samples, with low H content,

relax due to dangling bonds.[163,191] Other anomalies in the behavior of T_1 have also been published.[169,181]

Reimer et al. measured the spin-lattice relaxation while suppressing homonuclear dipole interactions, and for partially deuterated and annealed samples.[156] This study provided evidence that relaxation centers were at higher concentrations in the regions associated with the narrow Lorenztian line.

Lamotte recently published magic-angle-spinning (MAS) proton data on a sputtered sample.[192] Spinning at the "magic angle" (Θ=54.7^{o} in the term $1-3\cos^2\Theta$) averages the secular dipolar Hamiltonian, equations (24) and (25), to zero if the spinning frequency, ω_r, exceeds the dipolar interaction strength, $\omega_r > \hbar/|H_D^{II}|$. Lamotte interpreted the resulting line shape as having a large component due to m-H_2. This interpretation has been questioned.[187]

NMR studies have been done on doped a-Si:H[155,160,193] and inorganic thin films such as a-Si:C:H.[159] A motionally narrowed line was observed in the inorganic films. Motionally narrowed proton line shapes have also been reported in the NMR studies of a-Si:F_x:H_y by Ueda and coworkers.[194-198]

III. EXPERIMENTAL DETAILS

A. Sample Preparation and Characteristics

Four samples, the Anode and Cathode, VAN150, and SHK#7, were studied in detail in this work. Parameters charaterizing their growth are summarized in Table 2.

The Anode and Cathode glow-discharge samples were provided by J. Reimer and J. Knights, and have been extensively studied by a variety of techniques (see Refs. 27 and 155 and Refs. therein). The details of the deposition

Table 2. Growth parameters for the a-Si:H samples

Sample	Preparative conditions
VAN150	GD, 35 watts, T_s=250°C, 10% SiH_4 in H_2
VAN400	400°C anneal for 15 minutes
VAN500	510°C anneal for 15 minutes
VAN550	550°C anneal for ~6 hours
Anode	GD, 18 watts, T_s=25°C, 5% SiH_4 in Ar
Cathode	GD, 18 watts, T_s=25°C, 5% SiH_4 in Ar
SHK#7	SP, 3.3 watts/cm^2, T_s=25°C
C45	SP, 3.3 watts/cm^2, T_s=25°C, 3.0 cc/min H_2
C70	SP, 2.9 watts/cm^2, T_s=25°C, 24.0 cc/min H_2

GD ≡ glow-discharge, SP ≡ rf-sputtered, T_s ≡ substrate temp

apparatus have been published elsewhere.[199] Both samples are characteristic of "poor" samples: they have a high density of dangling bonds, 10^{18}-$10^{19}/cm^3$, as measured by the intensity of the ESR line at g = 2.0055, and show discernible features in electron micrographs.[38,120] IR analysis shows them to have ≡SiH, $=SiH_2$, $-SiH_3$ and $(SiH_2)_n$ bonding groups.[121]

VAN150 was provided by P. Vanier at Brookhaven Labs, and is characteristic of a "good" quality glow-discharge sample. ESR measurements verify that the dangling bond density is $<10^{16}/cm^3$. IR analysis of similarly prepared samples shows only ≡SiH bonding, and no features are present in the electron micrographs. The design of the deposition apparatus has recently been published.[200] Of interest for a later section, samples prepared under similar conditions have never shown oxygen contents >1.0 at%.[201]

SHK#7 is a good quality rf-sputtered sample provided by H. Shanks at the Ames Laboratory. Again, this sample has only ≡SiH units and $<10^{16}$ e^-/cm^3. Two other rf-sputtered samples have been studied less extensively, C45 and C70 (the same designations as Lowry et al.[165,166,191] uses), provided by M. Lowry and R. Barnes of the Ames Laboratory. All three sputtered samples were prepared on the same system at the Ames Laboratory.[202] More details about C45 and C70 can be found in the literature.[34,165-167,191]

All samples were grown on an Al substrate. An HCl acid etch was used in all cases to obtain the a-Si:H powder. I etched only VAN150, since all the other samples were provided already in powder form. For VAN150, a 0.1M HCl solution was used, ~750 ml for each 300 mg of a-Si:H. The sample was then carefully washed with deionized H_2O. All the samples were inserted in a high-precision 5mm NMR tube, and dried overnight at 150°C (thus the designation VAN150) under $\sim 10^{-5}$ torr in a grease-free vac-line. The samples were then sealed under ~10 torr He.

An annealing experiment was performed on VAN150 to check this sample's quality. A small amount, < 1 mg, of sample was mounted in an ultra-high vacuum (UHV) system. The sample was pinned against a heater block with a 200 mesh Ni grating. The hydrogen evolution during the anneal was monitored using a mass spectrometer tuned to amu=2. The base pressure of the system before starting the anneal was $<10^{-9}$ torr. A background run on just the wire mesh was run, and although the hydrogen background did rise with increasing temperature (to $\sim 10^{-7}$ torr at 1000 K), this background was always an order of magnitude smaller than the intensity measured in the presence of the sample. The temperature was measured with a W5%Re-W26%Re thermocouple spot-welded next to the sample. The heating rate was controlled manually (trial runs were necessary to obtain a reasonably uniform rate) to ~35°/min.

The hydrogen evolution, dH_2/dt, versus temperature is shown in Figure 4. Clearly, no significant evolution takes place < 680 K. Any $-SiH_3$ or polymeric $(SiH_2)_n$ groups would evolve by 650 K, and usually display a very strong peak in poor samples.[125-128] This confirms that VAN150 is a good quality sample, as assumed from its conditions of deposition.

B. NMR Spectrometers

Two homebuilt spectrometers were used, one operating at a proton frequency of 56MHz, the other at 220MHz. Both are similar to the design published from this group.[203]

1. Timing of the CPMG experiment

The rf pulse sequences are set using a microprocessor controlled pulse programmer (PPG).[204] Of specific interest for the CPMG experiment is the use of the PPG's sample-and-hold circuit. This feature has adjustable delay and integrate periods which allow for "stroboscopic" observation during multiple-pulse sequences. The sample-and-hold circuit is triggered by the PPG using a trigger, T3. At this trigger, a dial selected delay time begins, at the end of which the integration period begins. The PPG must be carefully programmed so that the integrate period will be centered on the echo peak. The situation is depicted in Figure 5 for the first three pulses of a CPMG sequence. The

Figure 4. Hydrogen evolution of VAN150. The ordinate represents the rate of amu=2 evolution (arbitrary units), with an average heating rate ~35^0/min.

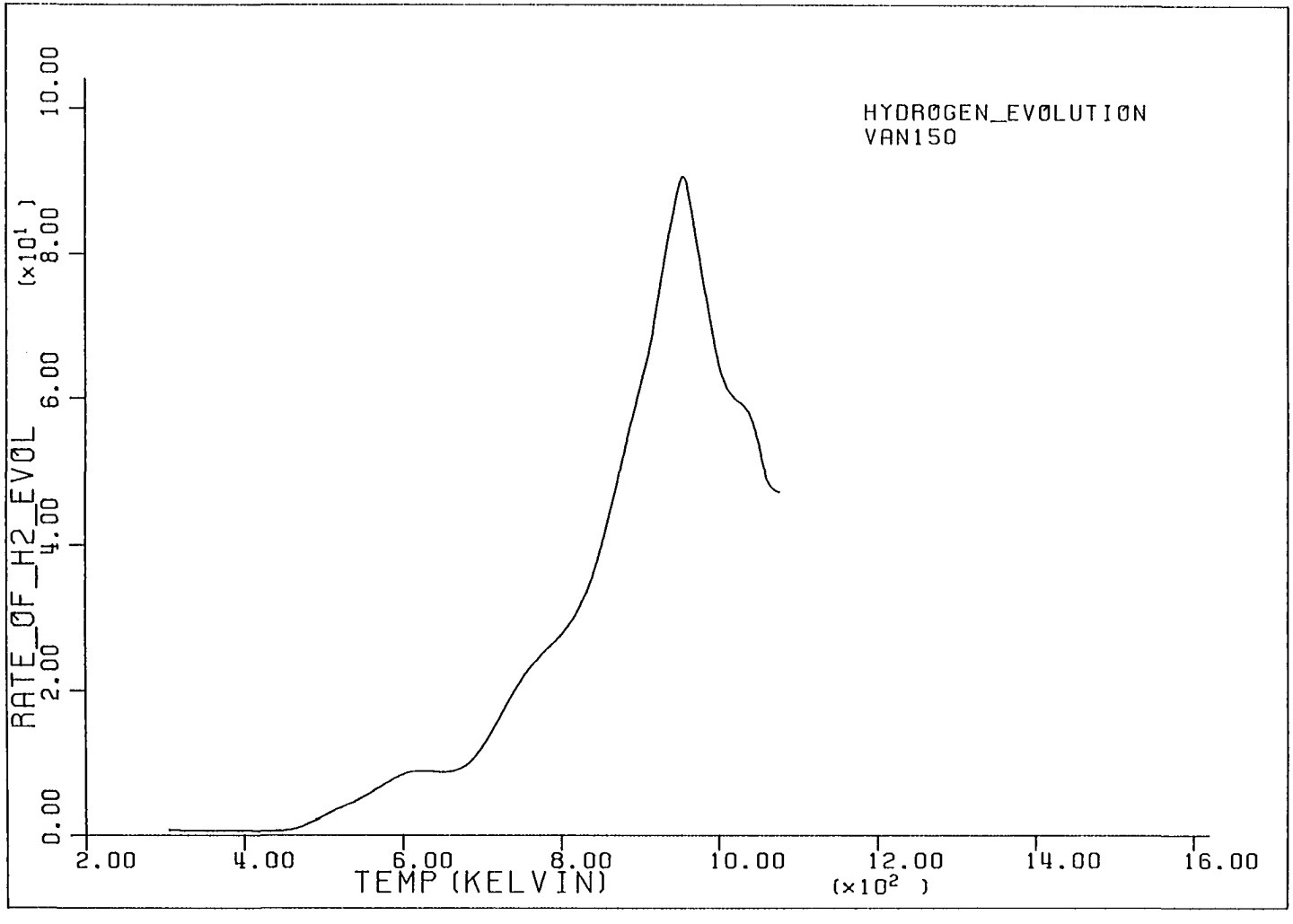
HYDROGEN_EVOLUTION
VAN150
RATE_OF_H2_EVOL
(×10¹)
0.00
2.00
4.00
6.00
8.00
10.00
2.00
4.00
6.00
8.00
10.00
12.00
14.00
16.00
TEMP (KELVIN)
(×10²)

Figure 5. Timing events during the CPMG sequence. t_c is the multiple pulse cycle time; t_p is the 90^0 pulse width; D1, D2 and D3 are programmed delays with T3 being a programmed trigger, all used in the PPG sequences; int and delay are dial adjustable integration and delay windows on the sample-and-hold circuit.[204]

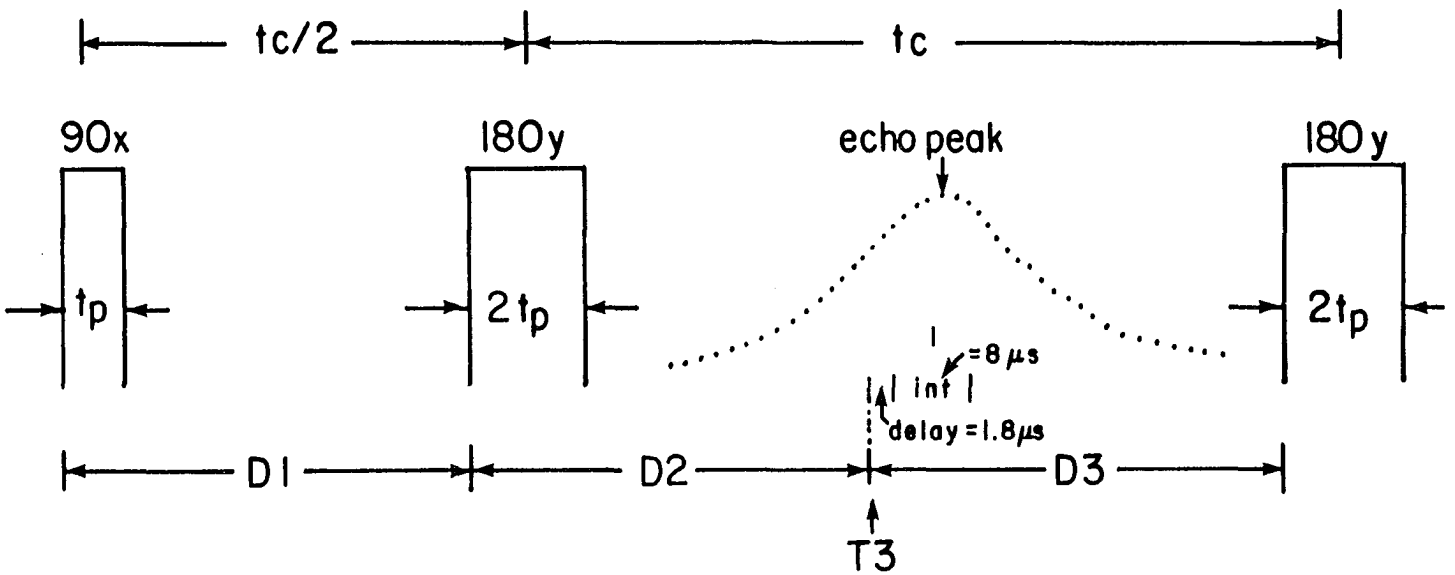

$D1 = (tc - tp)/2$

$D2 + D3 = tc$

$D2 = \frac{tc}{2} - \frac{int}{2} - delay + tp$

settings most commonly used were a delay period set to the minimum value of 1.8μs, and an integrate period set to the maximum value of ~8μs. In Figure 5, D1, D2, and D3 are programmed delays that set the timing of the PPG rf sequence. Tuning P1 ≡ 90_x, P2 ≡ $90_{\bar{x}}$ and P3 ≡ 180_y pulses, the PPG sequence would be

```
P1 D1 I
(P3 D2
D3
P3 D2
T3 D3)2048
```

where each line represents a timing event (all commands on a line begin at the same time), and 2048 is the number of digital points per scan. The I in the first line stipulates that on alternate scans P2 is substituted for P1, and the resulting transient is subtracted from the accumulated signal. This technique cancels some base line artifacts and DC drift, which can be fairly large when using the sample-and-hold circuit (from thermal effects).

The ability of the sample-and-hold circuit to give accurate decay rates was checked by doing a CPMG experiment on an H_2O sample both while using the sample-and-hold circuit and under normal observation. (Note also, as discussed in Section IV, that the CPMG experiments performed on the a-Si:H samples were always done using both modes.) The decay rate

of the echo amplitudes under each method gave T_2 = 0.90 ± .05 sec.

Background signals were an experimental problem constantly being attacked during this work. The spectrometers used are very "clean" spectrometers: background signals rarely exceed an apparent intensity of 10^{18} protons (<0.5% of the number of protons in a typical NMR sample). But many experiments done in this work were performed to observe <10^{19} total protons in the a-Si:H sample, and thus background signals could become non-negligible. Background problems from spurious signals were most discernible during the CPMG experiments. The background was constantly checked by taking data without the sample, and then taking an identical background run to make sure proton signals exterior to the sample, and other spurious signals were being properly subtracted from the data. Background runs were always taken for all experiments (CPMG, T_1, FID's, etc.), and background signal intensities were always kept less than 20% of the true proton signal intensity.

2. Doubly wound coils for solid state double-resonance and multiple pulse NMR

A critical part of probe construction in modern solid state NMR spectrometers is the coil. The inductance of the coil determines the quality factor Q, which in most cases is

a major factor determining both the overall sensitivity and the ring-down time of the spectrometer's receiving system. A coil design was used in this work, similar to one suggested by Stephen B. W. Roeder,[205] which has some advantages over the usual coil designs.

The basis of this coil is a parallel double winding arrangement. The coil design is shown in Figure 6a. Doubly wound coils have been discussed in the literature (see Refs. 206 and 207 and discussions therein), but not with the interwoven design shown in Figure 6a. Theoretically, inductively uncoupled parallel inductors would give one-eighth the total inductance when compared to the inductance of a singly wound coil having the same number of turns, radius and length.[208] In actual designs, there is enough mutual inductance to cause the total inductance to be reduced by approximately two. Triply wound coils have total inductances reduced by ~4, but with coils of <15 turns the end effects become too large for this design to be useful.

The reason for using this configuration is to construct a coil with a length (l) to diameter (d) ratio, $l/d \gg 1$, to maintain a relatively homogeneous B_1 field, while keeping the inductance sufficiently low to tune the circuit containing the coil to resonance at ~300 MHz. The advantage of being able to decrease the inductance of the coil is being able to correspondingly increase the capacitance of the isolation

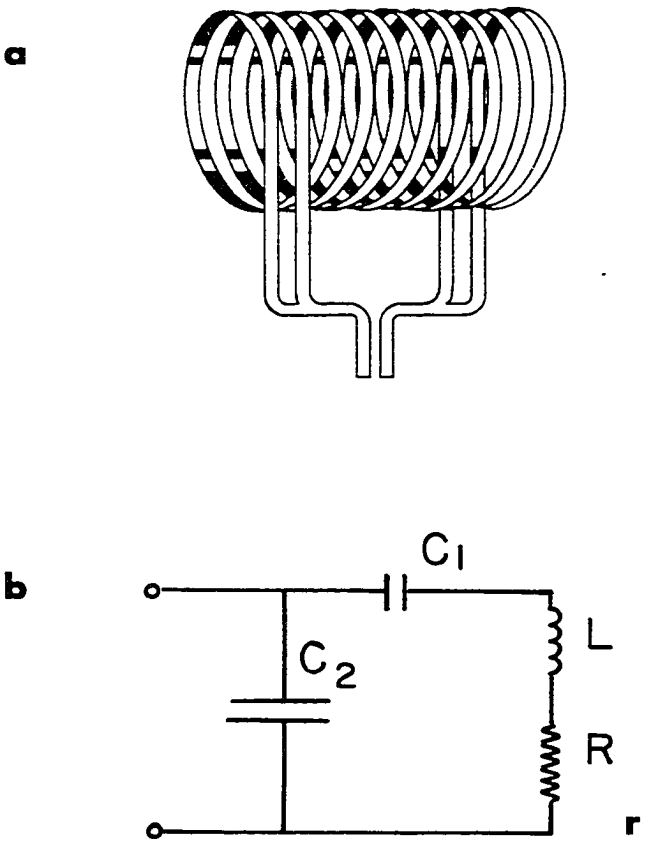

Figure 6. The doubly wound coil

a) Design of the doubly wound coil.

b) Circuit diagram of a multiple pulse ^{1}H probe.

tuning capacitor (C_1 in Figure 6b). A lower inductance with a more uniform B_1 is especially an advantage for NMR of protons at high frequencies. A 10 turn - 5 turns in each parallel winding - 5mm diameter coil as shown in Figure 6a has an inductance of ~0.09 μH at 220 MHz, compared to ~0.18 μH for the corresponding singly wound coil. This decrease in inductance allows a multiple-pulse proton probe to be tuned with a 0.8-10 pf Polyflon variable capacitor.[209] The Q of the probe was adjusted to the optimal value of 23.[210] The rf homogeneity of the coil is shown in Figure 7 for a 5mm spherical water sample under the normal $\pi/2$ tuning pulse sequence.[147,211,212] With the singly wound coil, the high inductance forced a lowering of the Polyflon's capacitance by adding a small ceramic capacitor[213] in series. This addition caused problems with structural stability and stray lead capacitances in the probes with singly wound coils.

This coil arrangement, albeit simple in concept, may be of greatest practical use in double-resonance circuits. Much labor has been expended in constructing the small isolation capacitor so important for double-resonance experiments (see for example Refs. 214 and 215). Doubling the allowed capacitance (in actual designs, we find that the capacitance is closer to four times as great as for the singly wound designs) for identical isolation should be advantageous. In addition, excellent B_1 homogeneities can be achieved with

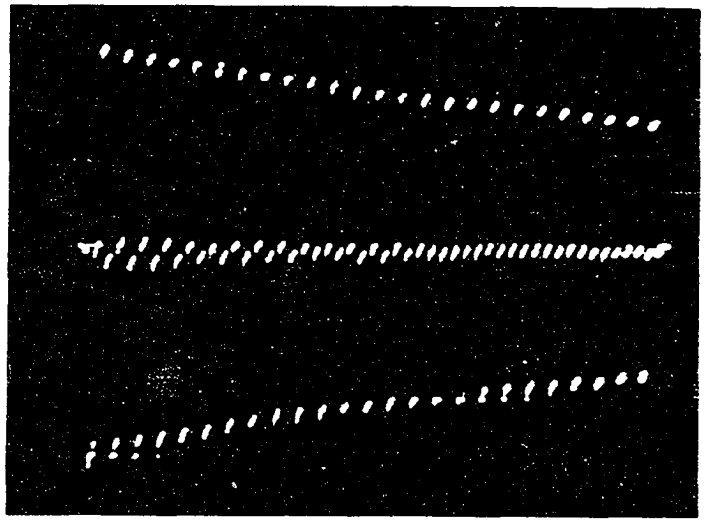

Figure 7. B_1 homogeneity of the doubly wound coil. Photographed is a $\pi/2$ tuning sequence using the doubly wound coil: $t_p \sim 1.2$ µsec, 400 µsecs between pulses, 40 msecs full scan.

doubly wound coils without any sacrifice in decoupling power.[216,217] This feature should allow for the construction of MAS double-resonance probes which can also perform multiple-pulse experiments.

C. Computational Techniques

In order to acknowledge the software used, and to discuss techniques for error analysis, I briefly mention the various computational techniques used in this work. The data acquisition at each spectrometer is controlled by a software routine called ALVIN, developed within the Ames Lab.[218] ALVIN is written specifically to interface a PDP-11 minicomputer with a Biomation 805 or 2805. In addition to controlling the data acquisition, ALVIN also performs small computational and data management chores. These include data transfer to other computer systems, data display on any x-y oscilloscope, fast Fourier transforms, zeroth-order base line adjusts, and linear phase adjustments, to name a few.

A compact (requiring only 28K bytes of memory) software package, FA1, was developed in our group by Dr. P. DuBois Murphy.[219] FA1 runs on the PDP-11's, and can perform most small computational tasks required by an NMR spectroscopist.

Single component relaxation data including inversion-recovery T_1, repetition-rate T_1, T_2, or $T_{1\rho}$ data can be

analyzed using a routine I developed called LSFT1. The T_1 data are assumed to be exponential, but the T_2 or $T_{1\rho}$ can have any user-specified time exponent. The raw data are input into LSFT1, including the corresponding errors, assumed to be instrumental[220] and significant only for the intensities. LSFT1 linearizes the data, and fits the linearized data using Bevington's linear least-squares fit algorithm, LINFIT.[220] The errors are propagated to give standard error limits on the final results (a relaxation time, and an initial intensity).

An example of this propagation of errors is as follows. For the repetition-rate method of measuring T_1 relaxation,[144] the data are fit to the equation

$$M(t) = M_0 [\, 1 - \exp(-t/T_1) \,] \qquad (65)$$

where M is the magnetization intensity, t is the time between pulses, and M_0 is the magnetization intensity for $t \to \infty$. The errors for each M(t) point are assumed to be equal, σ_m, except for M_0 which has an different error, σ_0. Equation (65) is linearized

$$Y(t) = \ln [1 - M(t)/M_0] \qquad (66)$$

The error in Y(t), σ_y, is easily found to be

$$\sigma_y^2 = \frac{1}{(M_0 - M(t))^2} \left[\sigma_m^2 + \sigma_0^2 \frac{M(t)^2}{M_0^2} \right] \quad (67)$$

Y(t), t, and $\sigma_y(t)$ are input by LSFT1 into LINFIT, which fits them as

$$Y(t) = a + bt \quad (68)$$

and returns a, σ_a, b, and σ_b. $T_1 = -1/b$, and the standard deviation of T_1, σ_T, then equals σ_b/b^2. LSFT1 then returns $T_1 \pm \sigma_T$.

More complex data were fitted using a generalized least-squares fitting routine, which will handle any function containing up to 48 parameters. This routine is the basis of PEAK15,[221] a software routine written by P. Murphy and modified by myself and Po-Jen Chu to accept ALVIN formatted frequency data. PEAK15 fits up to fifteen peaks having specified Gaussian, Lorentzian, or Gaussian*Lorentzian character. A two component decay analysis routine, TCDA, written by myself, will fit an ALVIN formatted time decay composed of two on-resonance decays of either Gaussian or Lorentzian character.

A disadvantage in the use of PEAK15 or TCDA is that no standardized error estimate on the fitted parameters is calculated other than a normalized sum of differences squared. Errors in actual fits were estimated by varying the

fit conditions and initial guesses, and observing how much a specific parameter could vary before noticable deviations from the raw data could be observed (especially in the difference spectra). Specific examples will be given in Section IV.

One last aspect of the analysis of importance is the relation between errors in two component fits to data in the frequency domain, relative to those in the time domain. Relaxation times obtained by fitting data in the time domain are sensitive to base line artifacts, but the fit in the time domain does extrapolate the data back to time zero to obtain "correct" relative intensities. In contrast, area measurements done in the frequency domain are always incorrect unless a correction is made for the loss of signal at small times due to pulse ring-down. Frequency domain data, however, are less sensitive to base line artifacts (which are Fourier transformed into a zero frequency peak for a slow DC drift, and thus out of the spectra). All two component fits done in the frequency domain in this work have been corrected for the pulse ring-down time. Fits were also done in the time domain, both with and without solid echoes,[144,222,223] and the results from all three methods were found to be self-consistent.

IV. RESULTS AND DISCUSSION

To ease the discussion in the rest of this work, I will introduce some nomenclature to reduce the wordage used to describe the various phenomena. It will be shown that four distinct proton environments exist in a-Si:H films. Three of these environments have already been introduced in Section II.C. The first two are the protons giving rise to the narrower Lorentzian line shape and protons giving rise to the broad Gaussian line shape observed in the Fourier transform (FT) of the proton free-induction-decay (FID) (see Figure 2). In the time domain FID, the narrow line gives a slower decaying component (a longer T_2), and the broad line a faster decaying component (a shorter T_2). I will refer to these two proton environments as the narrow line and the broad line, respectively. Later on, these environments will also be referred to as the monohydride and void protons, even though in some respects the use monohydride may be misleading (the void protons can also be monohydrides, but not the monohydrides specifically being referred to). The third proton environment is the molecular hydrogen, i.e., m-H_2.

The fourth proton environment will be attributed to protons which are isolated (defined more precisely later) from the rest of the proton bath. These protons I will refer to as isolated protons, or isolated monohydrides.

The isolated protons and the m-H_2 give rise to a echo component in some NMR experiments. In the early parts of this section, I may refer to the m-H_2 and isolated protons together as the echo component, or the Hahn echo component.

A. Line Shapes and Spin Counting

A typical line shape of the Fourier transform (FT) of a free-induction-decay (FID) following a 90^0 rf pulse was presented in Figure 2. The data were fit using PEAK15 to a superposition of a broad Gaussian line shape, equation (35), and a narrower Lorentzian line shape, equation (36). The resulting linewidths and relative intensities are typical of the results given in the literature.[33,155,165,166] Similar fits to all the samples studied in this work give results as listed in Table 3. The relative intensities of the two peaks have been corrected as described in the Appendix.

In Table 3, the widths of some of the Lorentzian lines narrow slightly (the Anode and SHK#7 do not) when going from a 5.2T field strength to 1.3T. VAN550 has only a single asymmetric narrow line shape, ~16ppm wide at 220 MHz and ~34ppm wide at 56 MHz. This narrowing of the Lorentzian lines will be discussed in detail in Section IV.F.1. The narrowing of the linewidths indicates that interactions proportional to the field strength, such as the chemical

Table 3. Line shapes and spin counts of a-Si:H samples

Sample	at% H	M_G	$FWHM_G$(kHz)	M_L	$FWHM_L$(kHz)
Anode	20±1	0.68±0.03[a]	30^{+4}_{-2}	0.32	3.4±0.4[a]
Cathode	28	0.71	27	0.29	4.9
SHK#7	16	0.70	28	0.30	3.7
VAN150	15	0.56	34	0.44	5.1
VAN400	13.3	0.55	31	0.45	3.8
VAN500	8.4	0.33	26	0.67	2.9
VAN550	1.3±0.2	0.0	--	1.0	3.5[b]
C45	5.9±0.7	0.59	27	0.41	4.0
C70	14.6	0.60	28	0.40	4.1

[a]Measured at 5.2T (220MHz for ^{1}H).
[b]Line shape was asymmetric (see text).

shift or magnetic susceptibility, are becoming large enough at 5.2T to be non-negligible. These are the first linewidths reported at such large fields, and thus are the first reported having a frequency dependence. The linewidths reported by other workers were all measured at lower fields (<1.3T), and all these linewidths have been field independent (to lower field strengths), indicative of line shapes dominated by dipolar interactions.[33,155,165,166]

Results of spin counting experiments are also listed in Table 3. These data were obtained by comparing the corrected (as described in the Appendix) initial intensity of the FID for an a-Si:H sample of known weight to the initial intensity of a water sample of known weight. The convention for reporting the atomic percent hydrogen, at% H ≡ 100α, in this work is the ratio of the total number of hydrogen times 100 to the total number of atoms (Si plus H). Some H content values in the literature report the total number of hydrogen over the total number of silicon, δ. The values here are derived from the total number of hydrogen atoms per gram, n_H, using

$$\alpha = \frac{n_H}{n_{Si} + n_H} = \frac{n_H M_{Si}}{N_A + n_H(M_{Si} - M_H)} \tag{69}$$

whereas

$$\delta = \frac{n_H}{n_{Si}} = \frac{n_H M_{Si}}{N_A - n_H M_H} \tag{70}$$

where N_A is Avogadro's number, M_{Si} is the molecular weight of Si, M_H the molecular weight of hydrogen and n_{Si} is the number of Si atoms per gram.

Spin counting gives the total hydrogen content of the a-Si:H sample. The H content can be measured by other means, but NMR is one of the easier and more accurate techniques available (see the review by Knights[106]). It should be

noted, however, that almost any systematic errors (careful attention is necessary to avoid these) in the NMR data lead to low values for the H content. These errors include the loss of proton intensity due to protons within a paramagnetic center's barrier or critical radius[224,225] (for an example of this occurring in a-Si:H, see Ref. 155), incorrect (too large) sample weights from part of the sample being stuck to the walls of the NMR tube outside the coil, incorrect pulse widths, rf phase errors, incorrect repetition rates (faster than $7T_1$), poor rf homogeneity, etc. Such sources of error were given careful attention during the measurements reported here, and are included in the listing of the error bars on the H content in Table 3. Still, it is important to keep in mind that the values are to some extent lower limits of the total H content. Some of the spin counting results listed in Table 3 were duplicated within the experimental errors by Joseph Iwamiya (for SHK#7 and Cathode). Most of the determinations were done at least twice on separate days.

It is important also to note that the relative intensities listed in Table 3, and reported elsewhere, are dependent on the assumption that the spectra are composed of a broad Gaussian line and a narrower Lorentzian line. This assumption will be shown to be questionable. The relative intensities will be reexamined in Section IV.D.1.

B. Goldman-Shen Experiments

The Goldman-Shen experiment, first introduced and named after M. Goldman and N. Shen,[6] will be discussed here primarily to introduce the next sections. The "anomalous" results described in this section led to the experiments discussed later. A modified Goldman-Shen experiment giving useful information about a-Si:H films will be described in Section IV.G.

Spin diffusion, so named to describe the diffusive transfer of magnetization through a sample by dipolar spin-flips caused by the B term in H_D^{II}, equation (25), can be described by a diffusion equation[3-5]

$$\frac{dM(\vec{r},t)}{dt} = D\,\nabla^2 M(\vec{r},t) \tag{71}$$

where T_1 is neglected (i.e., for times $t \ll T_1$). In a powder, the transition rate of mutual spin flips, W, is approximately[3,4]

$$W = \frac{\sqrt{M_2}}{30} \tag{72}$$

where M_2 is the second moment as in equation (42). The spin diffusion coefficient is defined as

$$D = Wa^2 \tag{73}$$

where a is an average internuclear spacing. Equations (72) and (73) are only approximate, but even so are quite useful.

As shown by Cheung and Gerstein,[7] a Goldman-Shen sequence applied to appropriate systems can be used to estimate domain sizes, and if accurate enough data are obtained, the Goldman-Shen experiment can also define the domain shape. The experiment can be visualized by a vector picture, as diagramed in Figure 8. The second pulse is applied at $\tau \sim 7T_2^b$ after the first pulse, where b indicates the broad line (fast decay). Just before this second pulse, there is no phase coherence left in the domains giving rise to the broad line. The only magnetization left is in the domains giving rise to the narrow line (slow decay), and this magnetization is "stored" along the z-axis by the second pulse. During the time t_1, the magnetization in the narrow line diffuses by spin diffusion into the broad line (obviously, broad line refers to the proton domains giving rise to the broad line; see the discussion about nomenclature on p. 73). After the third pulse, the amount of diffusion is monitored by measuring the regrowth of the broad line. This recovery is defined as

$$R(t_1) = \frac{M_b(t_1)}{M_b(t_1 \to \infty)} \tag{74}$$

Figure 8. The Goldman-Shen sequence. At the top is a vector diagram illustrating the motion of the on-resonance magnetization. Below is illustrated the expected regrowth of the fast decaying component as t_1 is lengthened. The fast decaying component grows back due to spin diffusion during t_1.

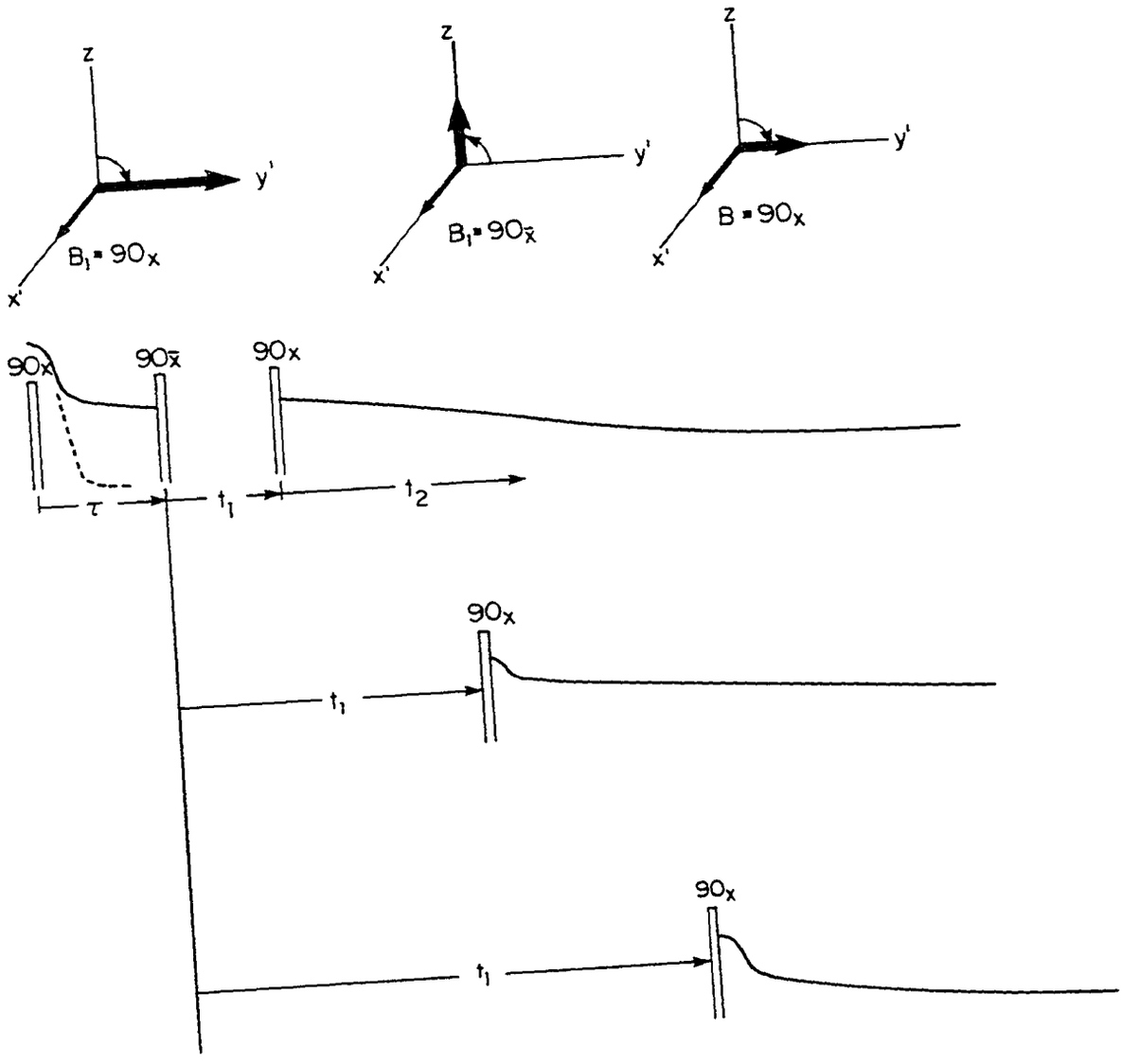
z
y'
x'
$B_1 = 90_x$
z
y'
x'
$B_1 = 90_{\bar{x}}$
z
y'
x'
$B = 90_x$
90_x
$90_{\bar{x}}$
90_x
τ
t_1
t_2
90_x
t_1
90_x
t_1

where $t_1 \rightarrow \infty$ implies a long t_1, but having $t_1 << T_1$. t_1 is long if it is much greater than $\bar{b}^2/D$, where $\bar{b}$ is the average length of the narrow line domain's longest dimension. The magnetization intensity at $t=\tau+t_1$ should be constant, since $t_1 << T_1$. Thus $M_b(t_1=0)=0$, and $M_b(t_1 \rightarrow \infty)+M_n(t_1 \rightarrow \infty)=M_n(t_1=0)$, where n denotes the narrow line.

In the theory developed by Cheung and Gerstein,[7] $R(t_1)$ for short t_1 is shown to be proportional to $2^m t_1^{1/2}$, where m is the dimension of the domain. For example, m=1 denotes a one-dimensional domain which has one length much larger than the other two. For long t_1, $R(t_1) \propto (\bar{b})^{m/2}$. Thus, for accurately measured $R(t_1)$, sizes and shapes of domains can be inferred.[7]

Most germane to the present discussion, however, are the qualitative features expected from the Goldman-Shen sequence shown in Figure 8. Following the second pulse, a flat base line is expected since all the magnetization is placed along the z-axis. Following the third pulse, a simple two component exponential decay is expected. These features have been observed, and the data analyzed in a similar vein as described above by many researchers.[7,226-229] When the sequence was tried on a-Si:H films, however, the time evolution observed was always similar to that shown in Figure 9. This photograph shows data obtained on the Cathode sample, with τ = 100μs and t_1 = 400μs. The initial

Figure 9. Echoes during a 90_x-τ-90_x-t_1-90_x-t_2 sequence. This photograph shows data obtained on the Cathode sample in the time domain; τ = 100 μsecs, t_1 = 400 μsecs, 2 msecs full scan. The initial magnetization decay after the first 90_x pulse begins well below the bottom of the photograph.

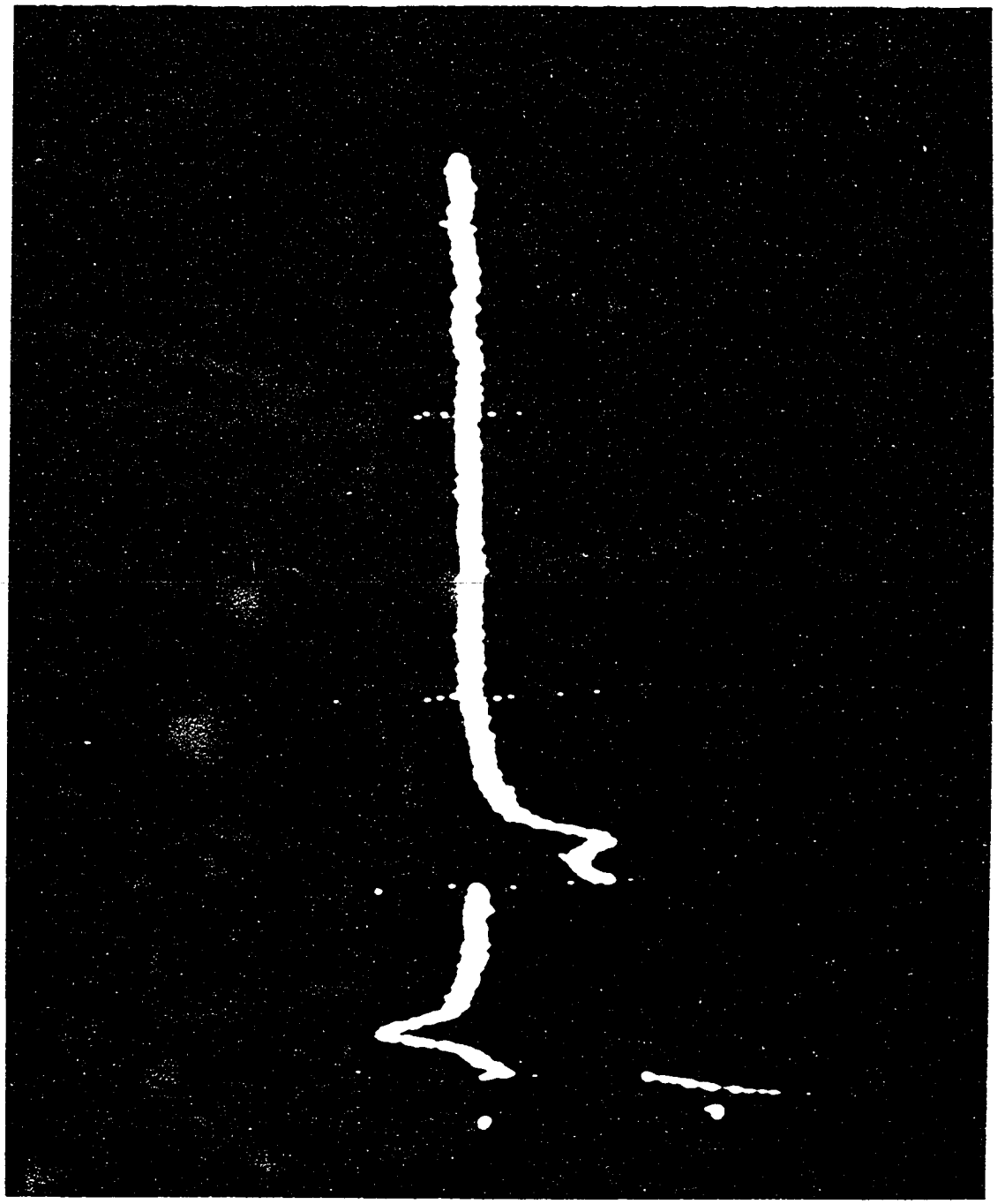

magnetization decay after the first pulse falls well below the bottom of the photograph. The echoes at time τ following the second and third pulses are the "anomalies" referred to earlier.

In a sample wherein the protons are experiencing static dipole-dipole interactions, meaning no protons are undergoing motions rapid enough to effectively narrow the static interaction, the behavior shown in Figure 9 is quite unexpected. This is not the case for protons experiencing rapid motions, such as in a liquid or gas. Still, existing published proton NMR results on a-Si:H all state that the linewidths are temperature independent to 4K (see Section II.C.1 and Refs. 27, 155, and 165). The echo intensity was determined to be ~5% of the total magnetization intensity, and for the reasons discussed in the Introduction, I undertook the project of discovering the source of the echoes with the hope of obtaining new information about the a-Si:H films.

Before leaving this section, there is some information which can be obtained from the Goldman-Shen experiment as described above. For increasing values of t_1 (and increasing τ), the echoes become less intense, until for $t_1 > 18$msec, no echo can be discerned at all after the third pulse. For $t_1 >$ 10msec, $R(t_1)$ can be estimated, and the values are listed in Table 4. The data are similar within error limits, ±0.05 on

Table 4. Values of $R(t_1)$ for a-Si:H

t_1(msec)	$R(t_1)$
10	0.65
20	0.85
50	0.90
100	0.93
500	1.0

$R(t_1)$, for the Cathode and Anode. Each point is obtained as an average value using many sets having differing t_1's. The errors in the fits, mainly due to the echo for t_1<18ms or simply due to poor signal-to-noise for t_1>18ms, kept more data from being listed in Table 4 with reliable precision. Still, comparison of the data in Table 4 with theoretical curves in Ref. 7 shows that the average narrow line domain spacing, $\bar{b} \sim 75\pm30$A for an assumed 3-dimensional domain, or $\bar{b} \sim 40\pm20$A for a 2-dimensional domain. These values, especially for the 3-dimensional case, are consistent with estimates obtained by other techniques[120,121,129,130,133-135] of the island sizes in a-Si:H.

C. Multiple Quantum Echoes

The first impression about the echoes shown in Figure 9 was that they were due to refocusing of multiple quantum (MQ) coherence during the rf sequence. The Goldman-Shen sequence

actually is better known as a standard sequence used to generate MQ coherence,[9,146,148,230-234] which for certain cases gives an echo at τ following the third 90^{o} pulse. (The echo following the second pulse is not expected for MQ refocusing, and in fact this observation led to the correct interpretation of the echo in Figure 9.)

MQ coherence has a useful feature that will be exploited here. To see how this feature comes about, it is desirable to express the spin operators I_{α} in terms of the irreducible spherical tensor operators, T^{k}_{q} (the density matrix formulation of quantum mechanics is independent of a choice of basis set)[146,231-233] which for k=1 are

$$T^{1}_{0} = I_{z} \quad ; \qquad T^{1}_{\pm 1} = \mp \frac{1}{\sqrt{2}} (I_{x} \pm iI_{y}) \tag{75}$$

The q in T^{k}_{q} represents the MQ order of the tensor operator; T^{k}_{q} connects states for which $q=|q'-q''|$. The relations

$$[I_{z},T^{k}_{q}] = q\, T^{k}_{q} \tag{76}$$

$$[I_{\pm},T^{k}_{q}] = [(k\mp q)(k\pm q+1)]^{1/2} T^{k}_{m\pm 1} \tag{77}$$

can be used to demonstrate that

$$e^{i\xi I_{z}}\, T^{k}_{q}\, e^{-i\xi I_{z}} = T^{k}_{q}\, e^{iq\xi} \tag{78}$$

Equation (78) defines the property of MQ coherence which will be used here.

To see how equation (78) relates to the present situation, the changes in the density operator through the Goldman-Shen sequence of Figure 8 must be followed. ρ before the first pulse was shown in equation (13) to be proportional to $I_z = T_0^1$. The first 90^0 pulse then gives $\rho(0)_+ \propto T_{\pm 1}^1$. Since all times in the experiment are much shorter than T_1, H_{int} cannot change q (which would require an energy transfer), but will mix k. The density operator just before the second pulse will then consist of a sum of $T_{\pm 1}^k$ terms. The second pulse will in general give all MQ orders possible, $q \leq |k|$.[9,146,231,232] During t_1, MQ coherence evolves, and if an operator of the type ξI_z exists, the density operator will evolve during t_1 according to equation (78). The final pulse rotates some of the MQ coherence into, after a period $\sim \tau$, observable single quantum order, $T_{\pm 1}^k$.

If an offset exists during a Goldman-Shen sequence, any MQ coherence should have an oscillatory dependence on t_1 described by equation (78). If the echo following the third pulse, then, is due to MQ refocusing, the echo intensity should oscillate proportional to the offset, the MQ order, and t_1;

$$\rho_{MQ}(t_1) \propto \sin(q\Delta\omega t_1) \tag{79}$$

This effect is not observed for a-Si:H (at least for τ=100μs). A selective double quantum experiment[232] was also performed to eliminate the possibility of differing MQ orders interfering with each other, and no double quantum coherence was observed for the parameters used. The echo intensity was found to be independent of offset, and decreased monotonically with increasing t_1 for a fixed τ, and similarly with increasing τ for fixed t_1 (this decay is plotted for a simplier sequence in Figures 15 and 16). MQ coherence should be observed in a-Si:H (as for any strongly coupled proton system) for a suitably selected choice of τ, but this value must be carefully chosen to make the MQ coherence refocus with observable intensity. In any event, for the conditions used to produce the data of Figure 9, the echoes are not due to MQ coherence.

D. Hahn Echoes in a-Si:H

The "anomalous" echo after the second pulse in Figure 9 is suggestive of an echo first observed by Hahn in his original paper, "Spin Echoes."[152] The echoes observed by Hahn are easily visualized (see Ref. 152 for Hahn's discussion accompanied by excellent illustrations) in liquids where the dominant T_2 interaction is linear in (proportional to) I_z - in Hahn's case, the static field inhomogeneity.

As previously pointed out, the linewidths in a-Si:H were believed to be dominated by the static Hamiltonian, H_D^{II}. The relative intensity of the echoes in Figure 9, however, is small enough so that it appeared possible that this portion of the proton magnetization might be dominated by an interaction linear in I_z, but not produce enough of an effect on the FID to be observable directly.

As discussed in Section II.B.2, a simplier sequence which refocuses interactions linear in I_z is the "Hahn echo" sequence shown in Figure 1; 90_x-τ-180_y-τ-echo. The time evolution of the Anode sample during this sequence is shown in Figure 10. The main advantage of the Hahn echo sequence compared to the Goldman-Shen sequence is that, neglecting small artifacts in the rf pulse tuning and shape, no MQ coherence using the Hahn echo can be generated into observable magnetization ($\propto T_{\pm 1}^k$). The echo observed in Figure 10 at a time τ after the second pulse, then, provides strong evidence that protons exist in a-Si:H which are dominated by an interaction linear in I_z.

Proof that the echo component is truly intrinsic to a-Si:H, as opposed to being an instrumental artifact or due to extrinsic protons, came from careful attention to the background signals and from carrying out the Hahn echo sequence on differing samples. The background signal intensities were found to be always less than 10% of the echo

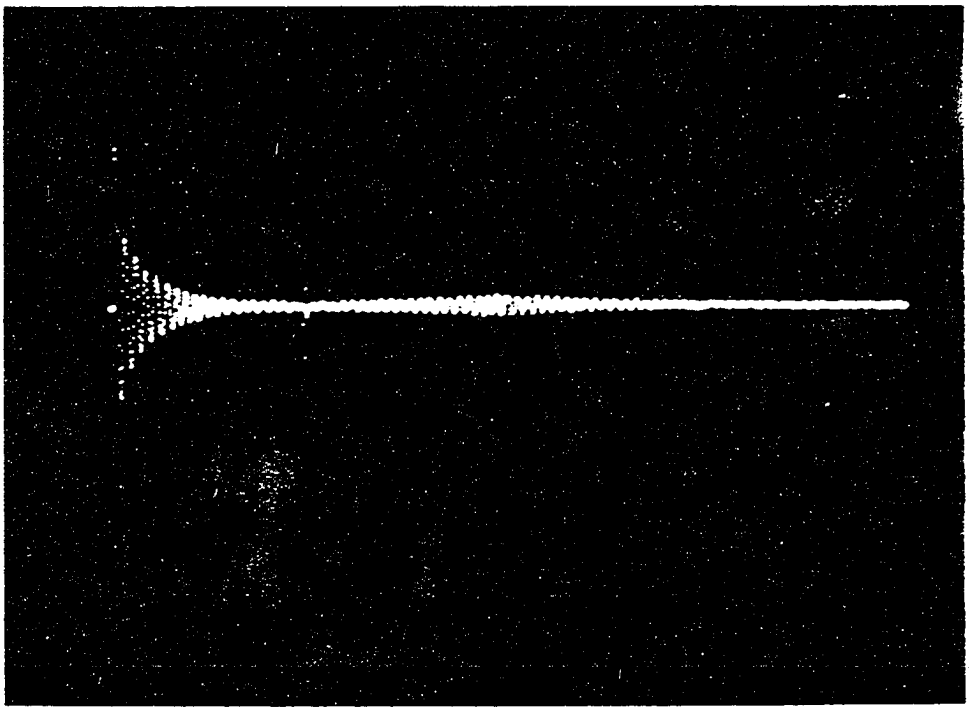

Figure 10. Hahn echo in the time domain. Photographed is the time evolution of the Anode sample during a 90_x-τ-180_y-t sequence; τ=500μs, +40kHz offset, 2 msecs full scan. The initial magnetization decay begins ~ at the bottom edge of the photograph (not observable).

intensity. The Hahn echo was observed in all the a-Si:H samples, but not on other solid samples such as polyethylene, nylon-66 or coals. In addition, the echo component in the a-Si:H's did not change in intensity or shape when the Hahn echo sequence was done on samples open to the atmosphere as compared to the normal dried (at 150°C overnight in a $<10^{-5}$ torr grease-free vac-line) and sealed (under ~10 torr He) samples.

1. Interaction dependence

A set of experiments was performed in an attempt to define what interaction(s) was dominating the echo component's T_2; i.e., to find what interaction is being refocused by the Hahn echo sequence. Hamiltonians which are linear in I_z are listed in Table 5, with the dependence of these Hamiltonians to a change in the static field strength, B_0, pointed out.

The B_0 inhomogeneity can be discounted immediately, since the measured (with various liquid standards) inhomogeneity for times up to 24 hours were < 0.5ppm on the 5.2T magnet, and < 2ppm on the 1.3T magnet. These broadenings are much too small to explain the echo component's T_2. Knight shifts can also be discounted since the echo component resonates very close to water, and a Knight shifted proton would be

Table 5. Hamiltonians linear in I_z

Hamiltonian	Field dependence	Spin operator
H_{cs}, chemical shift	linear	$\vec{I}_z.\overleftrightarrow{\sigma}.\vec{B}_o$
$H_{\varepsilon i}$, B_o inhomogeneity	variable	$\varepsilon_i I_{zi} B_o$
H_c, magnetic susceptibility	linear	$\chi_i I_{zi} B_o$
H_D^{IS}, heteronuclear dipole-dipole[a]	none	$A_{ij} I_{zi} S_{zj}$
H_K, Knight shift	linear	$\vec{I}_z.\overleftrightarrow{K}.\vec{B}_o$

[a] S_{zj} must be static for this interaction to refocus.

expected to have a large downfield shift (although this is not always the case).

To differentiate between the heteronuclear dipole-dipole interaction and the other interactions listed in Table 5, Hahn echoes were taken at both 5.2T (220MHz) and at 1.3T (56MHz). The data were taken off-resonance (10-20 kHz; the second pulse was timed to occur when the magnetization vector aligned with the y-axis, although any 180^o transverse pulse will give a Hahn echo), with a trigger starting the data accumulation at the top of the echo peak in the time domain. The FT of the resulting FID gave spectra such as shown in Figure 11. The spectra have reproducible asymmetry, as shown in Figure 11, but this asymmetry varies from sample to

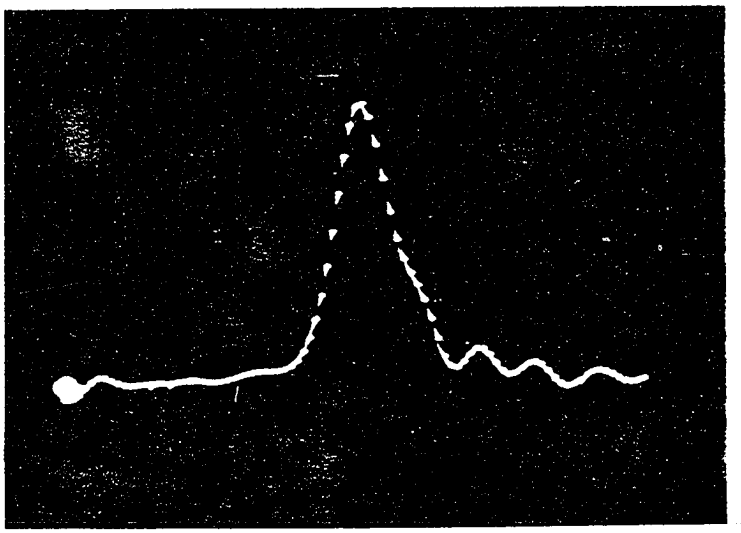

Figure 11. Fourier transform of the Hahn echo. Photographed is an 8K Fourier transform of the time evolution data displayed in Figure 10. The digital resolution is 122 Hz/pt, and upfield is to the right. $\sigma_{\perp} \sim 4.5$ppm, $\sigma_{||} \sim 0.5$ppm relative to TMS.

sample. The approximate linewidths are listed in Table 6 for both the 1.3T and 5.2T field strengths.

The main features of Table 6 are the approximately linear relation of the echo linewidth with the field strength, and the broader linewidths seen in the better samples. Heteronuclear dipole-dipole interactions thus do not appear to be the dominant interaction of the echo component. Although ^{29}Si has a relative abundance of ~5%, which might be associated with the 5% relative intensity of the echo component, there is no clear explanation as to how the proton homonuclear dipolar interaction could become small enough to allow the ^{1}H-^{29}Si interaction to be dominant. The echo component's T_2 must then be dominated by the chemical shift interaction or possibly by magnetic susceptibility effects.

Table 6. Linewidths of Hahn echoes at 1.3T and 5.2T field stengths

Sample	FWHM(ppm) at 1.3T	FWHM(ppm) at 5.2T
Anode	8.5±1.5	7±1
Cathode	7	7±2
VAN150	30±4	18±3
SHK#7	14±2	14±2
C70	-	14±2

A discussion of the slight broadening both by going to better samples and by decreasing the field strength, is deferred until Section IV.E.1.b.

It was originally assumed that motion must be averaging the homonuclear dipole-dipole interaction of the protons giving rise to the echo component. The linewidths, however, do not change down to 77K. This eliminates the possibility that mobile SiH_2, SiH_3 or SiH_4 comprise part of the echo component. These motionally averaged bonding species are observed in inorganic thin films,[159] and in a-Si:H:F,[194-198] but their linewidths have a temperature dependence above 77K. It will be shown that part of the echo is in fact motionally averaged (the m-H_2), whereas most is not (the isolated protons).

2. Three component fits

Also assumed early on was that the echo component was as a whole a single third species in a different environment than the monohydride or void protons. This new species should then be fit using PEAK15 to the FT of the FID's along with the broad Gaussian and a narrower line shape (either Gaussian or Lorentzian, determined, if possible, by the quality of the corresponding three component fits). Such a three component fit, with the broadest line a Gaussian shape, the other two Lorentzians, is shown in Figure 12 for the

Figure 12. Two and three peak fits of an Anode FTFID

a) Three peak fit of an Anode FTFID. The fit was generated using PEAK15 - the crosses are the raw data taken at 220 MHz. The data was fit by forcing one peak (1) to have a % area and FWHM corresponding to that observed in the Hahn echo. The other two peaks were allowed to vary. The results of this procedure gave as a best fit:

Peak	Type	% area	FHWM
1	Lorentzian	5.6	6. ppm
2	Lorentzian	33.2	4.8 kHz
3	Gaussian	61.2	30. kHz

b) Two peak fit of the same Anode FTFID. The fit is similar to a), but without the narrowest peak (1 above). All the parameters were allowed to vary. The results of this procedure gave as a best fit:

Peak	Type	% area	FWHM
1	Lorentzian	32.	3.4 kHz
2	Gaussian	68.	30. kHz

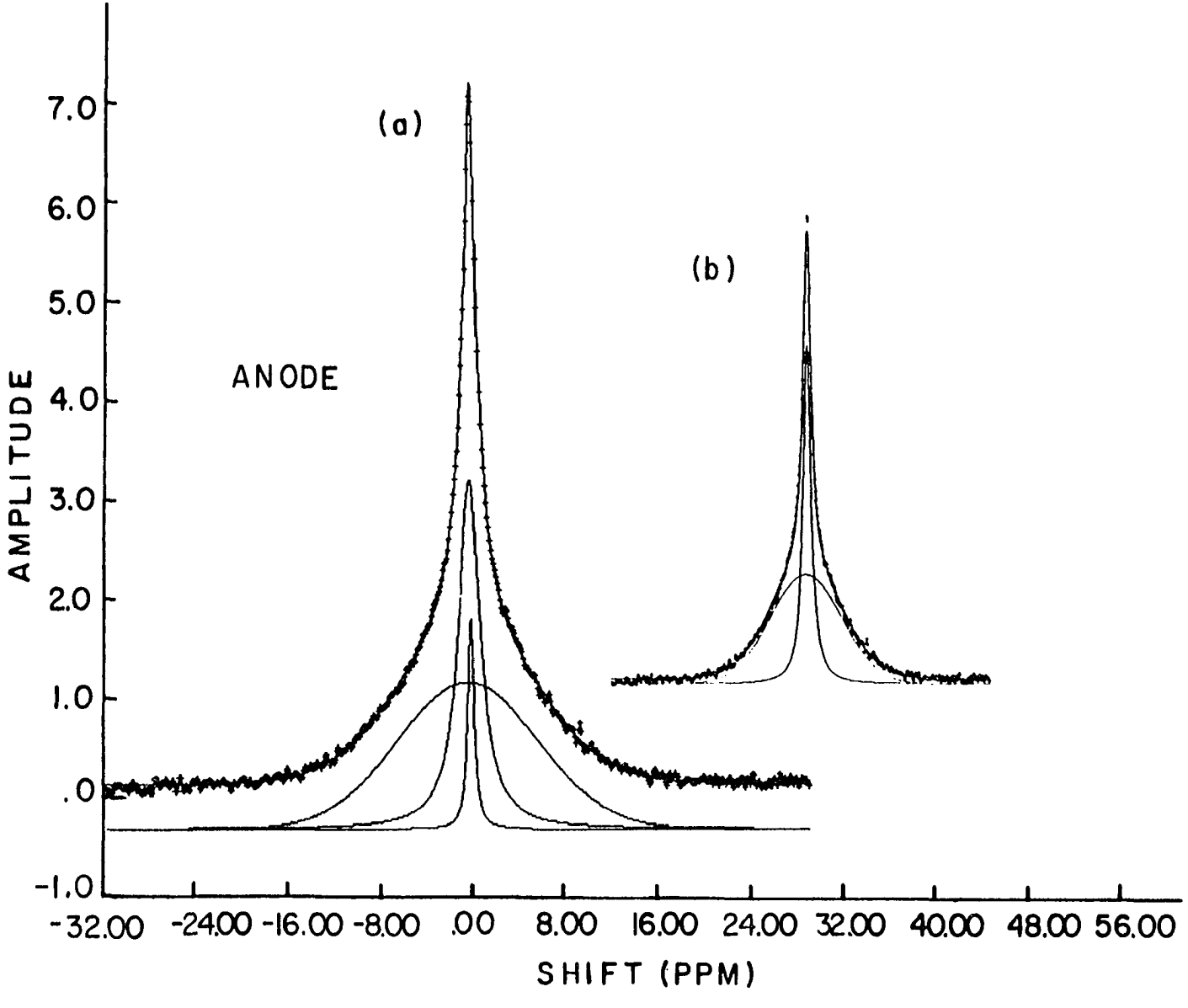
(a)
(b)
ANODE
AMPLITUDE
7.0
6.0
5.0
4.0
3.0
2.0
1.0
.0
-1.0
-32.00
-24.00
-16.00
-8.00
.00
8.00
16.00
24.00
32.00
40.00
48.00
56.00
SHIFT (PPM)

Anode sample. Inset in Figure 12 is the two component (broad Gaussian, narrower Lorentzian) fit, which was used to give the results in Table 2.

The three component fit in Figure 12 was generated by forcing PEAK15 to give a width of ~7ppm and an area ~5% for the peak that represents the echo component of the Anode sample (quantitative information about the echo component is deferred until the next section; see Table 7). The parameters for fitting the other two components were allowed to vary. As can be seen in Figure 12, the three component fit actually simulates the data, especially at the peak, better than the two component fit shown in the inset. Similar results - excellent fits using three components - were observed for SHK#7 and VAN150.

The three component fit to the FT of the FID of the Cathode sample, however, cannot be made to simulate the data within the experimental precision. An example of one attempt to fit the data is shown in Figure 13. The fitted line is too narrow at the peak to match the data when the echo component linewidth is set to ~7ppm and the area to 5%. Attempts to improve the fit using asymmetric line shapes, or four or five components all ended with the same conclusion; the Cathode data can not be fit using a third component resembling the echo line shape unless the echo line shape area is reduced to < 2%. Needless to say, this result caused

Figure 13. Three peak fit of a Cathode FTFID. The fit was generated using PEAK15 - the crosses are the raw data taken at 220 MHz. The fitting procedure was initially identical to that described for Figure 12 a). The % area of Peak 1 in this fit, however, was decreased in an attempt to obtaining a better fit. The results were:

Peak	Type	% area	FWHM
1	Lorentzian	2.8	7.8 ppm
2	Lorentzian	30.	6.0 kHz
3	Gaussian	67.2	27. kHz

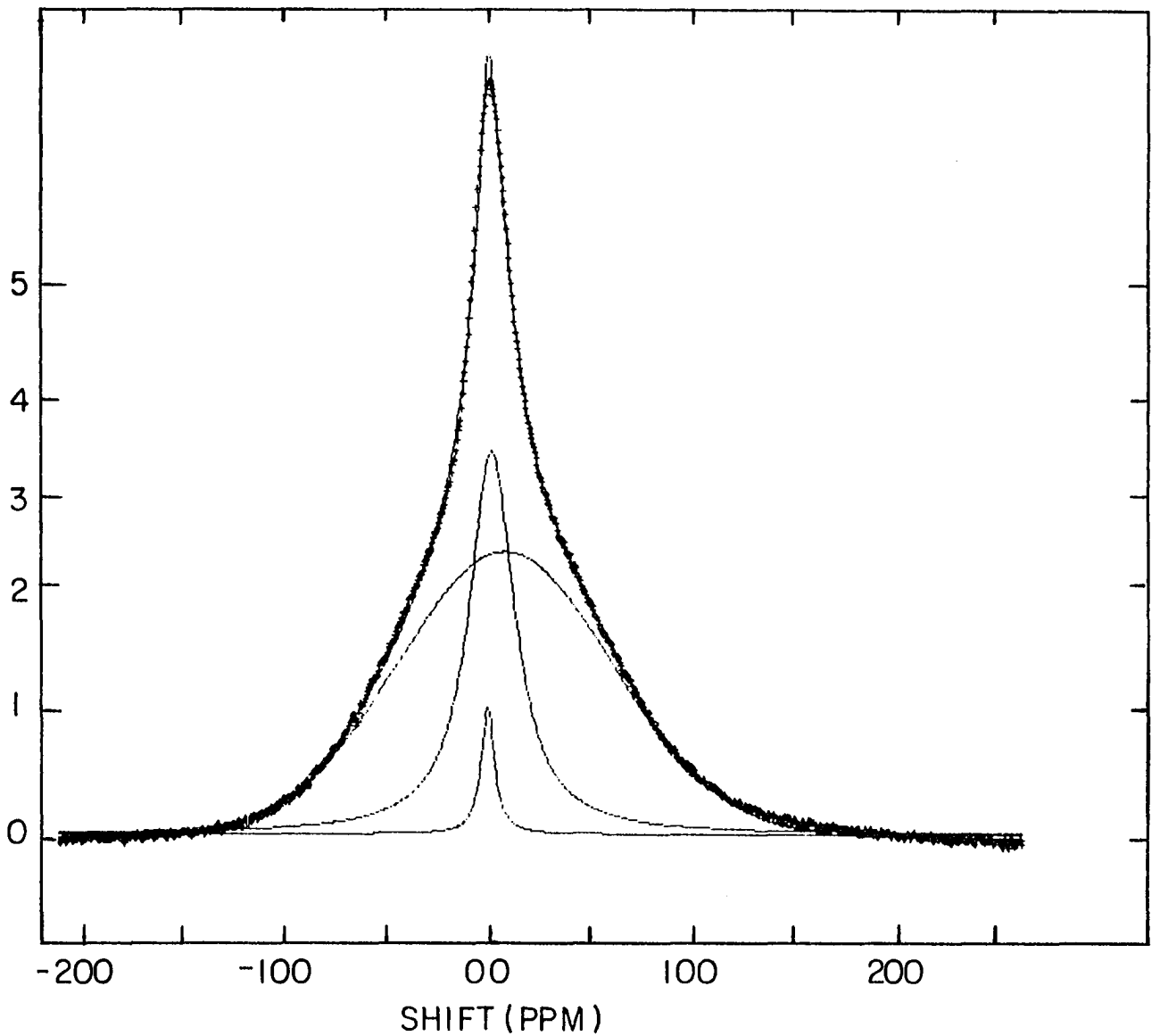
5
4
3
2
1
0
-200
-100
00
100
200
SHIFT (PPM)

considerable consternation, and provided motivation for the next experiment.

E. Nuclear Relaxation of Hydrogen in a-Si:H

1. The CPMG experiment

A natural extension of the Hahn echo sequence is the Carr-Purcell-Meiboom-Gill sequence, as discussed in Section II.B.2. This experiment re-echoes the linear I_z interaction, leaving only homogeneous line broadenings as interactions which damp the echo intensity. These homogeneous interactions are either bilinear in $\vec{I}$ - the homonuclear dipolar and J-coupling interactions, or lifetime broadening - or a heteronuclear interaction where S_z is time dependent (over the time scale of the experiment). The time evolution of the proton magnetization in VAN150 at 220 MHz during a CPMG experiment (2τ = 600μs) is shown in Figure 14.

a. Spin counting The CPMG sequence was originally performed in order to obtain a more accurate estimate of the percentage of protons which echo (especially important, in view of the foregoing discussion). By taking the plot of the echo peak intensities versus the echo times, and extrapolating these intensities back to zero time, a number proportional to the total number of protons echoing, M_0^{echo}, is obtained. Such a plot is shown in Figure 15. Of

Figure 14. CPMG echoes; raw data. Photographed is the time evolution of the VAN150 sample during a 90_x-τ-$(180_y$-2τ-$)_n$ sequence; 2τ=600us, 20 msecs full scans. The FID following the 90_x pulse can be seen decaying from above the top of the photograph.

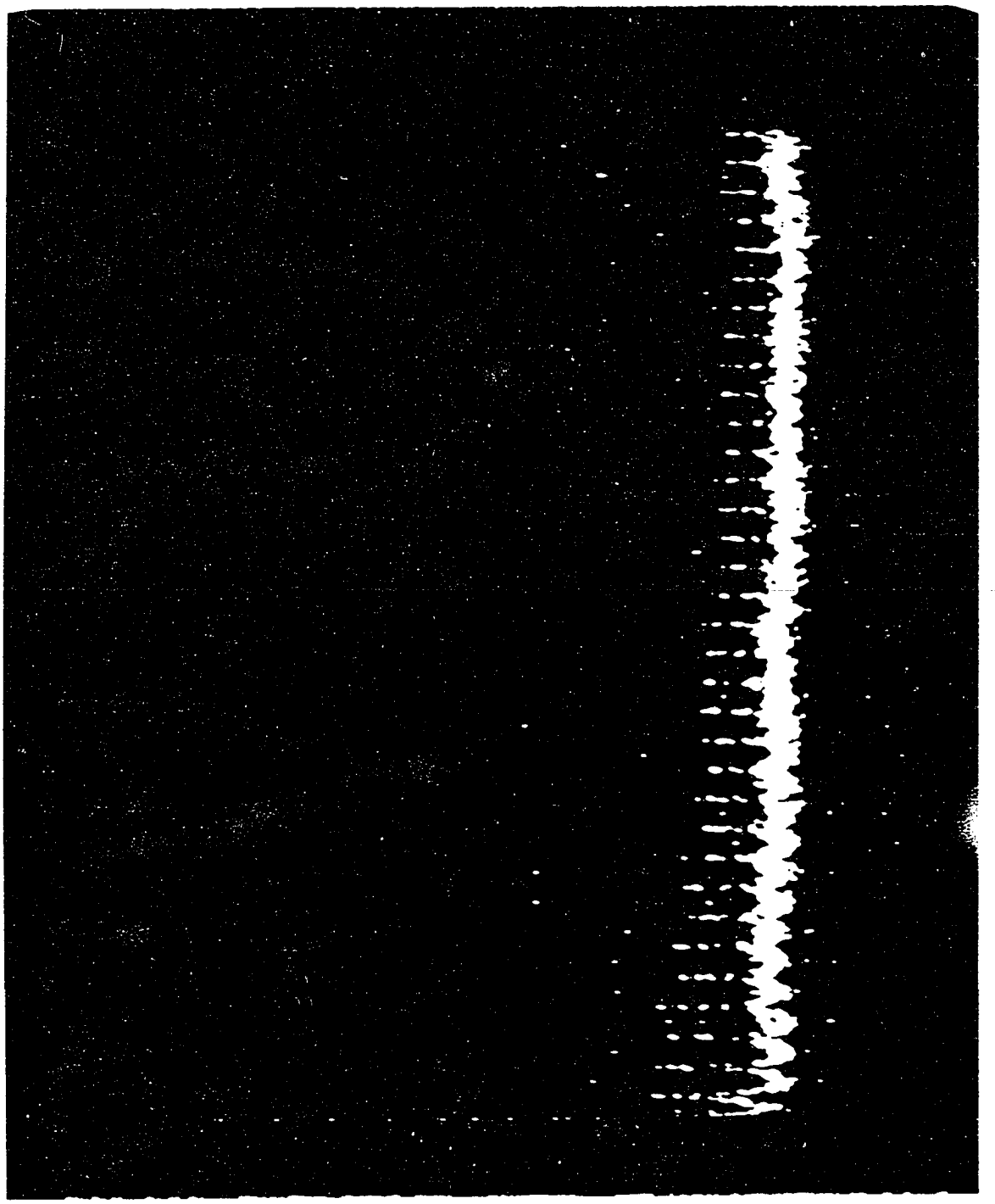

particular interest in this plot is the existence of two identifiable decay rates. The total number of protons, M_0^{total}, is proportional to the extrapolation of the FID (using TCDA) after the initial 90^o pulse back to time zero. Obviously, the % H^{echo} is the ratio of the two initial intensities, $100M_0^{echo}/M_0^{total}$.

Similar plots resulted in the data listed in Table 7. All the data are given for a field strength of 5.2T since the signal-to-noise ratio was much better at this field. There are two major contributions to the error limits given in Table 7. The first is the signal-to-noise ratio in the echo peaks, which is a serious problem because of low sensitivity (low in order to not clip the FID after the initial 90_x pulse), and the long T_1's (see Section IV.E.2). The second contribution to the error comes from the ability of TCDA to extrapolate M_0^{total} back to time zero (the digital resolution was poor for this fit since the time/point was long in order to give enough echoes for an accurate plot).

b. Spin-spin relaxation The two decay rates observed during the CPMG experiment are also given in Table 7. These decay times, however, are best measured using "stroboscopic" observation of the echo amplitudes. This method of taking data during a multiple pulse experiment, and for the CPMG experiment specifically, was described in detail in

Figure 15. Plot of the CPMG echo amplitudes versus echo times for VAN150. M_0^{total} is obtained by extrapolating the FID following the initial 90_x pulse back to t=0. M_0^{echo} is obtained by computer fitting the sum of two exponentials to the echo data, and extrapolating back to t=0. Lines drawn through the points are shown for visualization only. The ratio M_f:M_s refers to the ratio of intensities of the fast to the slow decaying components.

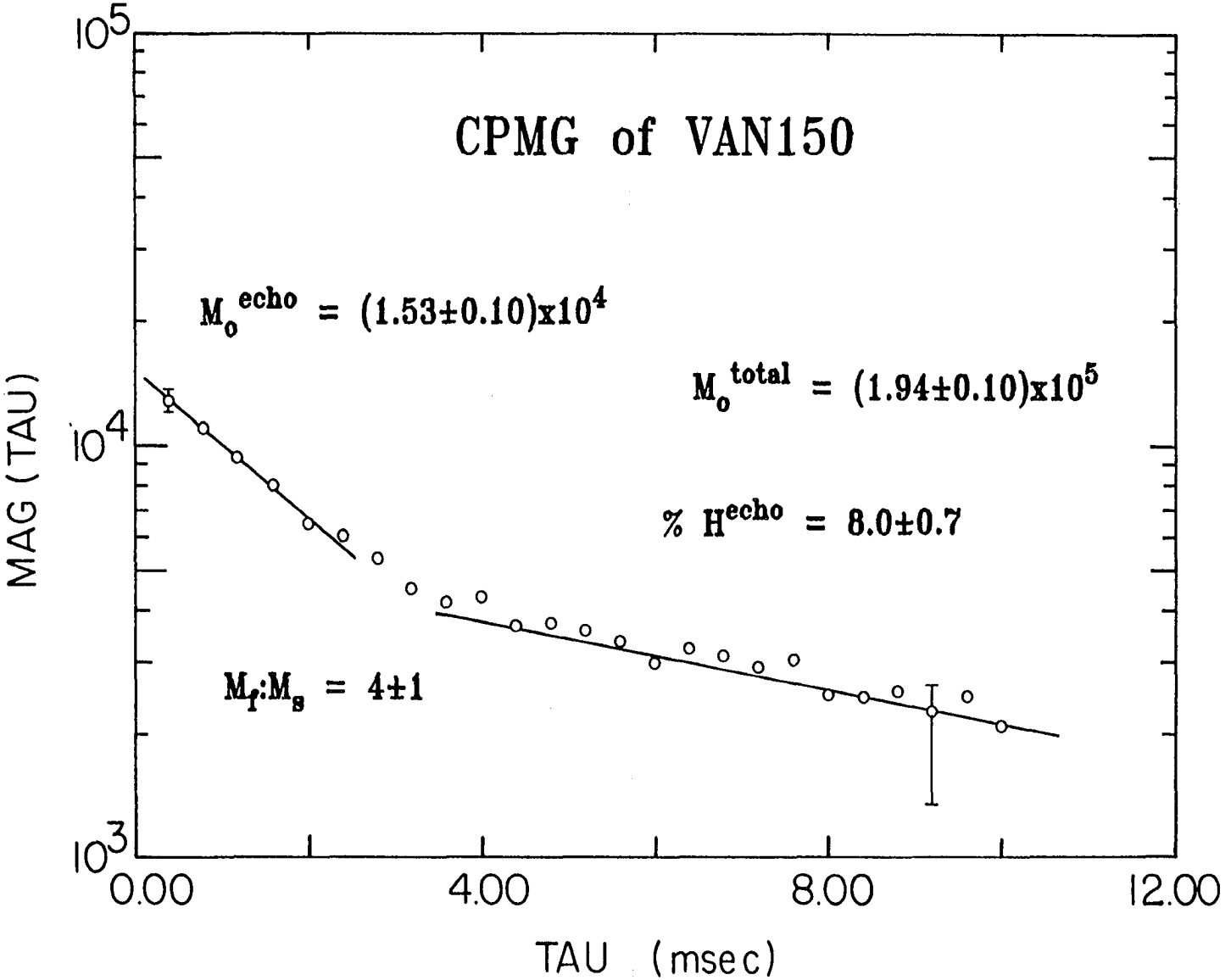
CPMG of VAN150
$M_o^{echo} = (1.53\pm0.10)x10^4$
$M_o^{total} = (1.94\pm0.10)x10^5$
% $H^{echo} = 8.0\pm0.7$
$M_l:M_s = 4\pm1$
MAG (TAU)
10^5
10^4
10^3
0.00
4.00
8.00
12.00
TAU (msec)

Section III.B.1. The advantages of the stroboscopic observation over the "normal" observation are three-fold. First, the stroboscopic experiment permits much more data to be obtained, since each point in the stroboscopic experiment represents an echo peak. Equally important, the analog signal is integrated for ~8μs for each point in the stroboscopic experiment, as compared to the ~130ns per point for the Biomation. Not only are more data points obtained during stroboscopic observation, but more signal is gathered

Table 7. Quantitative determination of the relative intensity of the echo component @ 5.2T

Sample	% H^{echo}	$M_f:M_s$	at $\%M_f$ [a]	T_2^f (msec)	at $\%M_s$ [a]	T_2^s (msec)
Anode	9±2	80:20[b]	1.5	1.0±.4	0.36	30
Cathode	9	85:15	2.2	0.7	0.39	15
SHK#7	10	75:25	1.2	2.5	0.40	14
C45	11	>87:13	0.56	4.5±2	<0.08	55
VAN150	8	80:20	0.96	1.8	0.24	30
VAN400	12.5	75:25	1.2	3.3	0.42	75
VAN500	20	65:35	1.1	5.5	0.59	70
VAN550	66±8	80:20	0.69	2	0.21	35±15

[a] These values were found using the at %H in Table 3.
[b] The relative error is 20%.

in each 8 us data window. Last, since quantitative information is not needed in this experiment (it is obtained from the non-stroboscopic experiment), the sensitivity can be increased until the echo intensity fills the digitizer. An example of stroboscopic observation during a CPMG experiment is given in Figure 16. These data are quite typical of all the stroboscopic data taken using the CPMG sequence.

The relatively large error limits given in Table 7 for the T_2's are due to two related factors. First, the values T_2^s were dependent on the time frame over which the fit was taken. T_2^s in Figure 16 was found to be 70 msecs when the fit covered the full 4 msec range of data, but decreased to 50 msecs when the fit was taken over just the first 2 msecs of data. This decrease is due in part to the truncation of the baseline. This effect is analogous to a loss of resolution occurring from a taper or truncation in the time domain, and seen in the Fourier transform of the FID (FTFID).

More importantly, the errors in the T_2's may result from the important assumption (derived from the best fit from Lorenztian-Guassian combinations) that both line shapes are simple exponentials. The assumption of only two decay rates is not only always justified, but also essential, unless evidence exists that implies more than two species are giving rise to the line shape. The assumption of exponential line

Figure 16. CPMG echoes; stroboscopic observation for VAN500. The raw data (crosses) were obtained using the sequence described in Section III.B.1 (see Figure 5 and the surrounding discussion); D1=48.8μs, D2=46.7μs, D3=53.3μs to give 200μs/pt over 2048 points. The data were then fit using TCDA to two Lorentzian decays, with the results listed in Table 7.

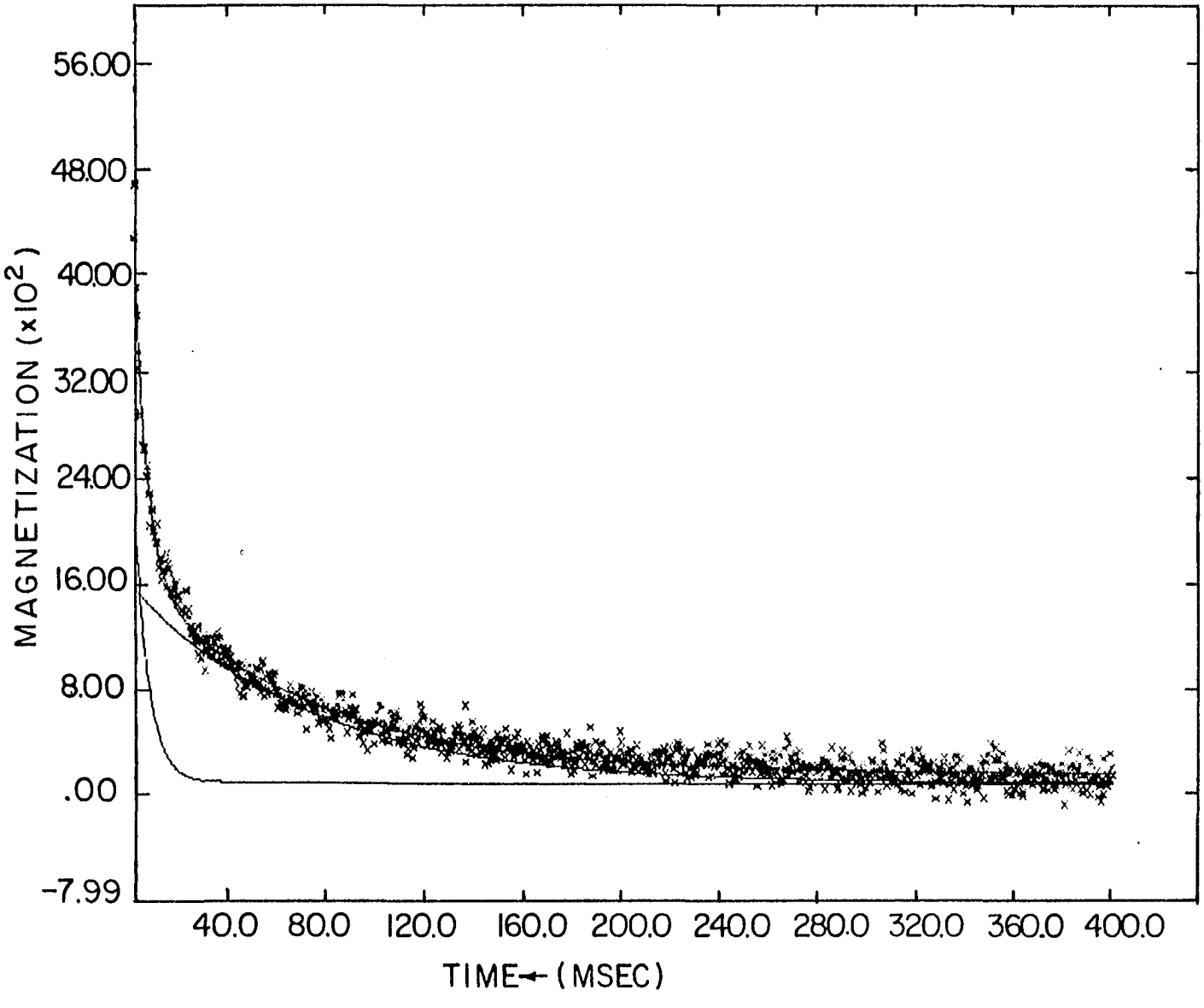
56.00
48.00
40.00
32.00
24.00
16.00
8.00
.00
-7.99
MAGNETIZATION (x10²)
40.0
80.0
120.0
160.0
200.0
240.0
280.0
320.0
360.0
400.0
TIME→ (MSEC)

shapes will be discussed more in the next sections, but it is important to point out here that all the data show systematic errors in the fitting similar to that seen in Figure 16: the fit falls just below, and then just above the data in the region where the fast decaying component is approaching zero amplitude. In reality, a distribution of relaxation times for two species or environments of protons in a-Si:H during a CPMG experiment is expected (see the discussion in Sections IV.F and IV.G), and a systematic fitting procedure was therefore used to provide values of T_2^s and T_2^f which have relative significance.

As already discussed in Section II.B.2, T_2 values determined using a CPMG sequence have errors associated with the experiment itself which may cause the longest T_2 to be only a lower limit value (i.e., T_2^s may be determined by experimental artifacts).

Finally, the relative intensities of the two components are greatly dependent on the type of line shape chosen for the fit. Gaussian line shapes significantly decrease the accuracy of the two component fits, such as that in Figure 16. But the long decaying component's relative intensity, at $\%M_s$ listed in Table 7, is most likely a lower limit. And, in fact, evidence will be presented in the next section supporting this idea.

2. Sample-wide and Hahn echo spin-lattice relaxation

Spin-lattice relaxation measurements were undertaken to help identify the echoing species. Initial measurements of the overall, or sample-wide spin-lattice relaxation time, T_1^{SW}, were also taken, and proved to be quite useful.

The experimental sequence used to measure spin-lattice relaxation rates is shown in Figure 17. Most of the rates reported here were measured using the repetition-rate method,[144] but some were measured using the inversion-recovery method. No differences within the experimental errors were observed between the two methods. The rep-rate method was used mainly because it allowed for faster determinations of the T_1's. Infinite time points were taken every other measurement, in order to obtain accurate T_1's.

A plot to determine T_1^{SW} of VAN150 is shown in Figure 18. Early in this study, the long time tailing of the magnetization decay was not observed. But after obtaining the data for T_1^{CS} on VAN150, as shown in Figure 19, and observing the two component decay in T_1^{CS}, one being ~20 secs, T_1^{SW} was carefully remeasured.

The results of these measurements are listed in Table 8. Note the absence of a single exponential T_1^{SW} for any of the samples. The Anode, Cathode and VAN150 data were close to single exponential, but carefully taken data showed clearly the nonexponentiality. In addition, the echo component has ~

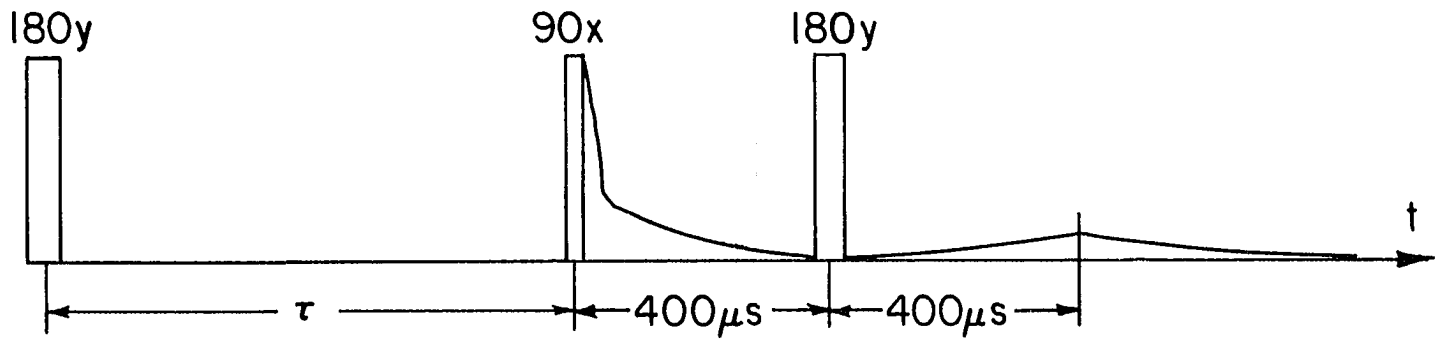

Figure 17. Pulse sequence for measuring T_1. This figure depicts all the sequences used in the present work for measuring T_1's.
a) The inversion-recovery method of measuring T_1^{SW} is done using the first 180_y, followed by the 90_x. The initial magnetization following the 90_x as a function of τ gives T_1^{SW}. During the same experiment, the echo amplitude as a function of τ gives the echo components' T_1^{CS}.
b) The repetition-rate method of measuring T_1's is performed similarly to the inversion-recovery method, but without the first 180_y pulse, and with τ being the time between consecutive experiments.

Figure 18. T_1^{SW} plot for VAN150. Using the repetition-rate method, the data at 220 MHz were adequately fit using two decay rates, T_{1f}^{SW} = 2.6 sec and T_{1s}^{SW} = 20. sec.

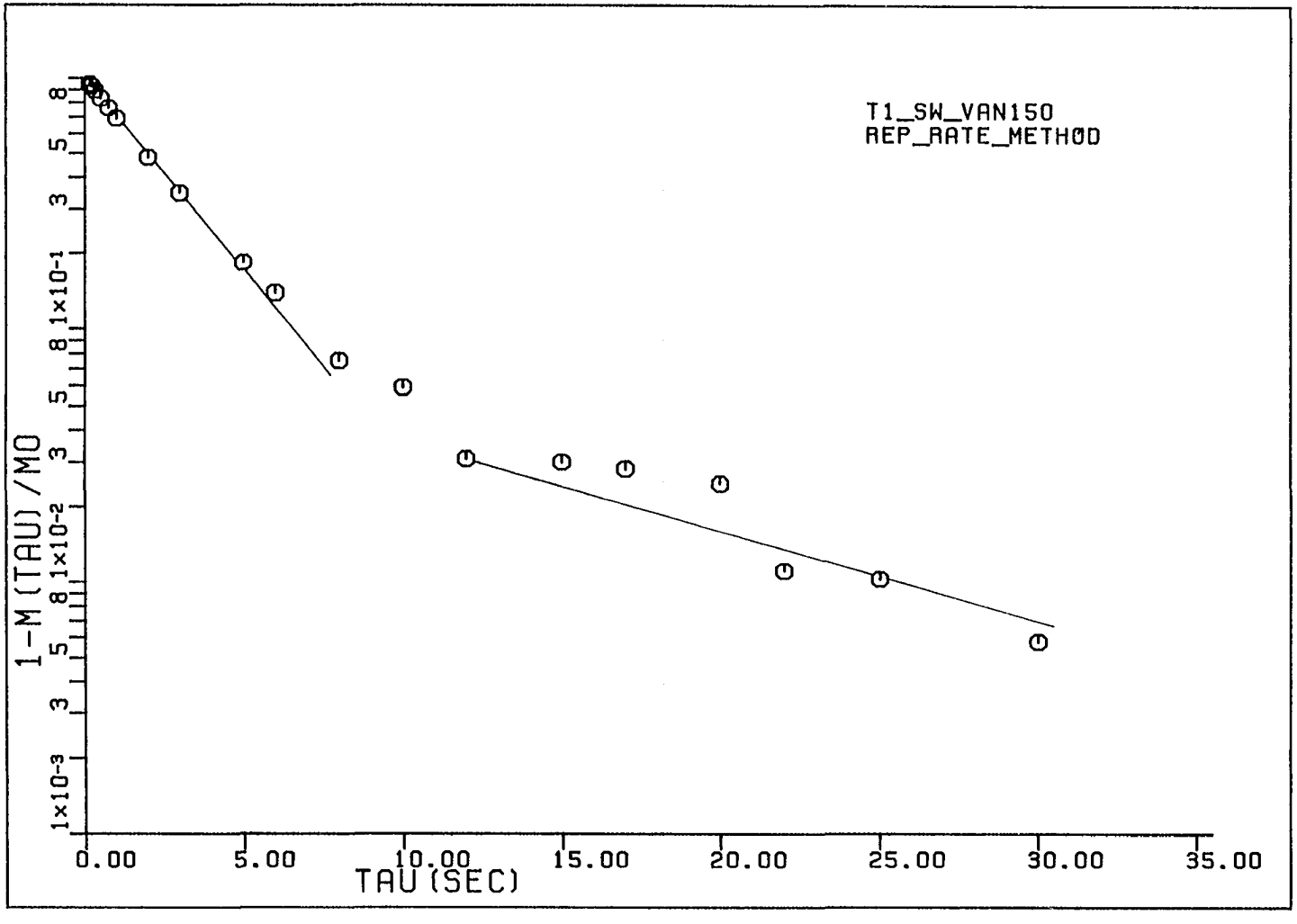
T1_SW_VAN150
REP_RATE_METHOD
1-M(TAU)/M0
1x10-3
3
5
8
1x10-2
3
5
8
1x10-1
3
5
8
0.00
5.00
10.00
15.00
20.00
25.00
30.00
35.00
TAU(SEC)

Figure 19. T_1^{cs} plot for VAN150. Using the modified repetition-rate method, the data at 220 MHz were adequately fit using two decay rates, T_{1s}^{cs} = 20±2 sec, T_{1f}^{cs} = 1.4 sec.

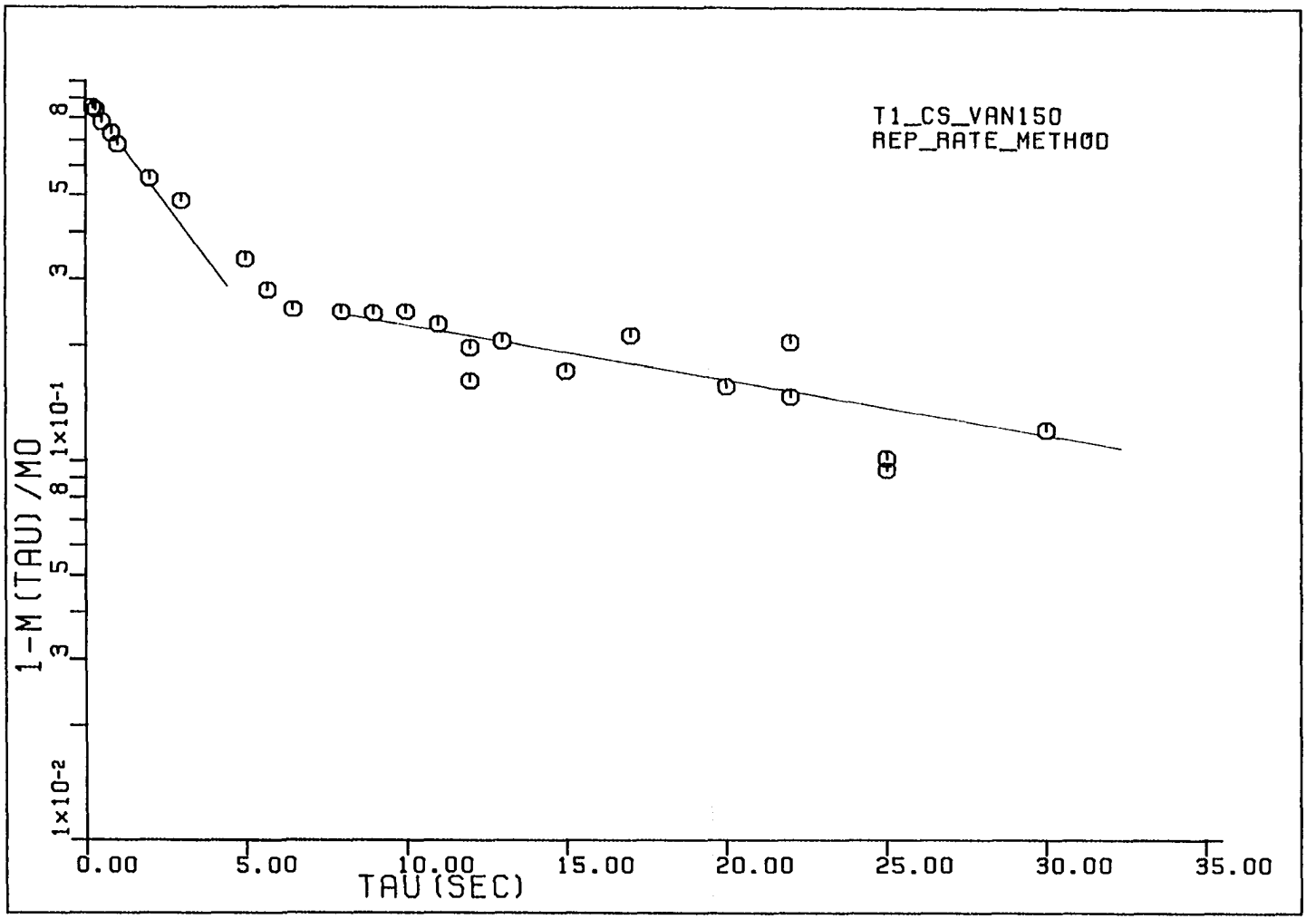
T1_CS_VAN150
REP_RATE_METHOD
1-M(TAU)/M0
8
5
3
1x10-1
8
5
3
1x10-2
0.00
5.00
10.00
15.00
20.00
25.00
30.00
35.00
TAU(SEC)

Table 8. Sample-wide and Hahn echo spin-lattice relaxation times in a-Si:H at room temperature

Sample	B_0 (MHz)	T_1^{sw} (secs)	$M_f:M_s$ (sw)	T_1^{cs} (secs)	$M_f:M_s$ (cs)
Anode	56	4.1±.1	100:0		
	220	5.5±.2[a]	100:0		
	220	1.2,6.1	12:88		
	220			~0.3[abcd]	
	220			~.45[abde]	
Cathode	56	5.4±.2	100:0		
	220	10.6±.3[a]	100:0		
	220	1.4,11	8:92		
	220	6.4±.1[bd]	100:0		
	56			0.3,1.8	20:80
	220			0.3,8	40:60
	220			8[adf]	
C70	220	44±3[a]	100:0		
SHK#7	220	2.2,14,40[g]	37:58:5		
	220			1.8,30	30:70
VAN150	220	2.6,20.	95:5		
	220			1.4,20	50:50

[a] Data are nonexponential, values given are approximate.
[b] Inversion-recovery method used.
[c] Fast component only.
[d] Temperature = -90°C.
[e] Temperature = -150°C.
[f] Not enough points to determine the fast T_1^{cs}.
[g] Data cannot be fit to two exponential decays, values are approximate.

two relaxation times, usually different by more than an order of magnitude. Another important point, not readily seen from Table 8, is that the fast T_1^{cs} increases slightly when going to lower temperatures (>120K).

F. Monohydride Distributions in a-Si:H

The data on VAN150 given in Tables 7 and 8 provoked the following interpretation. Note that the long T_1^{sw} component in all the data is very close to the long T_1^{cs} value. Fast repetition of the CPMG experiment (not a routine experiment because of the high power requirements) confirmed that the long T_1^{sw}-T_1^{cs} component gives rise to the fast T_2^f in the CPMG experiment. In addition, the density of protons having the long T_1^{sw} equals the density of protons determined to echo with T_2^f in the CPMG experiment (the most accurate determination of this result is for VAN150, where the % protons having T_1^{sw}~20s equals 5±2 and the % protons having T_2^f~1.8ms equals 6.4±2).

1. Reinterpretation of line shapes in the FID

The above observations led to the following important conjecture: the long T_1^{sw}-T_1^{cs}, fast T_2^f component is due to "isolated" monohydrides which are the large separation tail of the random distribution of monohydrides which comprise the Lorentzian line shape in the a-Si:H sample.

There are three reasons for this interpretation. First, as previously discussed in Section II.C.1, the narrow Lorentzian line is thought to arise from a random distribution of monohydrides within the bulk regions of the a-Si:H film.[26,155] Consider Reimer et al.'s values of 7.7A as the average internuclear spacing, with a standard deviation of 1.7A for the monohydride distribution.[155] At 220 MHz, a proton having a chemical shift anisotropy of 20ppm, and also being >6A from its nearest-neighbor protons experiences $H_{cs} > H_{dip}$. In this case, the proton will echo under a Hahn echo sequence. There is, therefore, a strong probability that at 220 MHz many of the monohydrides in the Lorentzian line will echo under a Hahn echo sequence.

The fact that the echoing protons in this case give rise to part of the Lorentzian line shape in a FID is crucial. Now, the Cathode FTFID shown in Figure 13 does not need to be fit with such a large echo peak area. Most of the echoing component, 85% for the Cathode sample (see Table 7), gives rise to the Lorentzian peak normally fit to FTFID's. The FTFID of the Cathode sample can easily be fit with three components where the narrowest Lorentzian peak has % area = 1.5, and the problem of the Cathode FTFID is thus resolved.

This conclusion lends support to the conjecture stated previously: the narrow line occurs from randomly distributed monohydride species throughout the sample.[26,155] This

conjecture was made in part to justify the Lorentzian line shape of the narrow line. Thus, the component T_2^f during the CPMG experiment is a natural part of the narrow line.

Moreover, I will show in Section IV.H that the long T_1^{sw} for the "isolated" monohydrides is easily explained, and, in fact, the "isolation" is in complete agreement with the value of T_2^f observed under the CPMG experiment.

2. The standard deviation of the monohydride distributions

The data derived from FTFID's and the CPMG experiments provide enough information to model the monohydride distribution without resorting to space-filling arguments.[155] Consider the following simplistic model. Assume the distribution of monohydrides giving rise to the (two-peak fit) Lorenztian line shape is completely random. This distribution of internuclear spacings is shown in Figure 20.

In order to estimate the spread, or standard deviation σ, in the random distribution, the following steps are taken. The average internuclear spacing for all the monohydrides is known from the FID, $r_L = \eta^{-1/3} = [7.6\gamma^2\hbar/FWHM]^{-1/3}$. The $FWHM_L$ is listed in Table 3. Next, r_i is defined as the smallest internuclear spacing at which the monohydride becomes "isolated", i.e., the spacing at which the monohydride will echo during a Hahn echo sequence (a more

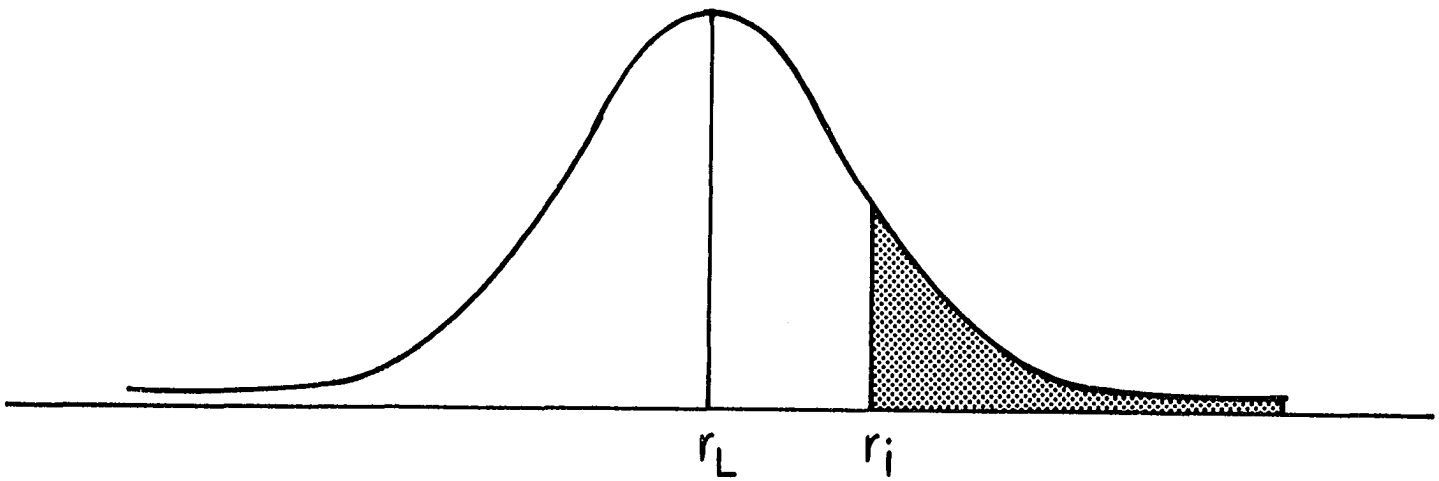

Figure 20. Random distribution of internuclear spacings. The probability distribution curve is shown with increasing internuclear separation, r, going toward the right. r_L is the average internuclear separation, and is found using Equation (45) with $r_L = \eta^{-1/3}$. r_i is the smallest internuclear separation at which a proton will echo during a CPMG experiment.

precise definition of "isolated" will be given in Section IV.H). The isolated monohydrides thus fall in the shaded region in Figure 20. r_i cannot yet be determined, but two other pieces of information derived from the CPMG experiment will give r_i. First, the average internuclear spacing of the isolated monohydrides, $\langle r \rangle_{iso}$, is obtained from T_2^f of the CPMG experiment. This T_2 is due only to the proton dipole-dipole interaction experienced at the isolated monohydrides, and the approximation can be made, using Equation (44):

$$\langle r \rangle_{iso}^6 \sim 5.1\ \gamma^2 \hbar^2 I(I+1)/M_2 \qquad (80)$$

Second, the fraction of monohydrides in the Lorentzian line which echo is known from the M_L fraction (in Table 3; corrected, if necessary for the amount of slow decaying protons in the CPMG), and the fraction, M_f^e, the T_2^f component comprises in the CPMG decay (in Table 7). The fraction, M_{iso}, of the curve in Figure 20 which is shaded equals M_f^e/M_L. M_{iso} is also equal to

$$M_{iso} = \frac{1}{\sqrt{2\pi}\,\sigma} \int_{r_i}^{\infty} \exp[-(r-r_L)^2/\ 2\sigma^2]\ dr \qquad (81)$$

Now it can be seen that

$$\langle r \rangle_{iso} = \frac{1}{\sqrt{2\pi}\,\sigma} \{\int_{r_i}^{\infty} r\ \exp[-(r-r_L)^2/\ 2\sigma^2]\ dr\}/M_{iso} \qquad (82)$$

Solving equation (82) for σ gives

$$\sigma = \sqrt{2\pi}\, \exp[-(r_i - r_L)^2 / 2\sigma^2]\, (\langle r\rangle_{iso} - r_L)\, M_{iso} \qquad (83)$$

r_i is easily determined from standard tables of normal distributions once M_{iso} is determined.

Table 9 gives all the values necessary to determine σ. The most important result of Table 9 is the small values of σ for the Anode and Cathode samples. These are samples with relatively high hydrogen content, and deposited with poor growth conditions (see Table 2). It appears that as the film grows, there is a variation in the amount of hydrogen available to the sample in the case of the Anode and Cathode. At one moment on the surface, a large number of hydrogens bond, and at another time much less. In fact, a better description would be to say that there is not enough thermal or rf energy in the system to adequately "scour"[155] the surface free of excess hydrogen. The surface then incorporates bundles of hydrogen at intervals. This gives rise to the small σ determined for the Anode and Cathode samples shown in Table 9. On the other hand, the films grown with the proper growth parameters incorporate hydrogen in a smooth fashion, with excess hydrogen continually being scoured off the surface. In this case, the monohydride distribution depends on the presumably random occurrence of dangling bonds at the surface, and leads to the larger

Table 9. Determination of σ for a random distribution of monohydrides. e stands for echo component. All distances given are in A

Sample	at%H	M_L	$\%M^e$	$M_f^e:M_s^e$	r_L	$\langle r \rangle_{iso}$	σ
Anode	20±1	.32	9.1±1	80:20	7.8	11.4	3.3
Cathode	28	.29	9.2	85:15	6.3	10.1	3.1
SHK#7	16	.30	10.	75:25	6.9	15.5	6.8
VAN150	15	.44	8.0	80:20	6.2	13.9	4.9
VAN400	13.3	.45	12.5	75:25	6.8	17.0	7.4
VAN500	8.4	.67	19.	65:35	7.5	20.0	8.7
VAN550	1.3	1.0	66±8	100:0	9.6	14.0	8.5
C45	5.9	.41	11.	>87:13	6.7	18.5	5.6

spread in the internuclear spacings, and thus in σ. This methodology of measuring the monohydride distribution in a-Si:H should prove helpful in studying the dynamics of a-Si:H film growth.

An identifying feature of the isolated monohydrides is their dependence on the B_o field strength. Since $H_{cs}>H_{dip}$ in order for the monohydride to echo, decreasing the field strength should decrease the amount of monohydrides which echo. This experiment has been carried out for VAN500 at 56 MHz, where M_f in the CPMG decay decreases from ~.65 at 220 MHz to ~.3 at 56 MHz. This measurement is preliminary

because of poor signal-to-noise at 56 MHz, but complementary data are seen for all the samples during the T_1^{cs} measurements, where an overall decrease in the $\%M^{echo}$ was always observed when going to lower fields.

This decrease in intensity for the isolated monohydrides also explains a problem with the Hahn echo linewidth as a function of field. Table 6 gives results showing that the total echo component's linewidth is ~ linear with the static field strength. The isolated monohydrides should have, however, a non-negligible dipolar interaction. The total echo linewidths do broaden slightly in the lower portion of the peak, but the linear linewidths measured must be due mainly due to the T_2^s component. The isolated monohydrides lose intensity at the lower fields, reducing their effect on the total linewidth.

Measuring M_f as a function of B_o would experimentally model the distribution of internuclear separations, P(r), for the monohydrides. The simplistic assumption incorporated in equation (80) could then be avoided by using instead

$$M_2 = A \int_{r_i}^{\infty} P(r)\ r^{-6} dr \qquad (84)$$

In conclusion, the assumptions used to obtain σ in Table 9 provide important information about the monohydride distributions in a-Si:H. A FID and CPMG experiment, giving

quantitative amounts and relaxation data for monohydrides provide the data necessary to carry out such an analysis. An interesting possibility for future work would be to discover if the large σ found for SHK#7 and C45 is indicative of sputtered samples in general, or not.

G. Molecular Hydrogen in a-Si:H

Now that the origin of the component T_2^f during the CPMG experiment is understood, the species responsible for the long T_2^s is still left to identify. I will show that this species is molecular hydrogen (m-H_2) trapped in the amorphous matrix. The quantitative amount of protons associated with T_2^s is close to that suggested by Conradi and Norberg[32] as the amount of m-H_2 necessary to explain the anomolous low temperature minimum in T_1. Moreover, this component has a shorter $T_1=T_{1f}^{cs}$ than the rest of the proton bath (~1/10th, at 25°C; see Table 8). The long T_2^s during the CPMG experiment by itself is a strong indication of m-H_2. The dipolar interaction found from T_2^s is so small that protons must be undergoing fast, <u>isotropic</u> motion. Since the CPMG results do not change with lowering temperatures, some small molecule must give rise to the T_2^s component. All the evidence points to this molecule being H_2.

To verify this identification, the CPMG experiment was performed on annealed samples of VAN150. The anneals were made to correspond to the annealing conditions of Lohneysen et al.[183] at 150°C and 400°C, Graebner et al.[184] at 500°C, and Carlos and Taylor[164] at 550°C. All the anneals were isothermal, lasting for 12 hours for VAN150, 15 min for VAN400 and VAN500, and 6 hours for VAN550.

1. Quantitative determination of m-H_2

Similar to the analysis done for the monohydrides, the quantitative amount of m-H_2 is determined from the CPMG experiment by extrapolating the slow T_2^s back to t=0, and taking the ratio with M_o^{total} (see Figure 15). These results, along with literature values measured or indirectly determined from similar samples, are listed in Table 10. Complete correspondence of the data from this work with the previously published results is not to be expected, since different samples were used in each case, and also because much of the analysis performed in the literature depends on a questionable assumption (see the following discussion). But the correlation between the data for VAN150, VAN400, VAN500, and C45 is apparent, especially in comparison to the calorimetry and Pake doublet NMR determinations. In addition, the amount of m-H_2 observed in the Anode and Cathode samples is reasonably close to the amount of m-D_2

Table 10. Quantitative determination of m-H_2 by our method, tabulated with values obtained by other methods[2]

Sample	at %H	% M^{echo}	% M_s	H_2[a] ($10^{19}/cm^3$)	H_2^{lit}	Ref.
VAN150	15±1	8±2	20±2	5.0[b]	6.4	183
VAN400	13.3	12.5	35	12.5	17.6	33,169,181
VAN500	8.4	20.0	35	12.6	25.0	183
VAN550	1.3	66±8	20	3.7	0	33
Anode	20.0	9.0	20	7.7	....	
Cathode	28.0	9.0	15	8.4	3.3	168
SHK#7	16.0	10.0	25	8.6	38.0	192
C45	5.9	11.0	<13	<0.9	0	191

[a]Density of 2 gm/cm^3 assumed.
[b]Relative error ±20%.

Leopold et al. indirectly determined for a similar sample (other than the deuterium substitution),[168] and the VAN150 contains m-H_2 in the same quantity as measured in similar samples.[169,181]

The observation of m-H_2 in relatively high concentrations in VAN550 was not expected. Following the results Carlos and Taylor found on annealed samples,[33] all the m-H_2 was expected to have been driven off by 530°C. It is possible that the temperature at which the m-H_2 is driven off is sample-

dependent. An alternative intepretation, however, has been supported by preliminary T_1 measurements on VAN550. In this sample, most of the protons have become so dilute in concentration that spin-diffusion between them and their nearest-neighbors has become an ineffective means of transverse relaxation (see the discussion in Section IV.H). Without spin-diffusion, these protons cannot relax through the m-H_2, and must instead relax similarly to Carlos and Taylor's sample annealed at 530^{o}C. The m-H_2 and any nearby protons would then relax very quickly. For VAN550 at 77K, a T_1 of ~20 secs for ~90% of the proton magnetization, and T_1 < 100 msecs for the other 10% was found.

Similar data on VAN500 showed clear nonexponential decays, as would be expected from a sample having fast relaxing m-H_2, moderately relaxing protons, and slow relaxing isolated monohydrides. This result, however, does not conform to most of the published literature, which state T_1's are single exponential. It is quite easy to misinterpret T_1 data, if one is not looking in specific regions of times (or is not careful). This is illustrated in Figure 21.

The three graphs in Figure 21 show theoretical T_1 relaxation curves for three-component systems. All the graphs have $M_s:M_i:M_f$ equaling 10:80:10, and T_1^i = 3secs and T_1^s = 20secs. T_1^f equals 0.1, 0.3 and 0.5 secs for the

Figure 21. Theoretical relaxation curves for a three-component system. All the graphs have $M_s:M_i:M_f$ equaling 10:80:10, and T_1^i = 3secs and T_1^s = 20secs. T_1^f equals 0.1, 0.3 and 0.5 secs for the top, middle and bottom graphs, respectively. The top curve in each graph is the correct theoretical relaxation curve. The lower curve, on the other hand, is the theoretical relaxation for the case where $M(\infty)$ in a rep-rate experiment is assumed to occur at 15 secs.

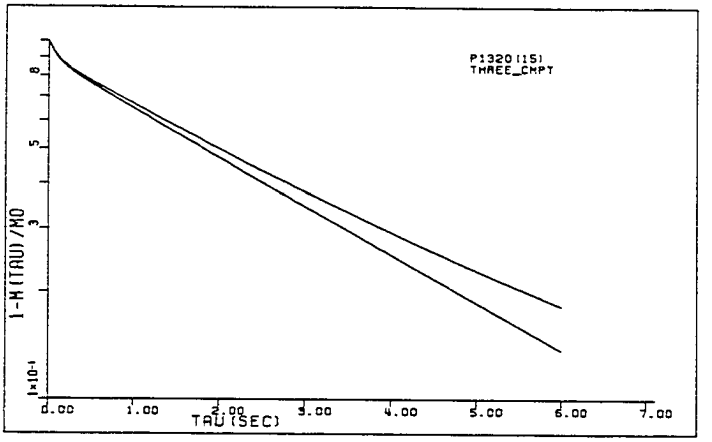
P1320(15)
THREE_CMPT
1-M(TAU)/M0
8
5
3
1x10-1
0.00
1.00
2.00
3.00
4.00
5.00
6.00
7.00
TAU(SEC)

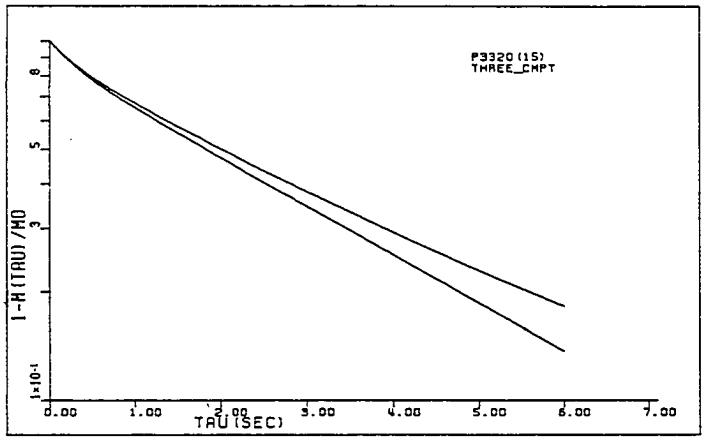
P3320(15)
THREE_CMPT
1-M(TAU)/M0
8
5
3
1x10-1
0.00
1.00
2.00
3.00
4.00
5.00
6.00
7.00
TAU(SEC)

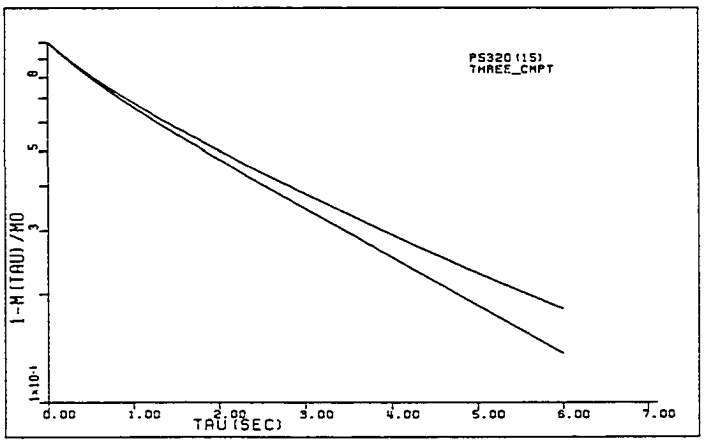
P5320(15)
THREE_CMPT
1-M(TAU)/M0
8
5
3
1x10-1
0.00
1.00
2.00
3.00
4.00
5.00
6.00
7.00
TAU(SEC)

top, middle and bottom graphs, respectively. The top curve in each graph is the correct theoretical relaxation curve:

$$M_c(t) = M_s\exp(-t/T_1^s) + M_i\exp(-t/T_1^i) + M_f\exp(-t/T_1^f) \qquad (85)$$

The lower curve, on the other hand, is the relaxation curve obtained when M(∞) in a rep-rate experiment is assumed to occur at 15 secs, giving

$$M(t) = \frac{M_c(t) - M(15)}{1 - M(15)} \qquad (86)$$

The lower curve is obviously straightened out, and if not many points are taken at very short times, the relaxation may incorrectly be assigned as single exponential. Certainly, the T_1^s component will not be observed.

The fact that m-H_2 is increasing during the anneals is provided from measurements of the sample-wide T_1 as a function of temperature. These data are shown in Figure 22 for VAN150 and VAN500 (T_1's for VAN500 are approximate, due to the above stated nonexponentiality). The most important thing to note is that the T_1 minimum decreases for VAN500, even though the average internuclear spacing for the monohydride distribution has increased. The increase in the monohydride spacings slows spin diffusion down, and if nothing else was happening, T_1 would be expected to increase.

Figure 22. T_1 versus temperature for VAN150 and VAN500. The squares are the measured, exponential T_1^{SW}'s of VAN150, whereas the triangles are T_1^{SW}'s of VAN500. The diamond is the long T_1^{SW} measured for VAN150 at room temp.

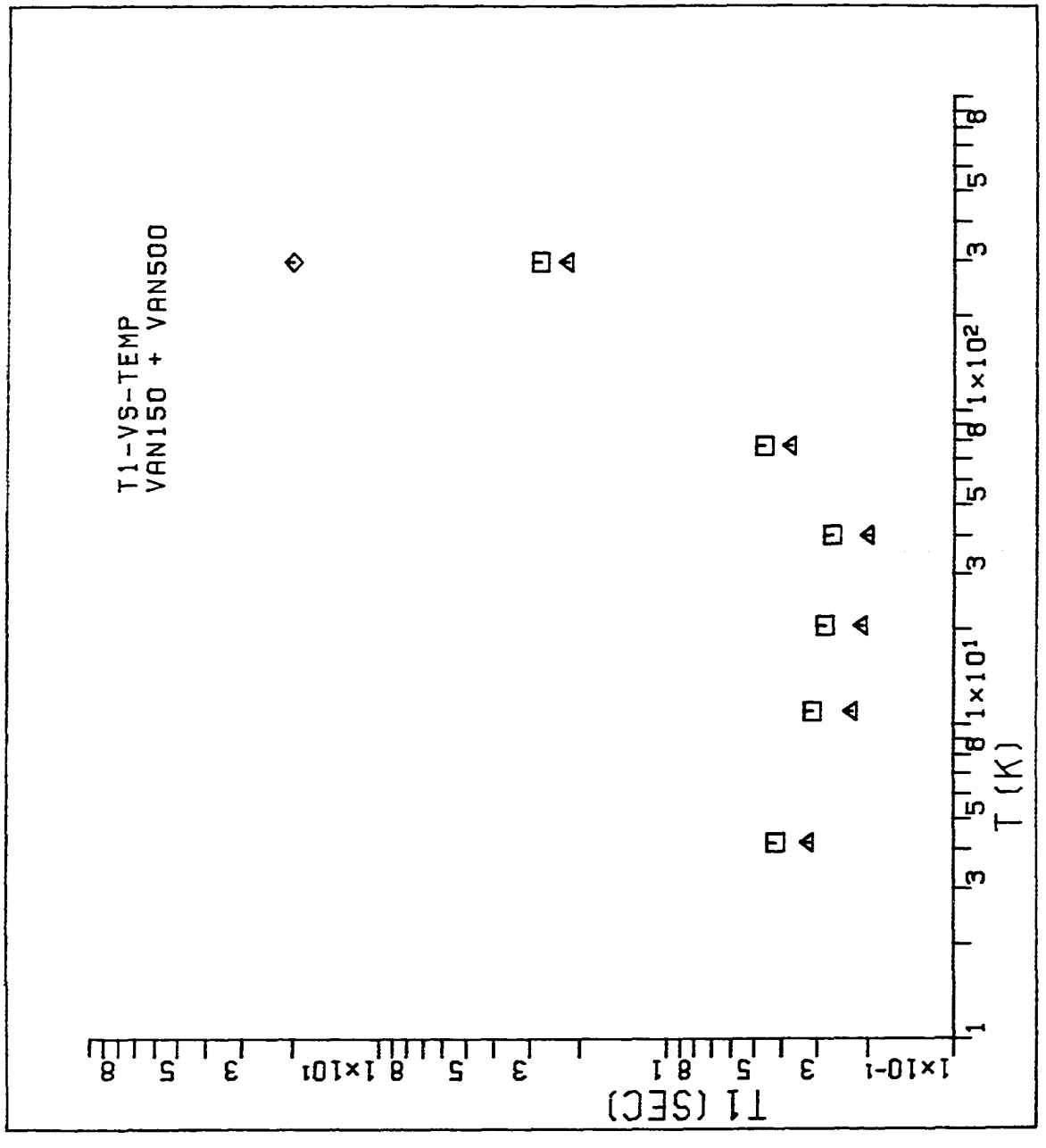
T1-VS-TEMP
VAN150 + VAN500
T1 (SEC)
T (K)
1×10-1
1
1×10¹
1×10²

It should be mentioned here that quantitative determinations of m-H_2 content from the T_1 curve versus temperature, as suggested by Conradi and Norberg,[32] has been shown to be invalid.[187,188] Only m-H_2 in a surface environment, meaning an environment where the m-H_2 experiences a strong EFG, has the Conradi and Norberg type relaxation. Figure 22 then shows the effect of an increase in the surface area of the voids, and the increase in T_2^s with increasing anneal is representative of the increased pressure due to the increased number of m-H_2 in the voids ($T_1^{-1} \propto \tau_c$).

2. Void sizes in a-Si:H

The CPMG measurements now provide another method with which m-H_2 may be studied in a-Si:H films. Questions at this point deal with: i) the nature of the void containing the m-H_2: the average void dimension, the density of the m-H_2, and the structure of the void wall, and ii) how the magnetization of the m-H_2 is connected to the rest of the spin bath.

Although the picture is not yet complete, these questions can be answered to some extent. The values of T_2^s from the CPMG experiments provide an upper limit on homonuclear dipolar (inter- or residual intramolecular) interactions, quadrupolar interactions, or lifetime broadening that the m-H_2 experiences. This was discussed in

detail in Section II.B.2. Accepting that the m-H_2 is rotating freely as a gaseous molecule - necessitated by the absence of the intramolecular dipolar interaction - T_2^s then represents homonuclear dipolar or lifetime broadening. Since T_2^s is greater than 10 msecs (see Table 8), I estimate the m-H_2 must be >10 A from nearest neighbor monohydrides. This estimation was made using a computer routine.

The routine placed upon a spherical surface, having a diameter inputted during execution, protons having an average separation which also is selected during execution. The routine then randomly selected positions within the sphere, and calculated the dipole-dipole interaction a m-H_2 would experience due to the surface protons, if the m-H_2 were static at the selected position. The computer then randomly selected another position inside the sphere, calculated the dipole-dipole interaction at this new position, and continued iterating 5000-10000 times to obtain an average dipole-dipole interaction for the chosen parameters. The calculation is dependent on the distance allowed for closest approach between the m-H_2 and the surface (I used 1-2A), but all the calculations gave >10A, and more likely 20A as the smallest diameter for which the observed T_2^s could be obtained for a hydrogenated void.

This result is of considerable importance, which is easily seen when reviewing the literature on void size

determinations in a-Si:H. EXAFS (Ref. 135 and refs. therein), small-angle x-ray[129,132] and neutron scattering[130,133,134] studies have led to considerable disagreement in the literature regarding the void sizes in a-Si:H, to the extent where some workers suggest voids are <10A in diameter, whereas others conclude voids are >100A in diameter. Recent IR[185,186] and NMR[187] studies have calculated void sizes, but these determinations depend on assumptions about the void shape. The void estimate given here, however, represents a <u>direct</u> measure of the minimum void size, and is only slightly dependent on the void shape. The CPMG experiment may introduce artifacts, but as discussed in Section II.B.2, these only affect the conclusion in a limiting manner as stated. Thus, the CPMG results give strong evidence, supporting recent studies by EXAFS[135] and SANS,[133,134] that voids in all a-Si:H films, glow-discharge and sputtered alike, are greater than 10A in diameter, and more likely are greater than 20A.

The m-H_2 can also be considered to be enclosed in a void containing no protons on the void wall. The connection of the m-H_2 to the proton spin bath then probably occurs spatially to monohydrides which are >10A away. This would account for the observations of Reimer et al.[156] and from modified Goldman-Shen experiments (see Section V) that the m-

H_2 are more closely situated spacially to the narrow line protons than the broad line protons.

A problem still to be addressed is the magnitude of the linewidths associated with T_2 for m-H_2 under a FID. A review of Table 6 shows that the m-H_2 are >5 ppm broad in a FID. The CPMG results verify, however, that the m-H_2 must be rotating isotropically at room temperature at a frequency large compared to the m-H_2 intramolecular dipolar interaction. This precludes chemical shift, which would be averaged by this isotropic motion, from being the dominant broadening mechanism. It appears that either magnetic-susceptibility shifts, or some kind of interaction with electron magnetic moments[169,182] must provide the broadening displayed for the m-H_2 during the FID.

The amount of m-H_2 measured in SHK#7 is almost four times smaller than the value reported by Lamotte[192] (a calculation from his data, assuming 3 at% H in his narrow line, gives 1.7 at% m-H_2). In addition, Chabal et al.[185] measured ~10^{21} protons/cm3 in a glow-discharge sample.

Obviously, there are many questions remaining about m-H_2 in a-Si:H. A combination of annealing with temperature dependent T_1 measurements, along with MAS and CPMG experiments, should lead to a better understanding of the role of hydrogen in a-Si:H materials. Naturally, the excellent recent work of Boyce and Stutzmann[187] will also

provide much new and clarifying information about m-H_2 and a-Si:H in general.

In conclusion, the CPMG experiment gives another method with which to study m-H_2 in a-Si:H. These measurements provide quantitative information about the m-H_2, but the most useful information may come from the relaxation data. These results are strong evidence that m-H_2 resides in voids having diameters of at least 20A, or proton free voids with nearest neighbor protons >10A away.

H. Spin Diffusion and Spin-Lattice Relaxation in a-Si:H

An important question still to be resolved is how the isolated protons can have such a long T_1 (~20secs) when they still have an apparent fast dipolar connection to the rest of the proton bath (T_2^f ~ 1 msecs). In other words, why does spin diffusion not relax these protons similarly to the proton bath?

The answer becomes somewhat apparent when it is realized that another interaction can make the B term in the dipolar Hamiltonian (equation (25)) nonsecular. This can be initially explained with the following arguments. It was previously stated that the isolated protons have $|H_{cs}| > |H_{dip}|$ due to the large internuclear spacing of the isolated proton to its nearest neighbor. Immediately, the possibility

that H_{cs} makes B_{ij} nonsecular must be considered: mutual spin flips have become non-energy conserving. In fact, this change of the B term to being nonsecular as an essential assumption for obtaining a Lorentzian line shape has already been discussed - see Section II.B.1. When this happens, spin diffusion to the isolated proton will suddenly become much slower, in essence becoming a T_1 process.

To make the discussion more explicit, consider two protons, proton 1 being part of the proton bath, the other, proton k, being an isolated proton. Of interest here is the transition rate for mutual spin flips between these two protons. The isolated proton can to a good approximation be considered as a single spin-1/2. But it becomes important to consider the other proton's connection to the spin bath. What does the A and B term mean for this proton? In the bath, mutual spin flips from the B term are occurring at a rate:[3,4]

$$W/t \sim \frac{1}{30T_2^{dip}} \tag{87}$$

where T_2^{dip} represents the inverse of the bath's homonuclear dipolar interactions. When these spin flips occur, the dipolar ordering is disturbed, and the change is transmitted by the A term very quickly ($<1/\omega_0$) to the rest of the bath, including proton 1. This information is also transmitted to

proton k, irrespective of $|H_{cs}|$, and is responsible for the homogeneous part of the two protons line shapes.

The calculation for the mutual spin flip transition rate starts with time-dependent perturbation theory[3] for the first-order transition probability between two states, $|l\rangle$ of proton l, and $|k\rangle$ of proton k, having $\Delta m_l = -\Delta m_k = \pm 1$:

$$W_{lk} = |\langle l|B_{lk}|k\rangle|^2 \; |(1-e^{i(\omega_l-\omega_k)t})/(\omega_l-\omega_k)|^2 \qquad (88)$$

ω_l and ω_k are not precise, but rather must be characterized by distribution functions $g_l(\omega_l)$ and $g_k(\omega_k)$ determined by the frequency spread caused by the A term in H_{dip} as discussed above. Invoking Fermi's golden rule of energy conservation in a quantum transition, the last term in equation (88) becomes

$$(1-\exp(i(\omega_l-\omega_k)t))/(\omega_l-\omega_k) \sim \pi h t \; \delta(\omega_l-\omega_k) \qquad (89)$$

Thus the transition probability per unit time now is:

$$W_{lk}/t \propto |\langle l|B_{lk}|k\rangle|^2 \; |\int\int d\omega_l d\omega_k \; g_l(\omega_l) g_k(\omega_k) \delta(\omega_l-\omega_k)|^2 \qquad (90)$$

$$W_{lk}/t \equiv P_{lk} \propto |\langle l|B_{lk}|k\rangle|^2 \; |\int d\omega_l \; g_l(\omega_l) \; g_k(\omega_l) \; |^2 \qquad (91)$$

where the integrals average the delta function over the frequency distributions. Fermi's golden rule, equation (89), implies that at any certain time there is negligible chance that the spins l and k have exactly matching energies

necessary to induce the mutual energy exchange. Equation (90) then describes the rate with which the spins' energy levels cross, at which time spin flip occurs. (A more proper quantum mechanical description would proceed by describing the probability that the transitions match. But being formal in such a way is not germane for the present discussion, since spin diffusion itself is a semiclassical concept which can not be thought of rigorously in the normal way.)

Equation (90) is valid for times τ where:[235]

$$2\pi/\omega_o \ll \tau \ll T_1 \tag{92}$$

which is true for all experimental times, and permits the use of the integrals in equation (90). The first term in equation (91) describes the mixing of states $\langle\alpha\beta|$ into $|\beta\alpha\rangle$ due to B_{1k}. Since this interaction is a small perturbation on the Zeeman wavefunctions, $|\langle 1|B_{1k}|k\rangle|$ is approximately independent of the chemical shift for all $|H_{dip}|$ and $|H_{cs}| \ll |H_z|$. Thus,

$$|\langle 1|B_{1k}|k\rangle|^2 \sim D^2/16 \tag{93}$$

This is exactly true for the case of two isolated spins-1/2.

Any changes in the transition rate for spin flips between protons 1 and k are therefore due to the overlap integral expressed in equation (91). For no chemical shift, the integral is proportional to the dipolar interaction strength.

But as the chemical shift becomes non-negligible compared to D, P_{1k} decreases depending on the overlap of $g_1(\omega_1,\delta_1)$ and $g_k(\omega_1,\delta_k)$, where the chemical shift terms, $\delta_i = \omega_o\sigma_i$, have been included in the frequency distributions. The situation is shown in Figure 23, for the case of

$$\delta \equiv \omega_o(\sigma_1-\sigma_k) = \Delta \tag{94}$$

where Δ is the half-width at half-height assumed equal for both distributions g_1 and g_k. Δ comes only from the dipolar interaction, and is initially assumed equal for both protons 1 and k. Figure 24 shows the numerical calculation for the overlap

$$P_{1k} \propto \left|\int d\omega\ g_1(\omega,0)\ g_k(\omega,\delta)\right|^2 \tag{95}$$

where the chemical shift difference, δ, has been included in the frequency distributions. In Figure 24, Gaussian distribution functions were used, and equation (95) can thus be rewritten as:

$$P_{1k} \propto \left|\int d\omega\ \exp\left[\frac{-(\omega-\omega_o)^2}{2\Delta^2}\right] \exp\left[\frac{-(\omega-\omega_o-\delta)^2}{2\Delta^2}\right]\right|^2 \tag{96}$$

From Figure 24, it is clear that for $\delta > 3.5\Delta$, spin-diffusion rapidly becomes ineffective.

Figure 23. Overlap of two chemically shifted peaks. These two peaks have $\delta = \Delta$ (DELTA≡Δ in the figure labels), and the transition rate calculated in Figure 24 is proportional to the overlap.

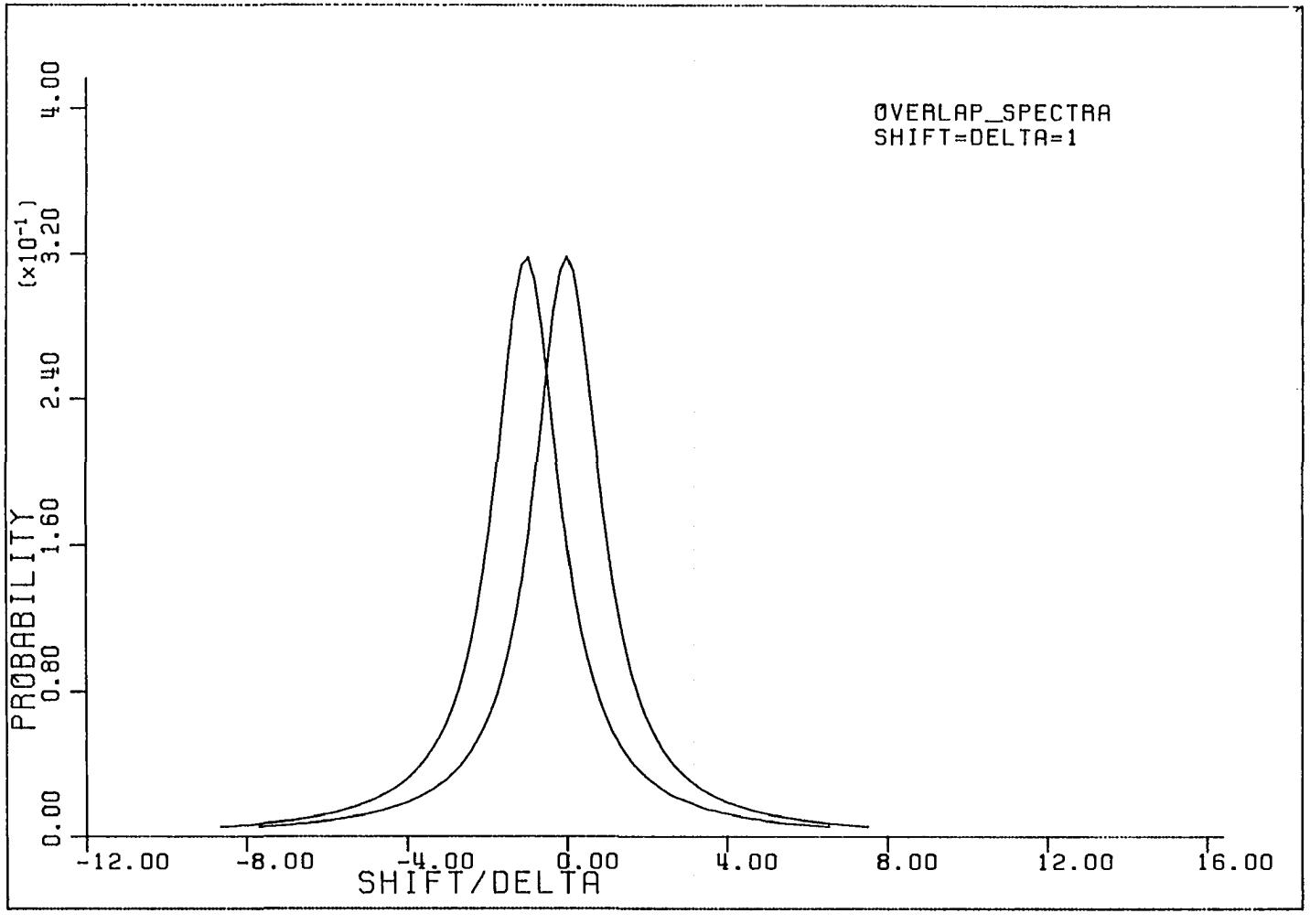
ØVERLAP_SPECTRA
SHIFT=DELTA=1
PRØBABILITY
(x10⁻¹)
0.00
0.80
1.60
2.40
3.20
4.00
-12.00
-8.00
-4.00
0.00
4.00
8.00
12.00
16.00
SHIFT/DELTA

Figure 24. Transition rate for mutual spin flips between two chemically shifted peaks. The two peaks have identical linewidths, in this case, $\Delta_{iso} = \Delta_{bath}$.

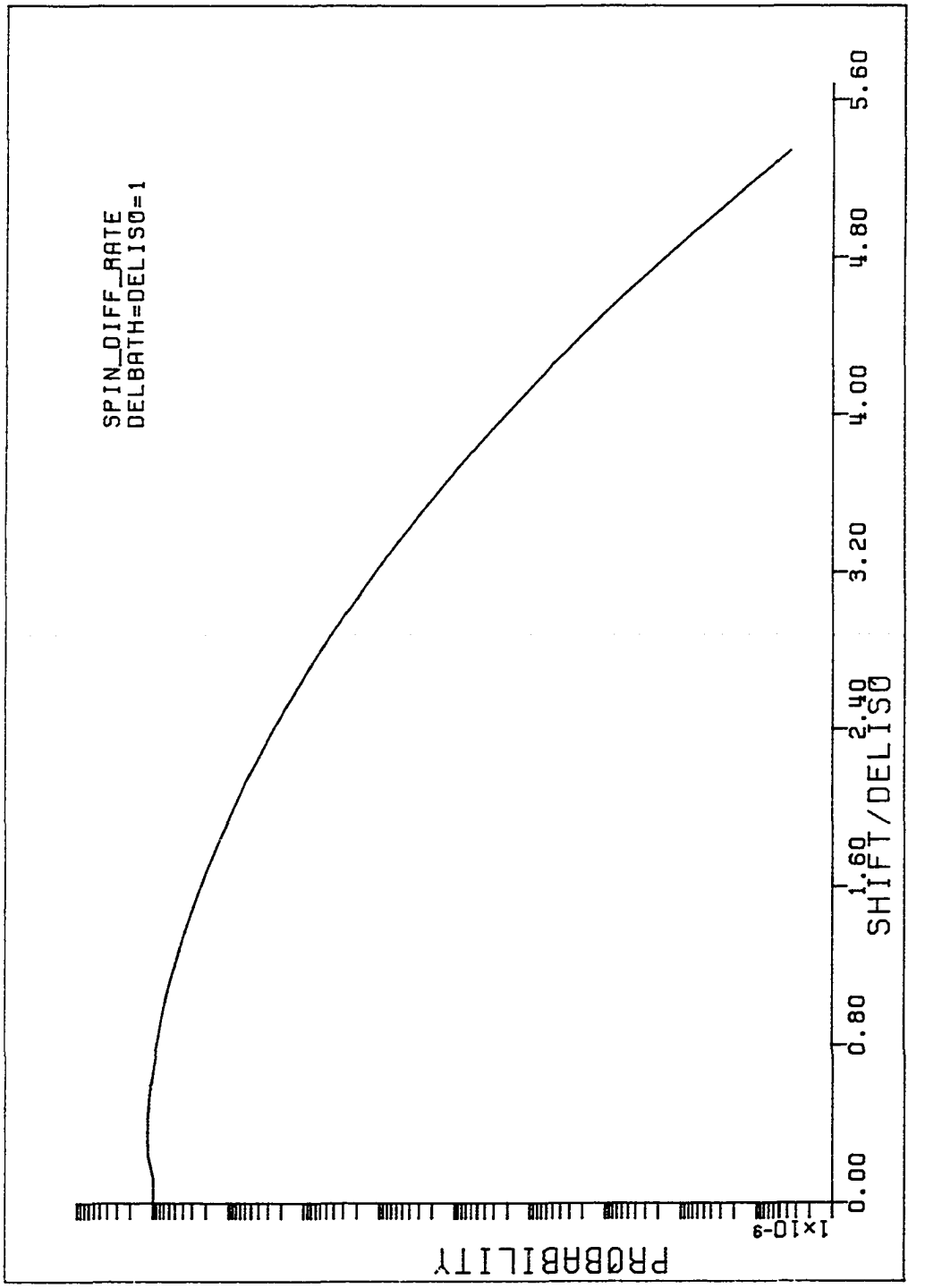
SPIN_DIFF_RATE
DELBATH=DELISO=1
PROBABILITY
1×10-9
0.00
0.80
1.60
2.40
3.20
4.00
4.80
5.60
SHIFT/DELISO

Now consider the more realistic case where the bath proton has a wider homogeneous width, Δ_{bath}, than the width for the isolated proton, Δ_{iso}. Figure 25 shows the calculated spin diffusion rates for Δ_{bath} being 1, 2, 5, 10 and 100 times larger than Δ_{iso}. The calculation includes the effect of Δ_{iso} decreasing as the spin diffusion term, B_{lk}, turns off. This narrowing of Δ_{iso} is calculated as

$$\Delta_{iso} = .67D + .33D*S \qquad (97)$$

The first term on right hand side is the homogeneous width due to the A term, whereas the second term is the contribution due to the B term which is scaled by the factor S as δ increases. The rates calculated in Figure 25 are not sensitive to the exact manner of calculating S for $\delta/\Delta > \sim 2$. The width was decreased for the data shown in Figure 25 as

$$S = 1 \qquad \text{for } \delta^2 \leq 48D^2$$

$$S = (1 + D^2/16\delta^2) - 1 \qquad \text{for } \delta^2 > 48D^2$$

Using $S(\delta) = \Delta(\delta=0)/\Delta(\delta)$, calculated in an interative manner, gave identical results as in Figure 25, except for small differences (slower decrease in $\Delta(\delta)$) for $\delta/\Delta < 2$.

Now it should be realized that for $\Delta_{iso} \leq 1/(2\pi\ 1msec) = 150$ Hz, δ on average can be up to 20-25 times larger. And to have $T_1 = 20sec$, which is $>10^4$ larger than 1msec, Figure

Figure 25. Transition rates for mutual spin flips between two chemically shifted peaks which have differing linewidths: a) $\Delta_{bath} = \Delta_{iso}$; this is the same curve as in Figure 24, b) $\Delta_{bath} = 2\Delta_{iso}$, c) $\Delta_{bath} = 5\Delta_{iso}$, d) $\Delta_{bath} = 10\Delta_{iso}$, and e) $\Delta_{bath} = 100\Delta_{iso}$.

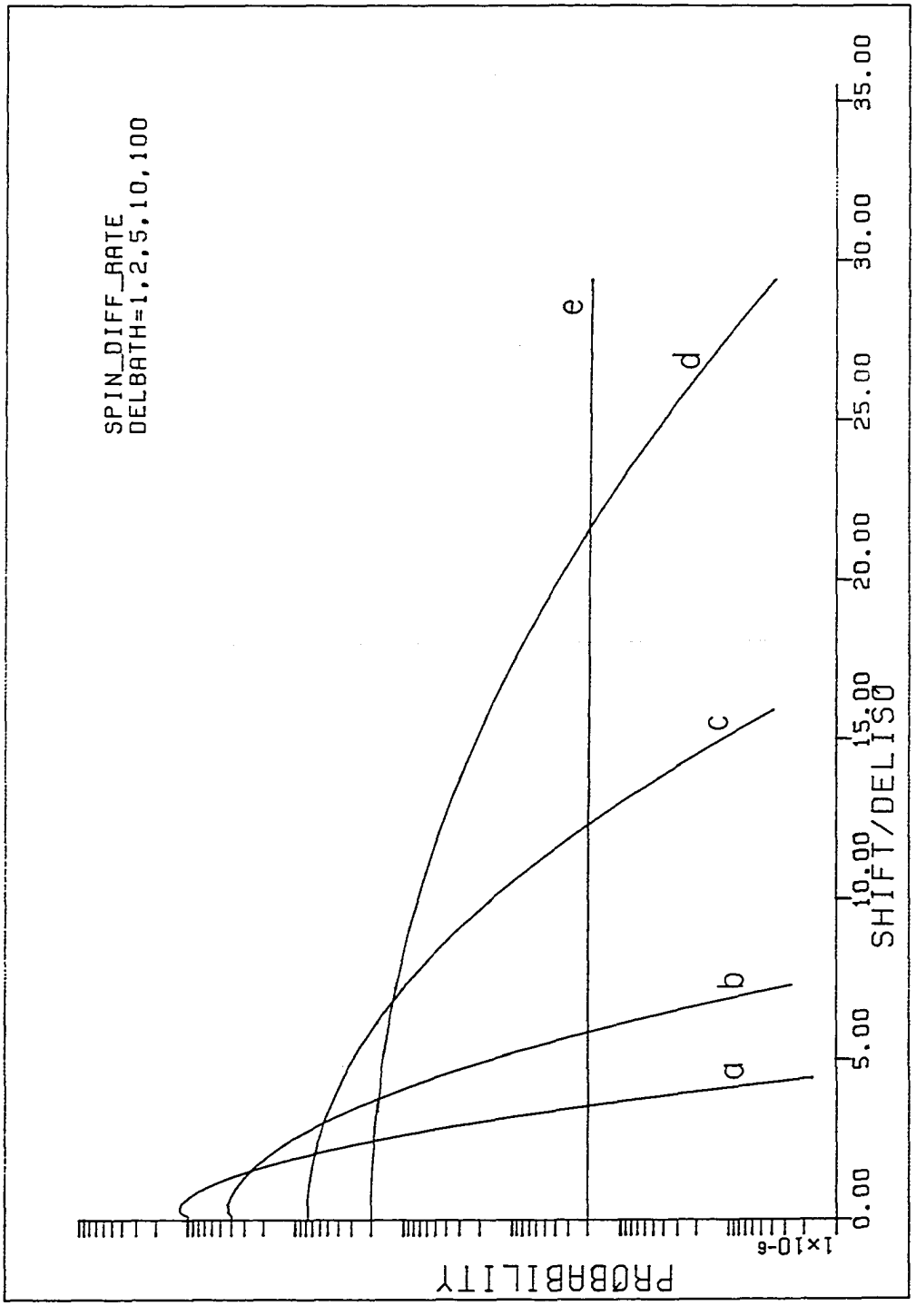
SPIN_DIFF_RATE
DELBATH=1,2,5,10,100
PROBABILITY
1x10-6
0.00
5.00
10.00
15.00
20.00
25.00
30.00
35.00
SHIFT/DELISO
a
b
c
d
e

25 shows that Δ_{bath} must be either less than ten times greater than Δ_{iso} (curve d), or greater than 100 times bigger than Δ_{iso} (curve e) where the bath proton self-decouples from the isolated proton.

Three cases can exist in a-Si:H: i) the bath proton is actually another isolated proton, ii) the bath proton is from the narrow line, or iii) the bath proton is from the broad line. Case iii) is perhaps the simplest. Δ_{bath} in this case is $\Delta_b \sim 25kHz \sim 170\Delta_{iso}$, and the broad line proton therefore is decoupled from the isolated proton. An isolated proton could then provide only a very slow connection of the narrow line proton bath to the broad line proton bath.

When the bath proton is from the narrow line, case ii), $\Delta_{bath} \equiv \Delta_n \sim 3.5$ kHz $= 23\Delta_{iso}$. From curves d and e in Figure 25, it is seen that the isolated proton still would have an appreciable spin diffusion transition rate with the narrow line proton. This implies that the number of isolated protons measured in a T_1^{cs} experiment would be $\leq$ the number measured in the CPMG experiment. This is just what is observed (see Tables 7 and 8).

In case i) where the bath proton is another isolated proton, $\Delta_{bath}/\Delta_{iso} < \delta/\Delta_{iso}$. Here the two protons may have spin diffusion contact with each other, or they may be decoupled, depending on the specific protons. Now we can understand why the Anode and Cathode have no long time T_1 for

the isolated protons, whereas SHK#7 and VAN150 do. Remember that the chemical shift interaction measured by the Hahn echo in SHK#7 and VAN150, ~13 and 25 ppm, were larger than in the Knights samples (~6ppm). The isolated protons in the Knights samples do not decouple from each other or from the narrow line bath because the differences in chemical shift are too small. In SHK#7 and VAN150, on the other hand, the chemical shift differences between the isolated protons are large enough so that they decouple from each other. Thus long T_1's are observed, even if the isolated protons are directly in contact with (at the boundary with) the narrow line bath.

Now consider the spin diffusion between the narrow line bath and the broad line bath. Similar Goldman-Shen results can be obtained from greatly different domains. In one case, the broad line domain is small, perhaps a divacancy, and spin diffusion at the boundary is very slow due to a connection between the baths by isolated protons. On the other hand, the two baths can be directly in contact with each other (the normal assumption in Goldman-Shen experiments). Then the Goldman-Shen results are as previously described. These two cases should be discernible by doing the Goldman-Shen experiment at different fields.

Since the narrow line protons have $\Delta_n \sim 3.5\text{kHz} \sim 7\Delta_b$, the transition rate across the two regions in contact with each other (separated by the average narrow line proton distance

of ~6Å) is < 1/30th the transition rate in the narrow line. Obviously, the picture described is too simplified. The two protons at the boundary surface would have modified Δ's compared to protons in the bulk - Δ_n^s larger than Δ_n, and Δ_b^s less than Δ_b (the superscript s denoting the surface protons). The boundary transfer rate could then be as large as a third of the spin flip rate in the narrow line. Still, it may be possible to find out whether the boundary is giving a rate-limiting step in the Goldman-Shen experiment or not. In the normal Goldman-Shen experiment, no field dependence is expected in the recovery term, R(t) (see Section IV.B). If the boundary is limiting the spin diffusion due to chemical shift differences, however, a definite field dependence would be expected. R(t) should increase in a predictable way with decreasing field strength.

The simplest way for the isolated protons to occur with the long T_1 (=20sec) is for them to have only other isolated protons for nearest neighbors. Another interesting possibility for isolated protons is that they occur between the narrow and broad regions, and are decoupled from the nearest broad protons. There does not appear to be any special experimental or physical justification for this description, it is only one of many possibilities. But if this turns out to be true, then the isolated protons would be in the important region connecting the broad and narrow

regions, and therefore could give important information concerning the electronic properties. A more detailed set of Goldman-Shen experiments on many samples perhaps would clarify the specific region of the isolated protons.

V. CONCLUSIONS AND SUGGESTIONS FOR FUTURE WORK

A. Conclusions

The island size in a-Si:H has been estimated to be ~75±30A for an assumed three-dimensional domain, or 40±20A for a two-dimensional domain. Spin-diffusion from the m-H_2 to the proton bath has suggested that the m-H_2 are closer spatially to monohydrides in the Lorentzian line than to the clustered protons in the Gaussian line.

Arguments have been given to suggest that the interpretation of the Lorentzian line shape being due to a random distribution of monohydrides distributed through the island, or bulk regions of the films should be reexamined. Several reasons, and some calculations provide motive for interpreting the Lorentzian line shape as due to monohydrides bonded to the interstitial surfaces parallel to the growth direction, where the surface has reconstructed to give the larger than expected internuclear separations leading to the narrow Lorentzian line shape. The Gaussian line shape would then occur from hydrogen bonded to surfaces perpendicular to the growth direction (parallel to the growth surface), and would occur on completely, or nearly so, hydrogenated surfaces.

A combination of spin-lattice relaxation measurements and the Carr-Purcell-Meiboom-Gill experiment led to the

identification of two hydrogen environments in addition to the monohydride distribution associated with the Lorentzian line shape and the clustered region associated with the Gaussian line shape. The fact that the Lorentzian line shape is due to a random distribution (it matters only peripherally whether this distribution is within the islands, or on the interstitial surfaces) gives part of the distribution of monohydrides having nearest-neighbor separations so large that these monohydrides echo during a Hahn echo sequence. The information obtained from these experiments led to the conclusion that poor films have a small deviation in internuclear spacings, whereas good films have a larger deviation in internuclear spacings. This result should be a good measure of the growth conditions during deposition.

Molecular hydrogen is identified and quantified using the CPMG experiment. The decay rate of the m-H_2 during the CPMG experiment give a direct measure of the strongest residual proton-proton dipolar interaction, which then gives a lower limit of 10A for void dimensions. This result is a clear measure of the void size.

Combining the information gathered during this work, a clearer picture of the spin-lattice relaxation processes in a-Si:H has been developed. This picture is illustrated in Figure 26. Here the m-H_2 relax quickly (at least surface m-

Figure 26. Schematic of T_1 pathways in a-Si:H. This depicts the T_1 pathways experimentally determined in VAN150 at room temperature. The m-H_2 relaxes directly to the lattice via spin-rotation angular momentum coupling of ~30 msecs. The monohydrides are coupled to the void protons in a time of ~10 msecs as determined by the Goldman-Shen experiments. These protons then relax via the fastest pathway, which is spin diffusion to the m-H_2. This rate is determined by the number of m-H_2 and the T_1 of the m-H_2. Some of the monohydrides, however, are removed far enough away from their nearest-neighbors so that they are decoupled from having effective spin diffusion with the rest of the proton bath. These monohydrides then can only relax directly to the lattice in a time of ~20 secs.

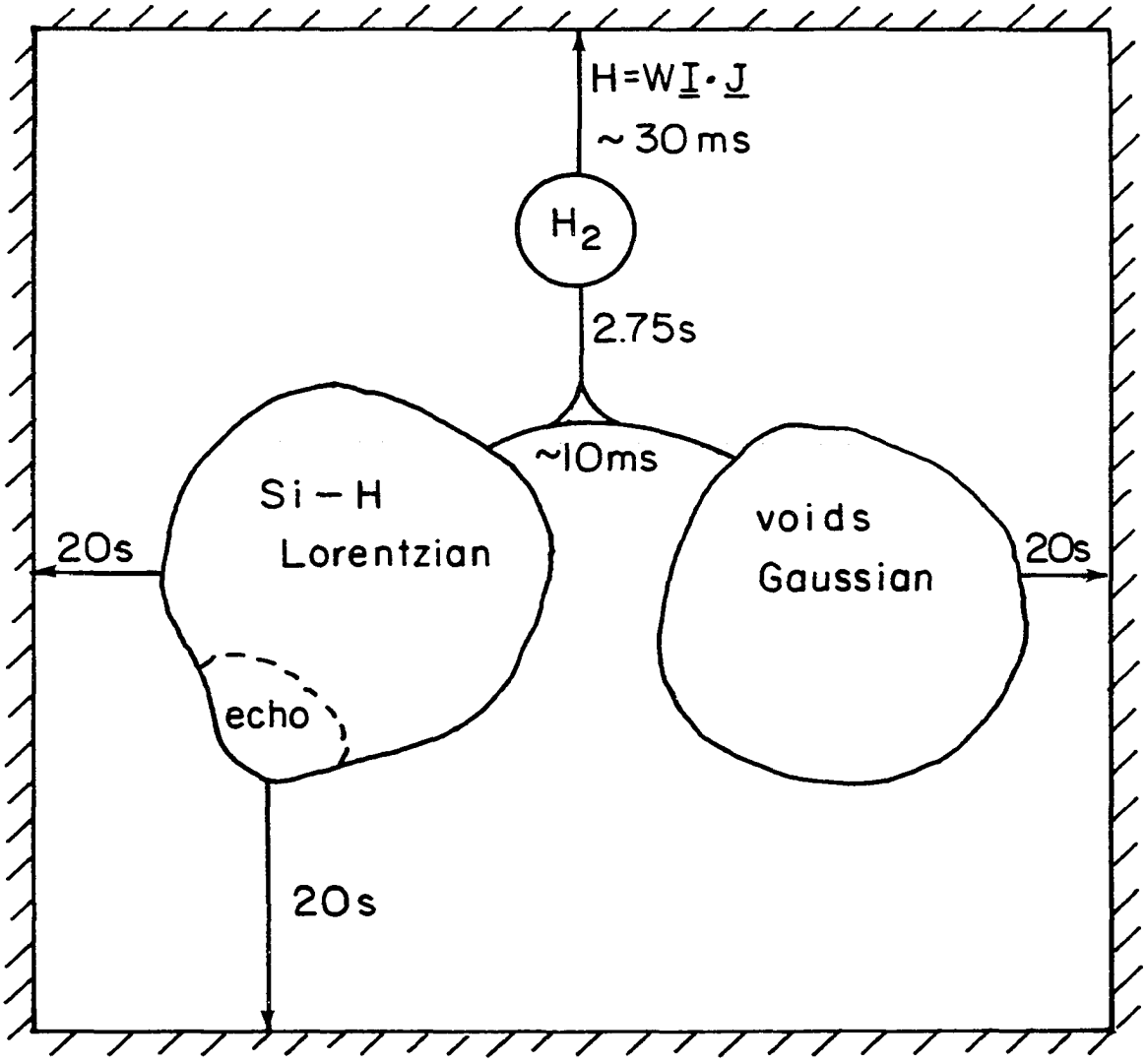
H=WI·J
~30 ms
H2
2.75s
~10ms
Si – H
Lorentzian
voids
Gaussian
20s
20s
echo
20s
Lattice

H_2) to the lattice, and provide a relaxation sink for the main proton baths. The monohydride and void environments are connected via spin diffusion to each other, and hence also to the m-H_2. A portion of the monohydride distribution, however, can be decoupled from the main proton bath, and then must relax directly to the lattice. The size of this region is a function of the static field strength, and annealing conditions.

B. Future Work

It appears the most promising area in the near future for further understanding a-Si:H using proton NMR is studying the behavior of m-H_2 at low temperatures (such studies are already well underway), where the m-H_2 can be observed directly as a Pake doublet feature.[187] The CPMG experiment should provide an excellent technique to extend the high temperature information obtained about m-H_2. At the melting temperature, ~30-40K, of the m-H_2, the Pake doublet will be averaged to a narrow line, and the CPMG experiment will become applicable. This should especially be useful for obtaining the m-H_2 T_1 as a function of temperature.

Also very promising should be a field dependent study of the isolated monohydrides. This study should be able to experimentally determine the distribution of monohydrides in a sample. An interesting contrast might be found between the

distribution in sputtered samples compared to the distribution in glow-discharge samples.

Certainly, the question of whether the Lorentzian line shape is due to monohydrides in the bulk regions of the films, or from monohydrides associated with interstitial regions is worth investigation. Neutron scattering perhaps is the most likely candidate for such a study.

Although Lamotte's recent work[192] using proton MAS NMR has been questioned,[187] MAS could be quite useful. For example, MAS at >4kHz will narrow all of the Lorentzian line shape, thus decreasing spin diffusion in this proton bath. A simple Hahn echo then, at high rep-rates could isolate the m-H_2, especially at low temperatures.

Last, studies involving more sample (>100mg) would greatly enhance the ability to study phenomena such as the Staebler-Wronski effect. I did attempt to see a change in the CPMG parameters when a sample was bathed in intense light, with negative results. More sample mass is a must for such an experiment. Moreover, EXAFS and/or neutron scattering studies done in conjuction with NMR studies would hopefully provide complementary results about void sizes.

VI. LITERATURE CITED

1. Benoit B. Mandelbrot, The Fractal Geometry of Nature (W. H. Freeman and Company, New York, 1977).

2. Richard Zallen, The Physics of Amorphous Solids (John Wiley & Sons, New York, 1983).

3. N. Bloembergen, Physica (Utrecht) 15, 386 (1949).

4. A. Abragam, The Principles of Nuclear Magnetism (Oxford University Press, New York, 1978).

5. T. T. P. Cheung, Phys. Rev. B 23, 1404 (1981).

6. M. Goldman and L. Shen, Phys. Rev. 144, 321 (1966).

7. T. T. P. Cheung and B. C. Gerstein, J. Appl. Phys. 52, 5517 (1981).

8. W. S. Warren, S. Sinton, D. P. Weitekamp, and A. Pines, Phys. Rev. Lett. 43, 1791 (1979).

9. Gary Drobny, Alexander Pines, Steven Sinton, Daniel P. Weitekamp, and David Wemmer, Faraday Symp. Chem. Soc. 13, 49 (1979).

10. Yu-Sze Yen and A. Pines, J. Chem. Phys. 78, 3579 (1983).

11. J. Baum, A. N. Garroway, M. G. Munowitz, and A. Pines, presented at the 26th Rocky Mountain Conference, Denver, 5-9 August 1984 (unpublished).

12. Richard Eckman, J. Chem. Phys. 79, 524 (1983).

13. R. Eckman, A. Pines, R. Tycko, and D. P. Weitekamp, Chem. Phys. Lett. 99, 35 (1983).

14. C. Ye, R. Eckman, and A. Pines, J. Magn. Reson. 55, 334 (1983).

15. Ad Bax, Nikolaus Szeverenyi, and Gary E. Maciel, J. Magn. Reson. 55, 494 (1983).

16. P. Caravatti, J. A. Deli, G. Bodenhausen, and R. R. Ernst, J. Am. Chem. Soc. 104, 5506 (1982).

17. James R. Bolton, Sol. Energy 31, 483 (1983).

18. Yoshihiro Hamakawa, Sol. Energy Mater. 8, 101 (1982).

19. W. D. Johnston, Jr., Solar Voltaic Cells (Marcel Dekker, Inc., New York, 1980).

20. Alan L. Fahenbruch and Richard H. Bube, Fundamentals of Solar Cells: Photovoltaic Solar Energy Conversion (Academic Press, New York, 1983).

21. Kasturi Lal Chopra and Suhit Ranjan Das, Thin Film Solar Cells (Plenum Press, New York, 1983).

22. R. H. Bube, "Solar Cells," in Handbook on Semiconductors, edited by C. Hilsum (North-Holland, New York, 1981), Vol. 4, Chap. 6A, p. 691.

23. Koji Okuda, Hiroaki Okamoto, and Yoshihiro Hamakawa, Jpn. J. Appl. Phys. 22(9), L605 (1983).

24. D. E. Polk, J. Non-Cryst. Solids 5, 365 (1971).

25. W. H. Zachariasen, J. Am. Chem. Soc. 54, 3841 (1932).

26. J. A. Reimer, J. Phys. (Paris) Colloq. 10, C4-715 (1981).

27. J. A. Reimer, R. W. Vaughan, and J. C. Knights, Phys. Rev. Lett. 44, 193 (1980).

28. E. Bustarret, B. Ranchoux, H. Hamdi, A. Deneuville, S. Huant, and P. Depelsenaire, Physica B+C 117-118, 950 (1983).

29. P. C. Taylor, in Hydrogenated Amorphous Silicon, edited by Jacques I. Pankove. Semiconductors and Semimetals (Academic Press, New York, 1984), Vol. 21, Part C.

30. Tatsuo Shimizu, Minoru Kumeda, and Shoichi Ueda, Oyo Butsuri 50, 1266 (1981).

31. D. L. Staebler and C. R. Wronski, Appl. Phys. Lett. 31, 292 (1977).

32. Mark S. Conradi and R. E. Norberg, Phys. Rev. B 24(4), 2285 (1981).

33. W. E. Carlos and P. C. Taylor, Phys. Rev. B 26, 3605 (1982).

34. M. E. Lowry, R. G. Barnes, D. R. Torgeson, and F. R. Jeffrey, in Nuclear and Electron Resonance Spectroscopies Applied to Materials Science, edited by E. N. Kaufmann and G. K. Shenoy (Elsevier North Holland, Inc., New York, 1981), p. 341.

35. J. A. Reimer, P. DuBois Muphy, B. C. Gerstein, and J. C. Knights, J. Chem. Phys. 74, 1501 (1981).

36. F. R. Jeffrey, P. DuBois Murphy, and B. C. Gerstein, Phys. Rev. B 23, 2099 (1981).

37. H. Fritzsche, Sol. Energy Mater. 3, 447 (1980).

38. John C. Knights, Jpn. J. Appl. Phys. 18, 101 (1979).

39. W. E. Spear and P. G. Le Comber, Solid State Commun. 17, 1193 (1975).

40. J. D. Joannopoulos and G. Lucovsky, eds., The Physics of Hydrogenated Amorphous Silicon I: Structure, Preparation, and Devices. Topics in Applied Physics (Springer-Verlag, New York, 1984), Vol. 55.

41. J. D. Joannopoulos and G. Lucovsky, eds., The Physics of Hydrogenated Amorphous Silicon II: Electronic and Vibrational Properties. Topics in Applied Physics (Springer-Verlag, New York, 1984), Vol. 56.

42. Jacques I. Pankove, ed., Hydrogenated Amorphous Silicon. Semiconductors and Semimetals (Academic Press, New York, 1984), Vol. 21, Parts A-D.

43. M. H. Brodsky, ed., Amorphous Semiconductors. Topics in Applied Physics (Springer-Verlag, New York, 1979), Vol. 36.

44. F. Yonezawa, ed., Fundamental Physics of Amorphous Semiconductors: Proceedings of the Kyoto Summer Institute, Kyoto, Japan, September 8-11, 1980. Springer Series in Solid State Sciences (Springer-Verlag, New York, 1981), Vol 25.

45. H. Fritzsche, Bull. Mater. Sci. 2, 295 (1980).

46. H. Fritzsche, Sol. Energy Mater. 3, 447 (1980).

47. John C. Knights and Gerald Lucovsky, CRC Crit. Rev. Solid State Mater. Sci. 9, 211 (1980).

48. William Paul and David A. Anderson, Sol. Energy Mater. 5, 229, (1981).

49. N. F. Mott, J. Phys. C 13, 5433 (1980).

50. John D. Joannopoulos and Douglas C. Allan, Festkorperprobleme 21, 167 (1981).

51. A. H. Clark, Thin Solid Films 108, 285 (1983).

52. D. K. Biegelsen, Mater. Res. Soc. Symp. Proc. Vol. 14, 75 (1983).

53. J. Robertson, Phys. Chem. Glasses 23(1), 1 (1982).

54. D. Adler, J. Phys. (Paris) Colloq. 10, C4-3 (1981).

55. J. C. Phillips, Comments Solid State Phys. 9(6), 191 (1980).

56. J. C. Phillips, J. Non-Cryst. Solids 34, 153 (1979).

57. J. C. Phillips, J. Non-Cryst. Solids 43, 37 (1981).

58. J. C. Phillips, in The Structure of Non-Crstalline Materials: Proceedings of the Second International Conference, edited by P. H. Gaskell, J. M. Parker, and E. A. Davis, Cambridge, UK, 12-15 July 1982 (Taylor & Francis, London, 1983), p. 123.

59. R. A. Street, Adv. Phys. 30, 593 (1981).

60. M. Cardona, Phys. Status Solidi B 118, 463 (1983).

61. B. C. Cavenett, Adv. Phys. 30, 475 (1981).

62. J. I. B. Wilson, J. McGill, and D. Weaire, Adv. Phys. 27(3), 365 (1978).

63. D. E. Carlson, Sol. Energy Mater. 3, 503 (1980).

64. Hellmut Fritzsche and Marc A. Kastner, eds., Transport and Defects in Amorphous Semiconductors: Proceedings of the International Topical Conference on Transport and Defects in Amorphous Semiconductors, 22-24 March 1984, Bloomfield Hills, Michigan. J. Non-Cryst. Solids 66, 1 (1984).

65. H. Fritzsche and D. Adler, eds., Science and Technology of Non-Crystalline Semiconductors. Sol. Energy Mater. 8, 1 (1982).

66. M. Averous, ed., Proceedings of the 16th International Conference on the Physics of Semiconductors, 6-10 September 1982, Montpellier, France. Physica B+C 117-118, Part II, Chap. 16, 864 (1983).

67. B. K. Chakraverty and D. Kaplan, eds., Proceedings of the Ninth International Conference on Amorphous and Liquid Semiconductors, 2-8 July 1981, Grenoble, France. J. Phys. (Paris) Colloq. 42(10), C4-1 (1984).

68. R. A. Street, D. K. Biegelsen, and J. C. Knights, eds., Tetrahedrally Bonded Amorphous Semiconductors, Carefree, Arizona, 1981. AIP Conference Proceedings No. 73 (American Institute of Physics, New York, 1981).

69. J. L. Stone, ed., Photovoltaic Material and Device Measurements Workshop, "Focus on Amorphous Silicon", 3-4 January 1980, San Diego. Solar Cells 2(3-4), 1 (1980).

70. William Paul and Marc Kastner, eds., Proceedings of the Eighth International Conference on Amorphous and Liquid Semiconductors, 27-31 August 1979, Cambridge, Massachusetts. J. Non-Cryst. Solids 35&36, 1 (1980).

71. Shoji Tanaka and Yutaka Toyozawa, eds., Proceedings of the 15th International Conference on the Physics of Semiconductors, 1-5 September 1980, Kyoto. J. Phys. Soc. Jpn. 49, Supplement A, 1 (1980).

72. P. H. Gaskell and J. D. Mackenzie, eds., Electronic Properties and Structure of Amorphous Solids. J. Non-Cryst. Solids 32(1-3), 1 (1979).

73. N. F. Mott and E. A. Davis, Electronic Processes in Non-Crystalline Materials, 2nd ed. (Clarendon Press, Oxford, 1979).

74. J. M. Ziman, Models of Disorder (Cambridge University Press, Cambridge, 1979).

75. Mauricio Schoijet, Sol. Energy Mater. 1, 43 (1979).

76. Charles E. Backus, "Photovoltaic Conversion," in Solar Energy Engineering, edited by A. A. M. Sayigh (Academic Press, New York, 1977), Chap. 12, p. 263.

77. H. J. Hovel, "Solar Cells," in Semiconductors and Semimetals, edited by A. C. Beer and R. K. Willardson (Academic Press, New York, 1975), Vol. 11.

78. Kasturi Lal Chopra and Inderjeet Kaur, Thin Film Device Applications (Plenum Press, New York, 1983).

79. D. S. Campbell, "Preparation Methods for Thin Film Devices," in Active and Passive Thin Film Devices, edited by T. J. Coutts (Academic Press, New York, 1978), Chap. 2, p. 23.

80. P. H. Gaskell, J. M. Parker, and E. A. Davis, eds., in The Structure of Non-Crstalline Materials: Proceedings of the Second International Conference, Cambridge, UK, 12-15 July 1982 (Taylor & Francis Ltd., New York, 1983).

81. M. F. Thorpe, Excitations in Disordered Systems (Plenum Press, New York, 1982).

82. Istvan Hargittai and W. J. Orville-Thomas, eds., Diffraction Studies on Non-Crystalline Substances (Elsevier, New York, 1981).

83. P. H. Gaskell, J. Phys. C 12, 4337 (1979).

84. C. S. Cargill III, Solid State Phys. 30, 227 (1975).

85. Shashanka S. Mitra, ed., Physics of Structurally Disordered Solids (Plenum Press, New York, 1976).

86. M. Cardona, ed., Light Scattering in Solids I, 2nd ed. Topics in Applied Physics (Springer-Verlag, New York, 1983), Vol. 8.

87. John Robertson, Adv. Phys. 32, 361 (1983).

88. G. A. N. Connell and R. A. Street, "Amorphous Semiconductors," in Handbook on Semiconductors, edited by S. P. Keller (North-Holland, New York, 1980), Vol. 3, Chap. 12, p. 689.

89. W. E. Spear, Adv. Phys. 26(6), 811 (1977).

90. W. E. Spear, ed., Proceedings of the Seventh International Conference on Amorphous and Liquid Semiconductors (CICL, Edinburgh, 1977).

91. B. T. Kolomiets, ed., Proceedings of the Sixth International Conference on Amorphous and Liquid Semiconductors (MCR Press, Moscow, 1976).

92. G. Lucovsky and F. L. Galeener, eds., Structure and Excitations of Amorphous Solids, Williamsburg, Va., 1976. AIP Conference Proceedings No. 31 (American Institute of Physics, New York, 1976).

93. M. H. Brodsky, S. Kirkpatrick, and D. Weaire, eds., Tetrahydrally Bonded Amorphous Semiconductors, Yorktown Heights, 1974. AIP Conference Proceedings No. 20 (American Institute of Physics, New York, 1974).

94. M. H. Pilkuhn, ed., Proceedings of the Twelfth International Conference on the Physics of Semiconductors, 15-19 July 1974, Stuttgart (B. G. Teubner, Stuttgart, 1974).

95. J. Stuke and W. Brenig, eds., Proceedings of the Fifth International Conference on Amorphous and Liquid Semiconductors, 3-8 September 1973, Garmisch-Partendirchen, Fed. Rep. Germany (Taylor & Francis LTD, London, 1974).

96. Proceedings of the Eleventh International Conference on the Physics of Semiconductors, 25-29 July 1972, Warszawa, Poland (Elsevier, New York, 1972), Vol. 1.

97. M. H. Cohen and G. Lucovsky, eds., Proceedings of the Fourth International Conference on Amorphous and Liquid Semiconductors, 9-13 August 1971, Ann Arbor, Michigan. J. Non-Cryst. Solids 8-10 (1972).

98. Sir Nevill Mott, ed., Proceedings of the Third International Conference on Amorphous and Liquid Semiconductors, 24-27 September 1969, Cambridge, UK. J. Non-Cryst. Solids 4 (1970).

99. Nevill Mott, Science 201, 871 (1978).

100. Nevill Mott, Rev. Mod. Phys. 50, 203 (1978).

101. David Adler, Sci. Am. 236, 36 (1977).

102. Jan Tauc, Phys. Today 29, 23 (1976).

103. Morrel H. Cohen, Phys. Today 24, 26 (1971).

104. P. W. Anderson, Phys. Rev. 109, 1492 (1958).

105. N. F. Mott, Adv. Phys. 16, 49 (1967).

106. J. C. Knights, "Structural and Chemical Characterization", in The Physics of Hydrogenated Amorphous Silicon I: Structure, Preparation, and Devices, edited by J. D. Joannopoulos and G. Lucovsky. Topics in Applied Physics (Springer-Verlag, New York, 1984), Vol. 55, Chap. 2, p. 5.

107. S. C. Moss and J. F. Graczyk, Phys. Rev. Lett. 23(20), 1167 (1969).

108. D. E. Polk and D. S. Boudreaux, Phys. Rev. Lett. 31(2), 92 (1973).

109. M. G. Duffy, D. S. Boudreaux, and D. E. Polk, J. Non-Cryst. Solids 15, 435 (1974).

110. R. J. Bell and P. Dean, Philos. Mag. 25, 1381 (1972).

111. P. Steinhardt, R. Alben, and D. Weaire, J. Non-Cryst. Solids 15, 199 (1974).

112. G. A. N. Connell and R. J. Temkin, Phys. Rev. B 9(12), 5323 (1974).

113. D. Weaire, N. Higgins, P. Moore, and I. Marshall, Philos. Mag. B 40(3), 243 (1979).

114. G. A. N. Connell and J. R. Pawlik, Phys. Rev. B 13, 787 (1976).

115. D. Kaplan, N. Sol, G. Velasco, and P. A. Thomas, Appl. Phys. Lett. 33, 440 (1978).

116. J. C. Phillips, Phys. Rev. Lett. 42, 1151 (1979).

117. D. E. Eastman, "Geometrical and Electronic Structure of Si(001) and Si(111) Surfaces: A Status Report," RC 8025 (#34875) 12/28/79 Research Report (IBM Research Division, San Jose, CA, 1979)

118. K. L. Chopra, Thin Film Phenomena (McGraw-Hill, New York, 1969).

119. A. Barna, P. B. Barna, G. Radnoczi, L. Toth, and P. Thomas, Phys. Status Solidi A 41, 81 (1977).

120. J. C. Knights and R. A. Lujan, Appl. Phys. Lett. 35, 244 (1979).

121. J. C. Knights, G. Lucovsky, and R. J. Nemanich, J. Non-Cryst. Solids 32, 393 (1979).

122. M. H. Brodsky, Manuel Cardona, and J. J. Cuomo, Phys. Rev. B 16(8), 3556 (1977).

123. G. Lucovsky, R. J. Nemanich, and J. C. Knights, Phys. Rev. B 19(4), 2064 (1979).

124. E. C. Freeman and William Paul, Phys. Rev. B 18(8), 4288 (1978).

125. M. H. Brodsky, M. A. Frisch, J. F. Ziegler, and W. A. Lanford, Appl. Phys. Lett. 30(11), 561 (1977).

126. H. Fritzsche, M. Tanielian, C. C. Tsai, and P. J. Gaczi, J. Appl. Phys. 50(5), 3366 (1979).

127. J. A. McMillan and E. M. Peterson, J. Appl. Phys. 50(8), 5238 (1979).

128. D. K. Biegelsen, R. A. Street, C. C. Tsai, and J. C. Knights, Phys. Rev. B 20(12), 4839 (1979).

129. A. J. Leadbetter, A. A. M. Rashid, R. M. Richardson, A. F. Wright, and J. C. Knights, Solid State Commun. 33, 973 (1980).

130. T. A. Postol, C. M. Falco, R. T. Kampwirth, I. K. Schuller, and W. B. Yelon, Phys. Rev. Lett. 45, 648 (1980).

131. J. F. Graczyk, Phys. Status Solidi A 55, 231 (1979).

132. P. D'Antonio and J. H. Konnert, in Tetrahedrally Bonded Amorphous Semiconductors, edited by R. A. Street, D. K. Biegelsen, and J. C. Knights, Carefree, Arizona, 1981. AIP Conference Proceedings No. 73 (American Institute of Physics, New York, 1981), p. 117.

133. R. Bellissent, A. Chenevas-Paule, and M. Roth, in The Structure of Non-Crstalline Materials: Proceedings of the Second International Conference, edited by P. H. Gaskell, J. M. Parker, and E. A. Davis, Cambridge, UK, 12-15 July 1982 (Taylor & Francis, London, 1983), p. 582.

134. R. Bellissent, A. Chenevas-Paule, and M. Roth, Physica B+C 117-118, 941 (1983).

135. C. E. Bouldin, E. A. Stern, B. von Roedern, and J. Azoulay, Phys. Rev. B 30, 4462 (1984).

136. S. Oguz, R. W. Collins, M. A. Paesler, and W. Paul, J. Non-Cryst. Solids 35/36, 231 (1980).

137. P. John, M. Odel, M. J. K. Thomas, M. J. Tricker, J. McGill, A. Wallace, and J. I. B. Wilson, J. Non-Cryst. Solids 35/36, 237 (1980).

138. E. M. Purcell, H. C. Torrey, and R. V. Pound, Phys. Rev. 69, 37 (1946).

139. F. Bloch, Phys. Rev. 70, 460 (1946).

140. F. Bloch, W. W. Hansen, and M. Packard, Phys. Rev. 70, 474 (1946).

141. A. Carrington and A. D. McLachlan, Introduction to Magnetic Resonance With Applications to Chemistry and Chemical Physics (Chapman and Hall, New York 1979).

142. Thomas C. Farrar and Edwin D. Becker, Pulse and Fourier Transform NMR: Introduction to Theory and Methods (Academic Press, New York, 1971).

143. C. P. Slichter, Principles of Magnetic Resonance, 2nd ed. (Springer-Verlag, New York, 1978).

144. Eiichi Fukushima and Stephen B. W. Roeder, Experimental Pulse NMR: A Nuts and Bolts Approach (Addison-Wesley, Reading, Massachusetts, 1981).

145. Ulrich Haeberlen, High Resolution NMR in Solids: Selective Averaging, edited by John S. Waugh (Academic Press, New York, 1976). Supplement 1 of Adv. Magn. Reson.

146. M. Mehring, Principles of High Resolution NMR in Solids, 2nd ed., edited by P. Diehl, E. Fluck, and R. Kosfeld (Springer-Verlag, New York, 1983). NMR - Basic Principles and Progress, Vol. 11.

147. B. C. Gerstein and Cecil Dybowski, Transient Techniques in NMR of Solids: An Introduction to the Theory and Practice (Academic Press, New York, in press).

148. Ad Bax, Two-Dimensional Nuclear Magnetic Resonance in Liquids (Delft Univ. Press and D. Reidel Publishing Co., Dordrecht, Holland, 1984).

149. N. Bloembergen, E. M. Purcell, and R. V. Pound, Phys. Rev. 73, 679 (1948).

150. J. H. Van Vleck, Phys. Rev. 74(9), 1168 (1948).

151. S. Meiboom and D. Gill, Rev. Sci. Instrum. 29, 688 (1958).

152. E. L. Hahn, Phys. Rev. 80, 580 (1950).

153. H. Y. Carr and E. M. Purcell, Phys. Rev. 94, 688 (1958).

154. W-K Rhim, D. D. Elleman, R. W. Vaughan, J. Chem. Phys. 59(7), 3740 (1973).

155. Jeffrey A. Reimer, Robert W. Vaughan, and John C. Knights, Phys. Rev. B 24(6), 3360 (1981).

156. J. A. Reimer, Robert W. Vaughan, and J. C. Knights, Phys. Rev. B 23(6), 2567 (1981).

157. Jeffrey A. Reimer and John C. Knights, in Tetrahedrally Bonded Amorphous Semiconductors, edited by R. A. Street, D. K. Biegelsen, and J. C. Knights, Carefree, Arizona, 1981. AIP Conference Proceedings No. 73 (American Institute of Physics, New York, 1981), p. 78.

158. Jeffrey A. Reimer, Robert W. Vaughan, and John C. Knights, Solid State Commun. 37, 161 (1981).

159. J. A. Reimer, R. W. Vaughan, J. C. Knights, and R. A. Lujan, J. Vac. Sci. Technol. 19(1), 53 (1981).

160. J. A. Reimer and T. M. Duncan, Phys. Rev. B 27(8), 4895 (1983).

161. W. E. Carlos and P. C. Taylor, Phys. Rev. Lett. 45(5), 358 (1980).

162. W. E. Carlos and P. C. Taylor, J. Phys. (Paris) Colloq. 10(42), C4-725 (1981).

163. W. E. Carlos, P. C. Taylor, S. Oguz, and W. Paul, in Tetrahedrally Bonded Amorphous Semiconductors, edited by R. A. Street, D. K. Biegelsen, and J. C. Knights, Carefree, Arizona, 1981. AIP Conference Proceedings No. 73 (American Institute of Physics, New York, 1981), p. 67.

164. W. E. Carlos and P. C. Taylor, Phys. Rev. B 25(2), 1435 (1982).

165. F. R. Jeffrey and M. E. Lowry, J. Appl. Phys. 52(9), 5529 (1981).

166. R. F. Jeffrey, M. E. Lowry, M. L. S. Garcia, R. G. Barnes, and D. R. Torgeson, in Tetrahedrally Bonded Amorphous Semiconductors, edited by R. A. Street, D. K. Biegelsen, and J. C. Knights, Carefree, Arizona, 1981. AIP Conference Proceedings No. 73 (American Institute of Physics, New York, 1981), p. 83.

167. M. Lowry, F. R. Jeffrey, R. G. Barnes, and D. R. Torgeson, Solid State Commun. 38, 113 (1981).

168. D. J. Leopold, J. B. Boyce, Peter A. Fedders, and R. E. Norberg, Phys. Rev. B 26(11), 6053 (1982).

169. D. J. Leopold, B. S. Coughlan, P. A. Fedders, R. E. Norberg, J. B. Boyce, and J. C. Knights, J. Non-Cryst. Solids 66, 121 (1984).

170. R. E. Norberg, Phys. Rev. B (in press).

171. D. J. Leopold, Peter A. Fedders, R. E. Norberg, J. B. Boyce, and J. C. Knights, Phys. Rev. B (in press).

172. C. Kittel, Introduction to Solid State Physics, 5th ed. (John Wiley & Sons, New York, 1976).

173. G. E. Pake, J. Chem. Phys. 16, 327 (1948).

174. Charles W. Myles, C. Ebner, and Peter A. Fedders, Phys. Rev. B 14(1), 1 (1976).

175. D. Weaire, "Random Structural Models for Amorphous Solids," in Excitations in Disordered Systems, edited by M. F. Thorpe (Plenum Press, New York, 1982), p. 579.

176. Toshio Sakurai and Homer D. Hagstrum, Phys. Rev. B 14(4), 1593 (1976).

177. B. Movaghar and L. Schweitzer, in Tetrahedrally Bonded Amorphous Semiconductors, edited by R. A. Street, D. K. Biegelsen, and J. C. Knights, Carefree, Arizona, 1981. AIP Conference Proceedings No. 73 (American Institute of Physics, New York, 1981), p. 73.

178. B. Movaghar and L. Schweitzer, J. Phys. C 14, 5185 (1981).

179. Peter A. Fedders, Phys. Rev. B 20(7), 2588 (1979).

180. Mark S. Conradi, K. Luszczynski, and R. E. Norberg, Phys. Rev. B 19(1), 20 (1979).

181. J. B. Boyce and M. J. Thompson, J. Non-Cryst. Solids 66, 127 (1984).

182. E. D. VanderHeiden W. D. Ohlsen, and P. C. Taylor, J. Non-Cryst. Solids 66, 115 (1984).

183. H. V. Lohneysen, H. J. Schink, and W. Beyer, Phys. Rev. Lett. 52(7), 549 (1984).

184. J. E. Graebner, B. Golding, L. C. Allen, D. K. Biegelsen, and M. Stutzmann, Phys. Rev. Lett. 52(7), 553 (1984).

185. Y. J. Chabal and C. K. N. Patel, Phys. Rev. Lett. 53(2), 210 (1984).

186. Y. J. Chabal and C. K. N. Patel, Phys. Rev. Lett. 53(18), 1771 (1984).

187. J. B. Boyce and M. Stutzmann, Phys. Rev. Lett. (in press).

188. F. Reif and E. M. Purcell, Phys. Rev. 91(3), 631 (1953).

189. P. A. Fedders, R. Fisch, and R. E. Norberg, Phys. Rev. Lett. (in press).

190. P. A. Fedders, Phys. Rev. B 30(7), 3603 (1984).

191. Mark E. Lowry, Ph.D. Thesis, Iowa State University, Ames, IA (unpublished).

192. B. Lamotte, Phys. Rev. Lett. 53(6), 576 (1984).

193. S. G. Greenbaum, W. E. Carlos, and P. C. Taylor, Physica B+C 117-118, 886 (1983).

194. S. Ueda, M. Kumeda, and T. Shimizu, J. Phys. (Paris) Colloq. 10(42), C4-729 (1981).

195. Shoichi Ueda, Minoru Kumeda, and Tatsuo Shimizu, Jpn. J. Appl. Phys. 20(6), L399 ()1981).

196. Tatsuo Shimizu, Kenji Nakazawa, Minoru Kumeda, and Shoichi Ueda, Jpn. J. Appl. Phys. 21(6), L351 (1982).

197. S. Ueda, K. Nakazawa, M. Kumeda, and T. Shimizu, Solid State Commun. 42(4), 261 (1982), 261.

198. Minoru Kumeda, Yasuto Yonezawa, Kenji Nakazawa, Shoichi Ueda, and Tatsuo Shimizu, Jpn. J. Appl. Phys. 22(3), L194 (1983).

199. R. A. Street, J. C. Knights, and D. K. Beigelsen, Phys. Rev. B 18, 1880 (1978).

200. P. E. Vanier, F. J. Kampas, R. R. Corderman, and G. Rajeswaran, J. Appl. Phys. 56(6), 1812 (1984).

201. P. E. Vanier, Brookhaven National Laboratory, Upton, Long Island, NY 11973, private communication (1984).

202. F. R. Jeffrey, H. R. Shanks, and G. C. Danielson, J. Appl. Phys. 50, 7034 (1979).

203. B. C. Gerstein, C. Chow, R. G. Pembleton, and R. C. Wilson, J. Phys. Chem. 81(6), 565 (1977).

204. D. J. Adduci and B. C. Gerstein, Rev. Sci. Instrum. 50(11), 1403 (1979).

205. Stephen B. W. Roeder, Department of Chemistry, San Diego State University, during a Poster Session at the 23rd Experimental N.M.R. Conference, Madison, WI (1982).

206. Stephen B. W. Roeder, Eiichi Fukushima, and Atholl A. V. Gibson, J. Magn. Reson. 59, 307 (1984).

207. T. E. Glass and H. C. Dorn, J. Magn. Reson. 51, 527 (1983).

208. Doug DeMaw, ed., The Radio Amateur's Handbook, 57th ed. (The American Radio Relay League, Newington, CT, 1980).

209. Model Number VC-10-12, Polyflon Corporation, 35 River St., New Rochelle, NY 10801.

210. P. DuBois Murphy and B. C. Gerstein, "Analysis and Computerized Design of NMR Probe Circuits", No. IS-4436, Ames Laboratory, DOE, Ames, IA 50011.

211. B. C. Gerstein, Philos. Trans. R. Soc. London Ser. A 299, 521 (1981).

212. S. Idziak and U. Haeberlen, J. Magn. Reson. 50, 281 (1982).

213. High-voltage ATC model B capacitors, American Technical Ceramics, 1 Norden Lane, Huntington Station, NY.

214. G. Scheler, U. Haubenreisser, and H. Rosenberger, J. Magn. Reson. 44, 134 (1981).

215. M. E. Stoll, A. J. Vega, and R. W. Vaughan, Rev. Sci. Instrum. 48(7), 800 (1977).

216. F. David Doty, Ruth R. Inners, and Paul D. Ellis, J. Magn. Reson. 43, 399 (1981).

217. Victor J. Bartuska and Gary E. Maciel, J. Magn. Reson. 42, 312 (1981).

218. D. V. Jensen, Ames Lab Virtual Interactive Network (ALVIN), unpublished computer program, available through the Instrumentation Group, Ames Laboratory USDOE, Ames, IA (1978).

219. Paul D. Murphy, Fourier Data Analysis Program (FA1), Ames Laboratory document # IS-4769 UC-32, Ames Laboratory USDOE, Ames, IA (1981).

220. Philip R. Bevington, Data Reduction and Error Analysis for the Physical Sciences (McGraw-Hill, New York, 1969).

221. Paul D. Murphy, PEAK15 (a multipeak fitting routine), available through D. V. Jensen, Instrumention Group, Ames Laboratory USDOE, Ames, IA (1979).

222. Irving J. Lowe, Bull. Am. Phys. Soc. 2, 344 (1957).

223. J. H. Powles and Peter Mansfield, Phys. Lett. 2, 58 (1962).

224. W. E. Blumberg, Phys. Rev. 119(1), 79 (1960).

225. H. E. Rorschach, Physica (Utrecht) 30, 38 (1964).

226. A. C. Lind, J. Chem. Phys. 66, 3482 (1977).

227. R. A. Assink, Macromolecules 11, 1233 (1978).

228. V. J. McBrierty and D. C. Douglass, Phys. Rep. 63, 61 (1980).

229. K. Dusek, J. Plestil, F. Lednicky, and S. Lunak, Polymer 19, 393 (1978).

230. Geoffrey Bodenhausen, Prog. NMR Spec. 14, 137 (1981).

231. S. Emid, Bull. Magn. Reson. 4, 99 (1981).

232. A. Wokaun and R. R. Ernst, Chem. Phys. Lett. 52(3), 407 (1977).

233. B. C. Sanctuary, Mol. Phys. 48(6), 1155 (1983).

234. B. C. Sanctuary, T. K. Halstead, and P. A. Osment, Mol. Phys. 49(4), 753 (1983).

235. A. S. Davydov, Quantum Mechanics, 2nd ed. (Pergamon Press, New York, 1976).

VII. ACKNOWLEDGEMENTS

To Mom and Dad
You started this for me

My wife has been my greatest asset. She has without complaint spent many nights alone in order to let me finish this work. Science surely would be meaningless without her or our son, who is the joy of my life.

I wish to thank Dr. Gerstein for his kind support and encouragement throughout the years. This work certainly is a reflection of his curiosity and love of science, and his ability to let a student roam.

I have truly benefited from a friendship with Dr. Peter Chueng. He always has an interest, and has given a great deal of guidance and support for this work and to me personally.

Dr. Tom Apple in many cases inspired this work, leading me away from the quandaries of muliple-quantum echoes.

I have had many good friends and coworkers which have made my years at Ames a pleasurable and productive experience. Joe Iwamiya, Serge Lacelle, and Po-Jen Chu have been the above and more. Drs. Paul Murphy, Bob Taylor, Larry Ryan, Gina Hoatson, and Paul Tindall deserve more of the same.

I wish to thank Dave Torgeson and Dr. R. Barnes for many conversations and kind help. I also want to thank Dr. Craig Taylor for the invitation to work at Salt Lake, and to Bert VanderHeiden for his generous help while I was there.

VIII. APPENDICES

A. Correction for Relative Intensities in a Fourier Transformed Free-Induction-Decay

For any line shape comprised of two overlapping lines having dissimilar linewidths, the usual Fourier transform (FT) of the free-induction-decay (FID) will give incorrect relative intensities in the two peaks. This error in the intensities comes about because the broader line decays away more in the FID during the receiver dead-time than does the narrower line. The broader line will appear in the FT to have a smaller relative intensity than it truly has. For a-Si:H's, this error can be >20%, but for the dead-times normal on our equipment (t_d~6-10μs) the error <5%.

Correct relative intensities can be obtained by fitting the time decay directly, since in this case the fit will extrapolate the decay back to time zero, t=0. In our group, it is only possible to fit on-resonance decays using TCDA. A fit to an on-resonance line shape is very sensitive to base line artifacts, so that the T_2's obtained in this case will be more uncertain than those obtained from a fit to frequency domain data. On-resonance fits have been done on some of the a-Si:H samples, giving results within the error limits of the results obtained by fits in the frequency domain. Taking FIDs both on- and off-resonance, however, is time consuming.

Moreover, obtaining correct T_2's was considered more important than getting accurate relative intensities, and a correction to the relative intensity error is simple. Thus, most FIDs were taken off-resonance, and FT into the frequency domain.

The relaxation of the magnetization in the rotating frame (which is the frame of detection) can be described as

$$\frac{M(t)}{M_o} = \frac{M_o^n}{M_o} e^{-t/T_2^n} + \frac{M_o^b}{M_o} e^{-t^2/2(T_2^b)^2} \qquad (8.1)$$

where $M_o = M_o^n + M_o^b$ is the total magnetization, and n denotes a narrow Lorentzian line, b a broader Gaussian line. During the dead-time, t_d, the magnetization has decayed to

$$\frac{M(t_d)}{M_o} = \frac{M_o^n}{M_o} e^{-t_d/T_2^n} + \frac{M_o^b}{M_o} e^{-t_d^2/2(T_2^b)^2} \qquad (8.2)$$

Since t_d is time zero for the Fourier transform, the "apparent" relative intensities (or areas) in the frequency domain, which are derived from the apparent initial magnetization in the time domain, are then

$$f_n = c \frac{M_o^n}{M_o} e^{-t_d/T_2^n} \qquad (8.3)$$

and

$$f_b = c \frac{M_o^b}{\bar{M}_o} e^{-t_d^2 / 2(T_2^b)^2} \tag{8.4}$$

where c is a normalization constant, since $f_n + f_b = 1$. To find the true relative intensities, equations (8.3) and (8.4) are solved with correct normalization to give

$$\frac{M_o^n}{\bar{M}_o} = \frac{1}{c} f_n e^{t_d / T_2^n} \tag{8.5}$$

$$\frac{M_o^b}{\bar{M}_o} = \frac{1}{c} f_b e^{t_d^2 / 2(T_2^b)^2} \tag{8.6}$$

where

$$c = f_n e^{t_d / T_2^n} + f_b e^{t_d^2 / 2(T_2^b)^2} \tag{8.7}$$

The frequency domain fitting routine, in this work PEAK15, returns f_n, f_b, T_2^n, and T_2^b, and t_d is known from experimentation (usually on water) done during the tune-up procedure. Equations (8.5-7) then give the corrected relative intensities.

One final aspect of the correction derived above should be noted here. The off-resonance oscillation, $\Delta\omega$, of the FID has been neglected. This procedure is correct only if the two peaks do not have a large difference in their first moments, $\Delta\omega_s$. If there is a large difference in the first

moments ($\Delta\omega_s \sim \Delta\omega$), then the two peaks will have a first order phase error which must be corrected. For two peaks having both a large difference in their linewidths, and a large difference in their first moments, the correction for the relative intensities becomes much more involved (quadrature detection with the rf frequency set exactly between the first moment difference would produce data which could be corrected as described above). In the case of a-Si:H's, however, the first moments are nearly identical ($\Delta\omega_s$ < 5ppm < 1.5 kHz), and only a zero order phase correction, identical for both peaks, need be made. The above correction scheme in this case is therefore correct.

B. Elaboration on the Lorentzian Line Shape

In this appendix, I will elaborate more fully (see Section II.C.1.b for previous discussions) on the possible morphological environments protons could have that would give rise to the Lorentzian line shape. In addition to the arguments given by Weaire et al.,[113,175] there are other reasons for reexamining the "standard" interpretation:[26] that the Lorentzian line is due to monohydrides randomly dispersed throughout the bulk regions of the film. Suppose this conjecture is true. Why, then, does this line always show a 3-4 at% concentration of monohydrides? It would seem most

likely that this concentration would depend strongly on the deposition conditions, just as with the Gaussian line. Moreover, what causes the "clustering" of these protons in some films, while not in others?[33,155,167,191] These questions, including those raised by Weaire, remain as troublesome problems.

While it is not the purpose of this discussion to answer the above questions, a different approach toward interpreting the Lorentzian line will be presented. Previous work[33,155,167] has assumed the Lorentzian line comes from a three-dimensional network of monohydrides. This assumption greatly affects space-filling arguments (it, in fact, is their origin). Consider instead a model of the film as shown in Figure 27. Islands of average width, k, grow up from the surface to form a film of thickness, d. The tissue region has a thickness, v, which would depend on the growth conditions. Suppose the Lorentzian line arises from monohydrides on the island surfaces. The main impact of this assumption comes from the decrease in the average internuclear spacing of the monohydrides giving rise to the Lorentzian line since these monohydrides now "see" a two-dimensional network of monohydrides about themselves. The number of nearest neighbors decreases from $\xi = 8.5$ for a three-dimensional cubic environment to $\xi = 6.3$ for a Si(111)

Figure 27. Monohydride bonding in an ideal a-Si:H film. d is the film thickness, k is the average island width, and v is the tissue thickness.

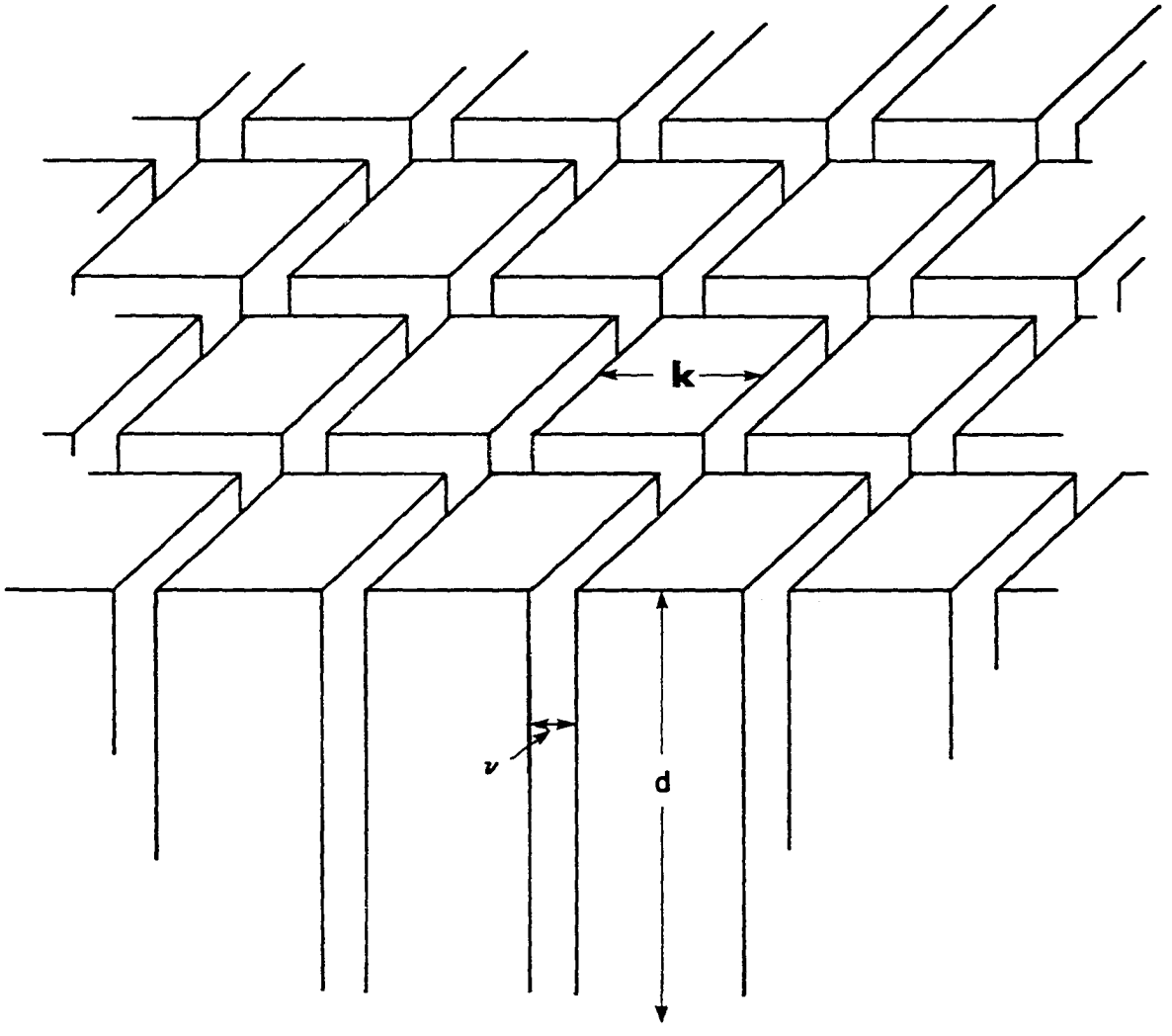
k
v
d

surface (see Table 1). Thus, the average spacing for the Lorentzian line would be (see equation (64)) ~5A.

A necessary test for any model of a-Si:H is the ability of the model to explain the density change from ~2.3 gm/cm^3 for crystalline silicon to < 2 gm/cm^3 for a-Si:H. The density of crystalline silicon is

$$\rho_c = \frac{M_{Si}}{N_A a_{Si}^3} \tag{8.8}$$

where a_{Si} is an average Si spacing ~2.7A (a diamond lattice contains eight atoms per unit cell, thus each atom takes up an equivalent volume of a_{Si}^3, where a_{Si} is half the unit cell length ~5.4A for crystalline silicon). For the model shown in Figure 27, there are $k^2 d/[a_{Si}^3 (k+v)^2 d]$ Si atoms/cm^3 and $4kd/[a_H^2 (k+v)^2 d]$ H atoms/cm^3 (a_H ~ 5A from the NMR linewidth). The a-Si:H density is then

$$\rho_a = \frac{k}{N_A (k+v)^2} \left\{ \frac{M_{Si} k}{a_{Si}^3} + \frac{4M_H}{a_H^2} \right\} \tag{8.9}$$

Now

$$\frac{\rho_a}{\rho_c} = \frac{k}{(k+v)^2} \left\{ k + \frac{4M_H}{M_{Si}} \frac{a_{Si}^3}{a_H^2} \right\} \tag{8.10}$$

which simplifies to

$$\frac{\rho_a}{\rho_c} \sim \frac{1}{(1 + \frac{v}{k})^2} \qquad (8.11)$$

The exterior surface area does not contribute, except for very thin films. The ratio of exterior surface area to interior surface area is

$$\frac{A_e}{A_i} = \frac{2(k+v)^2}{4kd} \sim \frac{1}{200} \quad \text{when } d=3\mu m.$$

Suppose 10% of the Si atoms are taken up as voids for the Gaussian line. Then

$$\frac{\rho_a}{\rho_c} \sim \frac{0.9}{(1 + \frac{v}{k})^2} \qquad (8.12)$$

which leads to

$$\frac{v}{k} \sim \frac{1}{14}$$

An a-Si:H film with a tissue thickness of v=10A and an island width of k=140A then gives the correct density change and ^1H NMR line shapes.

The other necessary test of the model is that the surfaces contain 3-4 at% monohydrides. This is easily calculated from the number of Si and H atoms/cm^3. α_L, the concentration of monohydrides in the Lorentzian line, as given in equation (69) is now

$$\alpha_L = \frac{4k/[a_H^2 (k+v)^2]}{4k/[a_H^2 (k+v)^2] + \frac{0.1}{a_{Si}^3} + k^2/[a_{Si}^3 (k+v)^2]} \quad (8.13)$$

or

$$\alpha_L \sim \frac{1}{1 + \frac{a_H^2 k}{4a_{Si}^3}} \quad (8.14)$$

For a_H=5Å and a_{Si}=2.7Å, equation (8.14) gives k = 75-105Å for α_L = 3-4 at%.

The line shapes can therefore be easily explained from second moments arguments using the island-tissue model. Moreover, the need for space-filling is completely avoided. Annealing behavior is also satisfied in this model, since silicon surfaces are known to evolve monohydrides similar to the high temperature evolution observed in a-Si:H.[176] It is interesting to speculate that if the island sizes are nearly the same in a-Si:H, irrespective of deposition conditions, then the 3-4 at% hydrogen concentration observed for the Lorentzian line could simply be due to the island wall monohydrides. This is a strong assumption, however, even without introducing the notion of reconstruction of the silicon surface. Experimental evidence is needed to consider such an interpretation further.

More relevant at the present time is to note the "coincidence" of a 3-4 at% hydrogen concentration in the Lorentzian line of all a-Si:H films compared to the universal 3 at% intrinsic defect concentration derived for a-Si[116] (see Section II.A.2). The tissue region seems a likely candidate for such defects, and certainly is intimately involved in hydrogen passivation. Surface effects, including reconstruction, must play an important role in the morphology of hydrogen in a-Si:H. Neutron and x-ray scattering techniques, combined with NMR, ESR, light-induced effects, and annealing have a good probability of resolving these questions in the near future.